

第8回コンピューショナル・マテリアルズ・デザイン(CMD)ワークショップ
NANIWA2001実習

Ab-Initio Quantum Dynamics Computation- Based Surface Reaction Design

笠井秀明¹、Wilson Agerico Diño^{2,3}

¹大阪大学大学院工学研究科

²大阪大学大学院理学研究科

³大阪大学ナノサイエンス・ナノテクノロジー研究推進機構

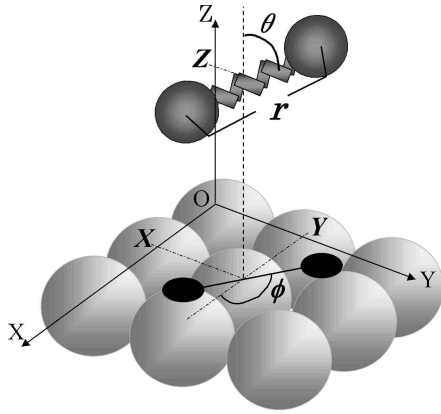


図 1.1: Cu(001) 上の水素分子 (H_2) の 6 つの自由度。X 軸は [100] 方向、Y 軸は [010] 方向にとる。また原点はオントップ・サイトにとる。 H_2 の重心 (X, Y, Z) 原子の相対座標 (r, θ, ϕ) 合わせて 6 次元、表面原子の自由度を含めると 7、8... 次元となる。

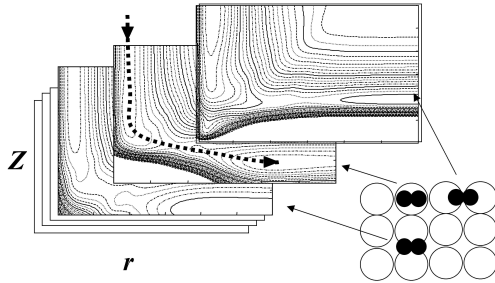


図 1.2: $\text{H}_2/\text{Cu}(001)$ 系の PES のイメージ図。各断面での等エネルギー線を示す (上図)。表面に投影した重心の位置 (下図: ○ Cu 原子、● 水素原子)。 $\theta = \frac{\pi}{2}, \phi = 0$ の場合を示した。PES は (r, Z, X, Y) の他に、(θ, ϕ) にも依存する。点線矢印は、特定の (r, Z, X, Y, θ, ϕ) の解離吸着プロセスにおける反応経路の例である。

1.1.1 カップルド・チャンネル法

本節では、水素-表面反応を例として、断熱近似 (ボルン・オッペンハイマー近似) の枠内で、第一原理の立場から理論的に解析するシミュレーション手法: カップルド・チャンネル法¹⁻⁶を用いた第一原理量子ダイナミクス計算を紹介する。従来の第一原理計算とは、イオン・コアの位置を固定し、電子系の状態を密度汎関数法で計算すること、若しくは第一原理分子動力学として、ある時刻のイオン・コア位置を確定し、その電子状態を密度汎関数法で計算し、それに基づいてイオン・コア位置の時間発展を古典力学に従って逐次的に追跡することを指す。これらに対し、第一原理量子ダイナミクス計算とは電子系とイオン・コアの運動も含

めた量子ダイナミクスを取り扱う計算手法である。図 1.1 に水素分子 (H_2) の運動の 6 つの自由度を表す。ここで、 Z は H_2 の重心位置の表面垂直距離、 r は H_2 を構成する 2 原子間の距離、 X と Y は H_2 の重心の表面平行位置を表し、Cu(001) では [100] 方向を X 軸、[010] 方向を Y 軸、そしてオントップ・サイトを原点として定義する。 θ は H_2 の配向で表面垂直方向と H_2 軸の成す角を表し、 ϕ は H_2 の方位角で H_2 軸の表面射影方向と X 軸とのなす角で定義される。まず H_2 のこれら 6 つの座標の関数として、電子系の基底状態の全エネルギーを電子状態の第一原理計算によって求める。計算は密度汎関数理論 (DFT: Density Functional Theory)^{7,8} に基づいて行う。求められた電子系の基底状態のエネルギーから 6 次元の断熱ポテンシャル・エネルギー (超) 曲面 [PES: Potential Energy (Hyper-) Surface] が得られる。そして次に、得られた PES 上での水素分子の運動を、多自由度系の量子ダイナミクス計算によって解析する。

固体表面に飛来する原子・分子の動的過程は、主として PES の形状や、原子・分子と表面自由度 (表面構成物質の電子系や格子系) 間のエネルギー交換の詳細によって決定づけられている。さらに、振動・回転等の内部自由度を持つ分子は、動的過程においてその内部自由度が変化している。例えば分子の持つ並進エネルギーの振動・回転自由度への移行も動的過程を決定づける要因となる場合もある。これらの要因の詳細を電子論に基づくミクロな立場から理解するために、 H_2 の 6 つの自由度を正確に記述した以下のハミルトニアンを出発点とする。

$$H = -\frac{\hbar^2}{2M} \left[\partial_X^2 + \partial_Y^2 + \partial_Z^2 \right] - \frac{\hbar^2}{2\mu} \partial_r^2 - \frac{2\hbar^2}{\mu r} \partial_r + \frac{1}{2\mu r^2} L^2 + V(r, Z, X, Y, \theta, \phi) \quad (1)$$

ここで、 M 、 μ はそれぞれ H_2 の全質量と換算質量である。 L は H_2 の回転運動を表す角運動量演算子である。また最後の項 $V(r, X, Y, Z, \theta, \phi)$ は、電子状態の第一原理計算より求めた 6 次元 PES である (図 1.2)。(表面原子の自由度を含めると 7、8... 次元となる。) 次に、 r, Z の直交座標系から反応経路に沿う湾曲座標 s とそれに垂直な一般化振動座標 v の系に変換し、ダイナミクスの計算を行う。¹⁻⁶この時、(1) は次のように書

き直される。¹⁻⁶

$$H = -\frac{\hbar^2}{2M} \left[\partial_X^2 + \partial_Y^2 \right] - \frac{\hbar^2}{2\mu} \left[\eta^{-1} \partial_s \eta^{-1} \partial_s + \eta^{-1} \partial_v \eta \partial_v \right] + \frac{\hbar^2}{2\mu} \frac{1}{r} L \frac{1}{r} L + V(s, v, X, Y, \theta, \phi). \quad (2)$$

ここでは質量の重みを付加した座標 s, v を導入している。 $V(s, v, X, Y, \theta, \phi)$ は反応経路座標系における6次元 PES である。 η は、変数変換のヤコビアンである。始状態の分子の並進エネルギー、振動エネルギー、回転エネルギーが実験で使われている分子ビームのそれぞれに対応する値を与えて、(2) をハミルトニアンとする Schrödinger 方程式を解く。

波動関数 $\Psi(s, v, X, Y, \theta, \phi)$ を、内部状態を表す波動関数 $\varphi_{\nu, m, n}^{j, m_j}(s; v, X, Y, \theta, \phi)$ を使って $\Psi(s, v, X, Y, \theta, \phi) = \sum \Psi_{\nu, m, n}^{j, m_j}(s) \varphi_{\nu, m, n}^{j, m_j}(s; v, X, Y, \theta, \phi)$ と展開し、 $\Psi_{\nu, m, n}^{j, m_j}(s)$ (量子数 ν, j, m_j, m, n はそれぞれ分子の振動状態、回転状態、角運動量ベクトル \mathbf{j} の表面垂直成分、表面平行方向の運動状態を表す量子数であり、チャンネルと呼ぶ) に対する coupled-channel type Schrödinger 方程式⁹ を導き、物理的に適切な境界条件下でこれを数値的に解き、吸着確率 $S(E_t, E_\nu, E_j, \Theta)$ 、脱離確率 $D(E_t, E_\nu, E_j, \Theta)$ を求めることが出来る。¹⁻⁶ ここで、 E_t, E_ν, E_j, Θ はそれぞれ分子の並進エネルギー、振動エネルギー、回転エネルギーと表面に対する入射・散乱角度である。

これまで、この方法により水素-表面系 (遷移金属、単純金属、半導体等の結晶表面、グラファイト、カーボンナノチューブ、芳香族分子等の表面等) を対象として、内部自由度をもつ複合粒子としての回折散乱過程、解離吸着 (飛来する H_2 が解離し、2つの H 原子となって金属表面に吸着する) 過程、会合脱離 (吸着している H 原子が会合し、 H_2 となって脱離する) 過程、剥ぎ取り反応 (表面に吸着している原子・分子を、飛来する分子・原子が剥ぎ取り持ち去る) 過程等を研究し、分子の振動・回転・並進運動の自由度それぞれに起因する効果 (ステアリング効果、回転から並進へのエネルギー移行効果、分子振動による吸着促進効果、表面格子振動による吸着促進・抑制効果、同反応鍵穴制御効果等) が見出されるとともに、多くの実験結果が再現された。^{1, 3, 10-22} これらは、イオン・コアの運動

における量子力学的効果の重要性を示すものである。

参考文献

- [1] 笠井秀明, W.A. Diño, 興地斐男: 日本物理学会誌 **52** (1997) 824.
- [2] W. Brenig, H. Kasai: Surf. Sci. **213** (1989) 170.
- [3] H. Kasai, A. Okiji: Prof. Surf. Sci. **44** (1993) 101.
- [4] W. Brenig et al.: Z. Phys. B **93** (1993) 91.
- [5] W. Brenig, R. Russ: Surf. Sci. **315** (1994) 195.
- [6] W. Brenig, A. Gross, R. Russ: Z. Phys. B **97** (1995) 311.
- [7] P. Hohenberg, W. Kohn: Phys. Rev. **136** (1964) B 864.
- [8] W. Kohn, L.J. Sham, Phys. Rev. **140** (1965) A 1133.
- [9] N 次元系では、反応座標 s に直交している $N-1$ 座標を Q とする。分子-表面反応では、 s が分子の重心の表面垂直方向の座標となり、その他の座標 (分子重心の表面並行方向の座標、分子の内部自由度を表す座標、表面原子の座標等) 全てを Q に繰り込んである。全エネルギーを E とおくと、質量の重みを付加した座標 Q を用いて、定常状態の Schrödinger 方程式は $H\Phi(Q, s) = -\frac{\hbar^2}{2\mu} \partial_s^2 \Phi + \hat{H}(Q) = E\Phi$ となる。波動関数 $\Phi(Q, s)$ を、波動関数 $\phi_n(Q)$ を使って、 $\Phi(Q, s) = \sum \Phi_n(s) \phi_n(Q)$ と展開し、 $\Phi_n(s)$ ($n = 1, 2, 3 \dots, N$: 量子数 n をチャンネルと呼ぶ) に対する coupled-channel type Schrödinger 方程式 $\partial_s^2 \Phi_m(s) = \sum \langle m | \hat{H}(Q) - E | n \rangle \phi_n(Q)$ を導く。
- [10] W.A. Diño, H. Kasai, A. Okiji: Prog. Surf. Sci. **63** (2000) 63.
- [11] H. Kasai, W.A. Diño, R. Muhida: Prog. Surf. Sci. **72** (2003) 53.
- [12] W.A. Diño, H. Kasai, A. Okiji: Phys. Rev. Lett. **78** (1997) 286.
- [13] W.A. Diño, H. Kasai, A. Okiji: J. Phys. Soc. Jpn. **67** (1998) 1517.
- [14] W.A. Diño, H. Kasai, A. Okiji: Surf. Sci. **418** (1998) L39.
- [15] W.A. Diño, H. Kasai, A. Okiji: Surf. Sci. **427-428** (1999) 358.
- [16] W.A. Diño, H. Kasai, A. Okiji: J. Phys. Soc. Jpn. **69** (2000) 993.
- [17] W.A. Diño, H. Kasai, A. Okiji: Surf. Sci. **493** (2001) 278.
- [18] R. Muhida et al.: J. Vac. Soc. Jpn. **45** (2002) 448.
- [19] Y. Miura, H. Kasai, W.A. Diño: J. Phys.: Condens. Matter **14** (2002) L479.
- [20] D. Fariás et al.: Chem. Phys. Lett. **359** (2002) 127.
- [21] K. Nobuhara et al.: Surf. Sci. **82** (2002) 507.
- [22] Y. Miura et al.: J. Vac. Soc. Jpn. **46** (2003) 402.



Oriental effects in dissociative adsorption/ associative desorption dynamics of H₂(D₂) on Cu and Pd

W.A. Diño^a, H. Kasai^{a,*}, A. Okiji^b

^aDepartment of Applied Physics, Osaka University, 2-1 Yamadaoka, Suita, Osaka 565-0871, Japan

^bWakayama National College of Technology, Gobō, Wakayama 644-0023, Japan

Abstract

With the advent of sophisticated experimental techniques to study various dynamical processes on solid surfaces, e.g., initial molecular state preparation, energy- and state-resolved detection techniques, the study of dynamical processes occurring on solid surfaces is now at the stage where there is a more direct link between what experimental studies observe and what theory predicts. It would not be an exaggeration to say that, in surfaces we have a playground for physics, and the study of dynamical processes occurring on solid surfaces, such as the ones mentioned above, is a rich field for new discoveries and observations of novel physical phenomena, filled with many possibilities. The most natural test particle of choice for these reactions is *hydrogen*, which has always played a central role in the development of modern physics. Of the several dynamical factors that influence the dynamics of hydrogen-solid surface reactions (e.g., relative coordinates of reactions partners—hydrogen molecule and solid surface, molecular internal degrees of freedom, surface degrees of freedom), one important factor is *molecular orientation*. In this review, we will consider the dissociative adsorption and associative desorption dynamics of H₂(D₂) molecules on/from Cu and Pd surfaces, which are typical examples of an activated and a non-activated system, respectively, and discuss how the orientation affects the dynamics of hydrogen on these surfaces and brings about such dynamical processes as steering and dynamical quantum filtering. © 2000 Published by Elsevier Science Ltd. All rights reserved.

* Corresponding author. Tel.: +81-6-6879-7857; fax: +81-6-6879-7859.

E-mail address: kasai@dyn.ap.eng.osaka-u.ac.jp (H. Kasai).

Nomenclature

CM	center-of-mass
DOF	degree(s) of freedom
DQF	dynamical quantum filtering
ETE	energy transfer effect
LIF	laser-induced fluorescence
PES	potential energy (hyper-) surface(s)
REMPI	resonance-enhanced multiphoton ionization
RTET(E)	rotational to translational energy transfer (effect)
SE	steering effect(s)
SP	sticking probability
SRE	surface recoil effect
TOF	time-of-flight
UHV	ultra-high vacuum

Keywords: Hydrogen; Deuterium; Copper; Palladium; Low index single crystal surfaces; Chemisorption; Dissociative adsorption/Associative desorption; Quantum effects; Potential energy surface; Density functional theory; Vibrational excitation; Rotational excitation; Coupled channel method; Steering effect(s); Energy transfer effect(s); Surface recoil effect; Dynamical quantum filter(ing)

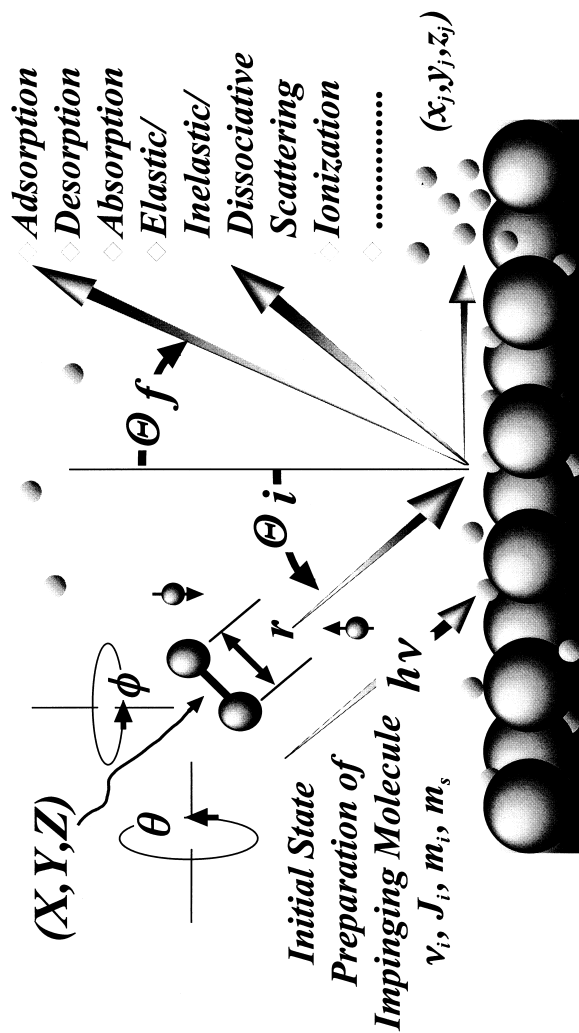
Contents

1.	Introduction	65
1.1.	Why hydrogen?	67
1.2.	Why dynamical calculations?	68
1.3.	Why this study?	69
2.	Model system	76
2.1.	Rigid surface	77
2.1.1.	One-dimensional activation barrier	77
2.1.2.	Orientationally anisotropic potential barrier and effective molecular bond-length for rigid surface	79
2.1.3.	Model Hamiltonian for rigid surface	81
2.2.	Dynamic surface	83
2.2.1.	Orientationally anisotropic potential barrier and effective molecular bond-length for dynamic surface	84
2.2.2.	Model Hamiltonian for dynamic surface	85
3.	Rotational effects in dissociative adsorption and inelastic scattering dynamics of D ₂ /Cu(111)	88
3.1.	Rigid surface	88

3.1.1.	Steering and energy transfer effects	88
3.1.2.	Incidence energy dependence	95
3.1.3.	Isotope effects	97
3.2.	Dynamic surface	98
3.2.1.	Surface recoil effect	102
3.3.	Steering, energy transfer and surface recoil effects	105
4.	Rotational effects in associative desorption dynamics of D ₂ /Cu(111)	107
4.1.	Consistency between dissociative adsorption and associative desorption results	107
4.2.	Rotational alignment and dynamical quantum filtering	110
4.3.	Isotope effects	117
5.	Rotational effects in dynamics of hydrogen on Pd-surface	120
5.1.	Rotational effects in dissociative adsorption dynamics	120
5.1.1.	Steering and energy transfer effects	123
5.1.2.	Isotope effects	125
5.2.	Rotational effects in associative desorption dynamics	126
5.2.1.	Rotational alignment and dynamical quantum filtering	126
6.	Conclusions and discussion	127
	Acknowledgements	130
	References	131

1. Introduction

There is a long-standing dream in the surface-science community to develop a material science of *heterogenous catalysis* (catalysis by powdered solids) [1]. The motivation is plain and simple. Billions of dollars in the world economy are being generated by catalytic chemistry. If it were possible to gain a detailed, atomic-level understanding of surface reactions, then it might be possible to design less expensive, more effective catalytic substrates. Thus, it can be said that, one of the most exciting challenges of present-day surface science is the task of developing a detailed picture of surface reactions. This would involve understanding the intra- and intermolecular motions of the reactants, as they undergo changes at a surface, and understanding the related issues of energy requirements, energy flow, and energy disposal for these microscopic interactions. Studies directed at describing atomic and molecular motion, and the relation between molecular motion and energy exchange throughout a surface process, such as chemisorption, physisorption or scattering, define the field of surface dynamics. The descriptions acquired from studies of surface dynamics can range from simple conceptual models, which yield insights into qualitative aspects of molecular interactions, to detailed theories, which can provide more quantitative information about the dynamical process involved. To make any headway in understanding such surface



Surface Phonon Excitation Electron-Hole Pair Excitation

Fig. 1. A schematic diagram of the several reactions that may occur when a diatomic molecule, prepared in a certain initial quantum mechanical state, interacts with a metal surface. The coordinates (X, Y, Z, θ, ϕ) give the location of the center-of-mass and the polar and azimuthal orientations of the impinging diatomic molecule with respect to some reference point. (v_i, J_i, m_i, m_s) correspond to the initial vibrational, rotational, azimuthal and spin quantum states of the impinging diatomic molecule, respectively. θ_i and θ_f correspond to the incidence and scattering angle of the diatomic molecule with respect to the surface normal, before and after a certain reaction occurs. The coordinates (x_j, y_j, z_j) give the location of the j th constituent atom of the diatomic molecule after a certain reaction, e.g. dissociative adsorption or interaction with a photon ($h\nu$) of light, occurs.

reactions, the most fundamental surface reactions must be understood. One such reaction which has been, and still is being, extensively studied is the interaction of a diatomic molecule with a surface.

When diatomic molecules, prepared in a certain initial quantal state, interact with metal surfaces, a number of processes can occur, depending on the initial conditions. Some may be adsorbed as molecules, or as dissociated atoms, which may then be absorbed into the metal. Some may undergo dissociative scattering, i.e. atomic fragmentation, with the products (fragmented/dissociated atoms) going back into the gas phase. Some may undergo elastic scattering (diffraction). Inelastic scattering via excitations of the molecular internal *degrees of freedom* (DOF) (e.g. rotation and/or vibration) or excitation of surface phonons and/or surface electron–hole pairs, may also occur. After undergoing dissociative adsorption, the adsorbed particles may also diffuse, or migrate, and later recombine with other adsorbed atoms/molecules and desorb. In Fig. 1, we show a summary of the possible processes that may occur.

In this review, we shall mainly discuss the dynamics involved in dissociative adsorption and associative desorption, which represent the initial and the final stages in any reaction. *Dissociative adsorption* is the initial process by which we can utilize the surface as a catalyst, or medium, and initiate the reaction of two reactants that may otherwise even be, normally, too stable to interact with each other. *Associative desorption* on the other hand, is a means by which we can harvest the resulting products of the reaction from the surface. In particular, we concentrate on the dissociative adsorption and associative desorption dynamics of hydrogen at copper and palladium surfaces.

1.1. Why hydrogen?

Hydrogen is probably the most important of all atoms both for its abundance in the universe and for its theoretical interest. It is the only stable neutral two-body system, and its energy levels (cm^{-1}) can be calculated with an accuracy far higher than for any other element (currently of the order 10^{-11}). In addition, atomic hydrogen possesses a rich spectrum of resonances ranging from radio to ultraviolet frequency and is thus a fertile ground for experimentalists. Several of its absorption resonances are particularly narrow and thus very suitable for metrology. For these reasons, the hydrogen atom has always played a central role in the development of modern physics, since, by performing measurements of its energy-level separations, one is able to make precise tests of current theories. (For more details regarding the role of hydrogen in modern physics and metrology, see Ref. [2].)

Furthermore, the understanding of how hydrogen interacts with metal surfaces is of broad interest. From a *practical* (technological) point of view [3–5], the interactions of hydrogen with solids are influential in a number of industrial processes (e.g. heterogeneous catalysis, material processing (*hydrogen firing*), purification of hydrogen by sorption or permeation, and fabrication of electronic devices), and in energy and power systems (e.g. fuel cells, nuclear reactors (tritium

containment)). The ability of hydrogen to alter the mechanical properties of metals to the point of rendering them unreliable is an outstanding technological problem [6,7]. Interactions with certain materials lead to severe degradations in the mechanical (embrittlement, stress corrosion cracking), electrical and magnetic properties of those materials. In the case of hydrogen-assisted cracking, in which crack initiation and propagation are controlled by a combination of stress and the presence of hydrogen, there is a relationship between the requisite stress and hydrogen-concentration: more hydrogen can reduce the failure stress. From an *environmental* point of view, with *water* as the only *emission* from hydrogen combustion, hydrogen is very attractive as an alternative *power source* of the future, with materials that readily adsorb hydrogen as potential fuel storage devices [8,9]. From an *academic* point of view, hydrogen is the simplest possible adsorbate. Thus, an understanding of how hydrogen behaves, when it approaches and subsequently comes into contact with a solid surface, should give the most fundamental view of gas–surface reaction.

1.2. Why dynamical calculations?

The main trend in the study of gas–surface reaction some 40 years ago was towards *kinetics* [10–12], i.e. the study of how external *macroscopic* variables (e.g. temperature, pressure and relative concentrations of the reactants) influence the overall reaction rate. It was the kinetic behavior of reactants near solid surfaces that was the focus for studying the chemically active species with surfaces. Although people then were wondering why some molecules stuck to some surfaces intact, some underwent fragmentation and some not at all [13–15], it was simply not possible then to compare state-resolved theoretical predictions with kinetic data obtained by experiments, because of the *vast degree of averaging* required to convert cross-sections into rate constants. However, with a number of diverse advances, both in the experimental and theoretical fields, it is now possible to gain a more *microscopic* view of gas–surface interactions, where one can focus attention on the detailed atomic/molecular motions that characterize an elementary reaction, i.e. the *dynamics* of the process. With the advent of sophisticated laser preparation and detection schemes (e.g. laser spectroscopy), combined with *ultra-high vacuum* (UHV) technology, it is now possible to perform experiments that can measure state specific information of molecules. Unfortunately, even though current experimental methods enable the exact motion of the nuclei in a reaction to be followed [16], there are still some microscopic details that remain inaccessible to direct investigations (e.g. time-dependence of the charge state of reacting species, correlated motion of a small cluster of atoms, etc.). Quantum mechanics tells us that it will always be *impossible* to follow the behavior of a molecule, as it interacts with a surface, without compromising the outcome. On the other hand, even though it is possible to write the exact Hamiltonian to describe the coupled electronic and nuclear motions as a reaction evolves, it is frequently impossible to find a solution, and the heart of the theoretical method is to make a simplified calculation, amenable to solution, that

will contain the essential physics of the problem. Dynamical calculations, using as input data from both theoretical and experimental studies, can be made to model the experimental problem and, in a way, allow investigation of areas not accessible to experimentalists and *other* theorists. The results of these dynamical calculations may then be compared with the numerous experimental data on this system (gas–surface interaction system), and provide us with a means to gauge just how close we are to having the important details of this system in our grasp.

1.3. Why this study?

The question of which forms of energy can best promote activated processes is central to the field of surface reactions. One important goal of this field is then to determine which physical factors (e.g. DOF) most affect the outcome of potentially reactive collisions. Such a detailed, atomic-level understanding of surface reactions should be of great value in optimizing reaction conditions and in controlling reaction yields. Furthermore, as mentioned earlier, it might permit the design of less expensive, more effective, novel catalytic substrates much needed in industry [1]. Many studies, both theoretical and experimental, have been done to understand the energetic requirements and energy disposal in elementary reactions. Although most of these works are concerned with gas-phase reactants [17,18], recent developments in theoretical and experimental techniques have made it possible to examine also the dynamics of gas–surface reactions [19,20], principally, the process of activated dissociative chemisorption. Over the years, the chemisorption of hydrogen on copper surfaces has become a benchmark for the study of gas–surface interaction dynamics, particularly in developing a dynamical description of activated adsorption [10,11,21–23].

Experiments (cf. Refs. [10,11] and references therein) using seeded molecular-beam scattering and state-resolved *time-of-flight* (TOF) measurements of desorption, have studied the detailed dependence of the dissociation probability on the translational, vibrational and rotational DOF and on surface temperature. From these experiments we now know that dissociation of hydrogen on the low index surfaces of Cu is hindered by a considerable energy barrier. This means that a certain amount of energy must be fed to the translational DOF of the hydrogen molecule before dissociative adsorption on a Cu surface can occur (cf. Refs. [10,11] and references therein). The dependence of the *sticking probability* (SP) on the angle of incidence of the molecular beam has also been measured. For Cu surfaces, *normal energy scaling* is found to be a good approximation [10,24], suggesting that only the component of the momentum perpendicular to the surface is effective in promoting dissociation. This is usually interpreted as implying that the surface appears to be *flat* to the dissociating molecule. Studies have also shown that the vibrational energy of incoming hydrogen molecules always promotes dissociation on the low index surfaces of Cu. For a fixed initial (vibrational, rotational and translational) state of the impinging hydrogen molecule, increasing the surface temperature slightly promotes dissociation for incidence energies a little lower than the effective energy barrier and slightly

hinders dissociation for incidence energies a little higher than the effective energy barrier, without changing the energetic location of the inflection point of the corresponding adsorption probability curves [25]. Furthermore, we also know that the dissociation of hydrogen on Cu is an orientation-dependent process, i.e. hydrogen molecules oriented parallel to the Cu surface dissociate more easily compared with perpendicularly oriented ones [26,27]. However, it is only now that we are beginning to understand how rotational energy or the molecular rotational DOF actually influences hydrogen dissociation.

Recently, TOF distributions for hydrogen molecules associatively desorbing from Cu(111) have been determined rotationally state resolved (cf. Refs. [28–33] and references therein). Earlier desorption measurements for H₂ and D₂ from Cu(110) and Cu(111) by Kubiak et al. [28,29] indicate that the mean rotational energy in desorption, associated with the detected low rotational states j of the hydrogen molecules, is slightly less than that appropriate to the surface temperature ($k_B T_s$) (*rotational cooling*). The measured rotational state distributions appear to have slightly enhanced populations at low rotational state j . Schröder et al. [30] observed a rather strong rotational cooling for the H₂ on Pd(100) system and recently, Michelsen et al. [31,32] observed distributions that show a non-monotonic dependence on the detected rotational state. Desorbing molecules with intermediate rotational states (e.g. $j = 4, 5, 6$) reach the detector faster than those that do not rotate at all ($j = 0$) or those in higher rotational states ($j \geq 10$). These experimental observations indicate a strong dependence on

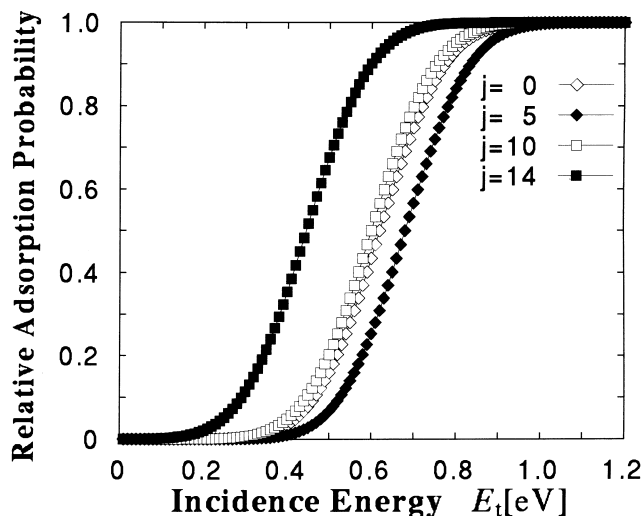


Fig. 2. Experimental rotational state j -dependent adsorption probabilities for D₂ in the vibrational ground-state. The curves were obtained by plugging-in experimental data of Michelsen et al. [10,31,32] into their proposed functional form for the sticking coefficient, and assuming a j -independent normalization factor ($A = 1$) [32]. The gas phase rotational constant of D₂ is $B \approx 3.8$ meV. From Ref. [36].

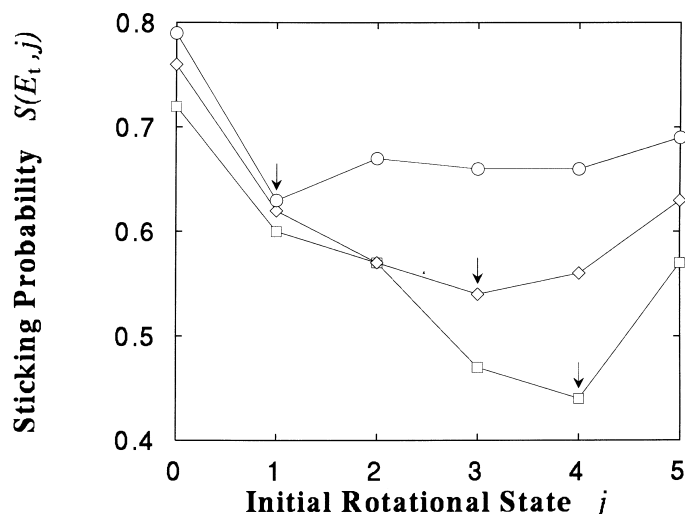


Fig. 3. Experimental results for the rotational state j -dependent sticking probability curves for H_2 on Pd(111) for fixed translational energies E_t . Arrows point to the corresponding minimum for each curve. The curves were obtained by replotting the experimental data of Gostein and Sitz (Table 2 of Ref. [39]). The statistical uncertainties for the sticking probabilities were omitted in the figure for clarity. The corresponding incidence energies E_t , and the location of the minimum for each curve j_{\min} , are as follows: \square : $E_t = 55 \pm 2$ meV, $j_{\min} = 4$; \diamond : $E_t = 73 \pm 3$ meV, $j_{\min} = 3$; \circ : $E_t = 94 \pm 5$ meV, $j_{\min} = 1$. The gas phase rotational constant of H_2 is $B \approx 7.6$ meV. From Ref. [40].

the molecular rotational DOF. Otherwise, the rotational distributions are expected to be in thermal equilibrium with the substrate temperature at which desorption occurs. By invoking the principle of *microscopic reversibility* [31–35], the dissociation behavior of hydrogen on Cu can be derived from these distributions. The non-monotonic j -dependence of the TOF peaks can be related to a non-monotonic j -dependence of the sticking (dissociation) coefficient¹. At low initial rotational states j , rotation inhibits sticking, while at high j , rotation promotes sticking (cf. Fig. 2).

With recent advances in molecular beam scattering techniques, it is now even possible to determine the initial rotational state of hydrogen molecules prior to being adsorbed on metal surfaces [37–39]. Gostein and Sitz [39] have directly observed, for the first time, that the sticking (dissociation) coefficient¹ of H_2 on Pd(111) is non-monotonically dependent on the initial rotational state of the impinging hydrogen molecule (Fig. 3), first decreasing with increasing initial rotational state ($j = 0 \rightarrow 3$), for low j , then increasing again for higher j ($j = 4, 5$). This interesting feature of the sticking coefficient of H_2 /Pd(111) as a function of the initial rotational state j of the impinging H_2 resembles the SP results inferred

¹ We will be using the terms adsorption, dissociation and sticking interchangeably to refer to the dissociation of hydrogen molecules into hydrogen atoms that are then adsorbed on the surface.

from rotationally state resolved TOF distribution results of Michelsen et al. [31] for D_2 associatively desorbing from Cu(111).

As for the orientational preference in associative desorption, Wetzig et al. [41], using the *laser-induced fluorescence* (LIF) detection technique [42–44], reported the first such measurement of the preferential steric orientation for D_2 desorbing from Pd(100) by determining the quadrupole alignment factor $A_0^{(2)}(j)$, given by Refs. [42–45]

$$A_0^{(2)}(j) = \left\langle \frac{3j_z^2 - \mathbf{j}^2}{\mathbf{j}^2} \right\rangle_j \quad (1)$$

assumes values in the range $[-1, 3j/(j+1)-1]$. For molecules exhibiting *cartwheel-like* motion ($|m_j| \approx 0$) with respect to the surface normal $\hat{\mathbf{n}}$, $A_0^{(2)}(j) < 0$, while those exhibiting *helicopter-like motion* ($|m_j| \approx j$) have $A_0^{(2)}(j) > 0$, with perfect alignment given by $A_0^{(2)}(j) = 3j/(j+1) - 1$, and as $j \rightarrow \infty$, $A_0^{(2)}(j) \rightarrow 2$. A spatially isotropic distribution of the angular momentum \mathbf{j} is described by $A_0^{(2)}(j) = 0$ (cf. Fig. 4). Wetzig et al. [41] observed that D_2 desorbing in the vibrational ground-state from Pd(100) have positive alignment (indicating a preference for helicopter-like motions) which vanishes for $j = 7, 8$ (spatially isotropic distribution). They later observed the same qualitative features for the desorption of H_2 from Pd(100) [46]. Similarly, for D_2 desorbing in the vibrational ground-state from Cu(111), Wetzig et al. [47] measured, for all final rotational states ($j = 1 \rightarrow 8$), a small quadrupole alignment factor that is almost compatible with a spatially isotropic distribution ($A_0^{(2)}(j) \approx 0$). Gulding et al. [48], using the

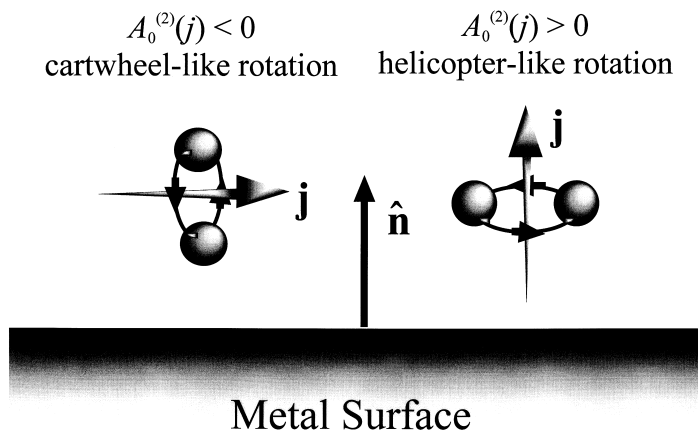


Fig. 4. Schematic diagram of how the molecular angular momentum \mathbf{j} is spatially oriented with respect to the surface normal unit vector $\hat{\mathbf{n}}$ for different $A_0^{(2)}(j)$ values. $A_0^{(2)}(j) < 0$ corresponds to a cartwheel-like rotational preference, with \mathbf{j} oriented predominantly perpendicular to $\hat{\mathbf{n}}$. $A_0^{(2)}(j) > 0$ corresponds to a helicopter-like rotational preference, with \mathbf{j} oriented predominantly parallel to $\hat{\mathbf{n}}$. $A_0^{(2)}(j) = 0$ corresponds to a spatially isotropic distribution of \mathbf{j} .

resonance-enhanced multiphoton ionization (REMPI) detection technique [49,50], also measured a quadrupole alignment factor corresponding to a small preference for helicopter-like motion, which, in turn, increased with increasing j .

Electronic (ab-initio) energy calculations [36,51–63] show that the H₂/Cu *potential energy (hyper-) surfaces* (PES) possess a barrier to adsorption of about 1 eV with a substantial increase in the equilibrium H–H internuclear distance near the crest of the barrier, or the so-called *transition-state* region of the potential. The existence of the activation barrier is due to the interaction between H₂ and the metal surface, and the interaction between the two constituent H atoms of H₂. The existence of the barrier for adsorption of hydrogen on simple metals has been illustrated via model calculations on a jellium surface [51]. As a H₂ approaches a metal surface, its molecular orbitals ($1\sigma_g$ and $1\sigma_u^*$) begin to overlap with the wavefunction of the metal s electrons. The H₂ molecular orbitals couple with the metal, producing H₂-metal bonding and anti-bonding states. While a bonding effect between the metal and H₂ can be initiated by a lowering of the $1\sigma_g$ orbital, an increase in the metal electron kinetic energy, brought about by an orthogonalization of the metal electron wavefunctions with the H₂ orbitals (via the Pauli exclusion principle) dominates as the H₂ molecule first approaches the metal surface, resulting in an activation barrier. As the H₂ comes closer to the metal surface, the $1\sigma_u^*$ antibonding molecular orbital broadens and its energy level lowered, becoming partially occupied at intermediate H₂-metal surface distances. This partial occupation means that the H–H bond weakens and the internuclear distance increases. Meanwhile, the H₂-metal bonding continues to increase. Finally, the H₂ internuclear bond breaks and the individual H atoms are free to bond with the metal surface. Once past the activation barrier that might exist, a H atom must bond to the surface. Hydrogen interacts with a metal surface in much the same way that H₂ does. However, because H has a half-filled orbital, it can accommodate an extra electron from the metal. The energy gain from the coupling of the H $1s$ -metal sp electrons results in a hydrogen bonding level typically 6–10 eV below the Fermi level, and explains all the measured chemisorption energy for H on the simple metals [64].

Results of dissociation dynamics calculations [34,35,66–69], consistent with the idea of molecular bond-length stretching in the transition state, suggest that the vibrational energy can help an incident molecule overcome the barrier to dissociation. On the other hand, quasi-classical and quantal calculations [34,70–76], most of them multidimensional, done to explain the role of rotational excitation on surface reactions, have varying conclusions. Some calculations show a SP that is: increasing with the initial rotational state j [70–72], independent of j [73], decreasing with j [34,71,74] and, recently, non-monotonically dependent on the initial rotational state j [75,76]. Ab-initio calculations of the PES for H₂ dissociating on Cu surfaces [58–63] also show a strong dependence on the molecular orientation (cf. ab-initio PES calculation results of Ref. [58] shown in Fig. 5) and significant corrugations within the unit cell [36,58–63]. This strong corrugation, most believe (e.g. Refs. [41,47,48,75,77–80]), is necessary in

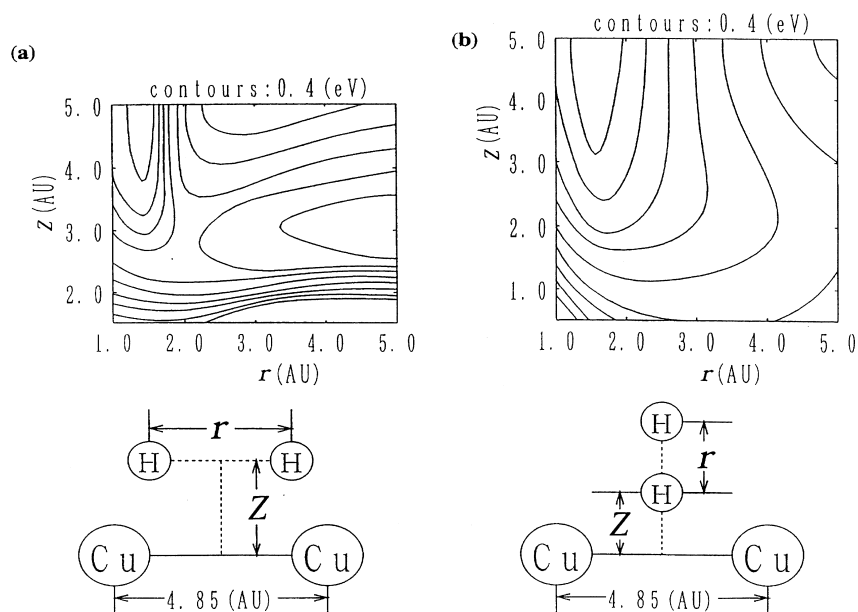


Fig. 5. Results of ab-initio potential energy calculations (GAUSSIAN88) [58] for H_2/Cu showing (a) parallel, and (b) perpendicular orientations of the H_2 relative to the Cu surface. Contour spacing is 0.4 eV and barrier height in (a) is approximately 1.6 eV. 1 AU (atomic unit) $\approx 0.5 \text{ \AA}$. From Ref. [36].

multidimensional calculations to understand and describe the trends found experimentally for the variation of the SP of H_2 on copper surfaces.

Of the several factors that influence the dynamics of hydrogen–solid surface reactions (e.g. relative coordinates of the reaction partners — hydrogen molecule and solid surface, molecular internal DOF, surface DOF — surface phonons and electron–hole pairs, influence of surface defects and steps), one of the more important is *molecular orientation*. Molecules, in general, are adsorbed on surfaces with preferential orientations, and we expect that such orientation preferences would ultimately determine how the molecule responds to the orientation dependence of the interaction PES describing the reaction. This review is based, in part, on earlier and ongoing studies [36,40,81–89] on orientational effects on the activated [36,81–86] and the non-activated [40] dissociation of hydrogen molecules on metal surfaces, and the reverse process of association and then desorption from metal surfaces [82–89]. In Section 2, we give a full description of the model adopted to study the dynamics of hydrogen on copper and palladium surfaces. We did quantal model calculations using the coupled-channel method [34,66] and the concept of a local reflection matrix [90]. Our model potential is based on qualitative features of available PES plots for the H_2/Cu surface [36,58–63] (e.g. ab-initio PES calculation results of Ref. [58] shown in Fig. 5) and H_2/Pd -surface [91,92] systems. We took advantage of the convenience gained in using the concept of a *reaction path* [66]. Section 3 provides a discussion of our results

concerning the rotational effects on the dissociative adsorption dynamics and inelastic scattering dynamics of hydrogen on a copper surface. A discussion of the corresponding rotational effects on the dynamics of the reverse process of associative desorption, is given in Section 4, where H(D) atoms initially adsorbed on the surface come together and desorb as H₂(D₂) from the surface. Our theoretical studies on the influence of molecular orientation on the dynamics of H₂(D₂) reactions with metal surfaces, viz. Cu(111) and Pd(111), which are examples of an activated and a non-activated system, respectively, show very interesting, surprising and general results. We show that, due to the *inherent orientational dependence* of hydrogen–solid surface reactions and the coupling between the different DOF involved, two factors, viz. *steering* or the *dynamical reorientation* factor and *rotational–translational energy transfer* (RTET) or the *rotational assistance via bond-length extension* factor, come into effect [36]. Furthermore, we will show that the *steering effect* (SE), which is due to the anisotropic nature of the PES, dominates over the *energy transfer effect* (ETE) for low initial rotational states j . For high j , the ETE, which arises from the strong coupling between the rotational motion and the motion along the reaction path, dominates. As a result of the competition between these two processes/factors, the dissociation probability of H₂(D₂) on Cu(111), a paradigm of an *activated system*, for example, shows a non-monotonic dependence on the initial rotational state of the impinging H₂(D₂), as observed experimentally. We also show that the efficacies of these two factors are strongly dependent on the incidence translational energy of the impinging hydrogen molecule [84]. This prediction was later observed for the H₂/Pd(111) system [39], an example of a *non-activated system*, which we discuss in detail in Section 5. We show that we were able to consistently relate the calculated adsorption results with that of the desorption results [84] and, for the first time, reproduce the experimentally observed initial cooling, then a mild heating, followed by a cooling again of the rotational temperature of the desorbing hydrogen molecules with respect to the surface temperature. Upon considering the reverse process of associative desorption, we show that due to the *inherent orientational dependence* of the hydrogen–solid surface reaction, another factor takes effect, viz. *dynamical quantum filtering* (DQF) [87–89]; and, by taking advantage of the inherent nature of the desorption process to be orientation dependent, we suggested that it might actually be possible to produce oriented H₂(D₂), which was up to now impossible. The process involves permeating H(D) atoms through the bulk of, e.g., a copper single crystal and using the Cu(111) surface as a DQF. Due to DQF, fast desorbing molecules exhibit helicopter-like rotational preference and slow desorbing molecules exhibit cartwheel-like rotational preference. By applying energy-resolved detection techniques [87–89], we can then select from among the desorbing molecules helicopter- or cartwheel-like rotating molecules. We also explain the experimentally observed surprisingly low rotational alignment [41,46–48]. Finally, the experimental observations for the dissociative adsorption and associative desorption dynamics of H₂ on Pd(111) are also explained by considering the three factors mentioned above, indicating that *steering*, *energy transfer via bond-length extension* and DQF are general, dynamical

features of orientation dependent reactions [40]. Overall conclusions and discussions appear in Section 6.

2. Model system

As mentioned in the previous section, one of the most exciting challenges of present-day surface science is, undoubtedly, the task of developing a detailed microscopic picture of dynamical processes occurring on solid surfaces. To this purpose, many systems have drawn considerable interest and studies, one of these being the hydrogen on metal system, which has become one of the benchmark systems, particularly on the nature of the dissociative adsorption process, and the reverse process of association and then desorption (cf. Ref. [23] and references therein). The dynamics of such interactions between a molecule and a surface is dependent on the relative coordinates of the reaction partners (molecule and surface) and the internal DOF of the molecule. To this list of variables we must add the surface DOF (e.g. surface phonons and electron–hole pairs) and recognize the possible influence of surface defects and steps. It is no doubt a formidable task to obtain a full theoretical description which includes all DOF. A way around this would be for us to choose model systems for which the influence of certain DOF is minimized. Alternatively, we could choose to systematically investigate only those DOF on which we can exert considerable control. However, since the positions and velocities of the nuclei and the electronic state of the system change throughout the interaction of a molecule with a surface, it is not possible to follow the ongoing events continuously. At best, we can only hope to infer the detailed dynamics from a series of information regarding the system, before, during and after the interaction.

Many of the dynamical processes (e.g. dissociative adsorption and associative desorption) occurring in nature are believed to be essentially electronically adiabatic [93] and governed by a single Born–Oppenheimer PES. Because of the smaller mass of the electrons, they may be considered capable of immediately reacting to the motion of the nuclei, relaxing virtually instantaneously, such that the force on the nuclei is that characteristic of the ground-state of the electron system. It is this electronic ground-state which will then contribute to the interaction potential of the interacting nuclei, serving as the potential energy function for the nuclear motion.

In studying the interaction of a gas-phase molecule with a solid surface, it is, thus, standard theoretical practice to adopt the Born–Oppenheimer approximation and formulate the problem in terms of the motion of some representative point or points over a PES. Then the problem of studying the interaction of a molecule with a surface reduces to (1) obtaining the relevant PES, and (2) solving the corresponding equations of motion. From the above reasoning it is obvious that, in order to make progress in understanding the dissociative adsorption and associative desorption of hydrogen molecules on or from metal surfaces, we require a good PES for the molecule–surface interaction.

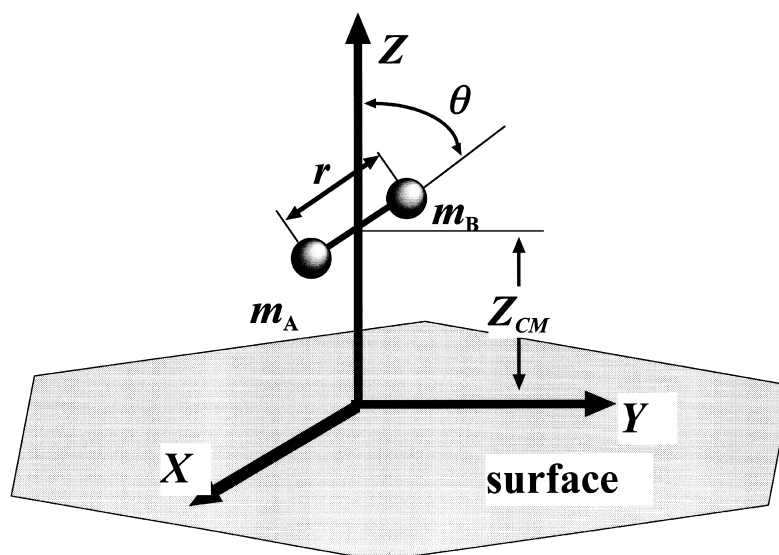


Fig. 6. The model system showing a diatomic molecule (molecular orientation with respect to the surface normal given by θ , surface to center-of-mass (CM) distance Z_{CM} , and bond-length r) approaching a flat surface perpendicularly. m_A and m_B correspond to the masses of the constituent atoms of the diatomic molecule. Note that there is no azimuthal dependence because normal energy scaling (a flat surface) was assumed. From Ref. [36].

Following the practice mentioned above, we did dynamical calculations, using the model system shown in Figs. 6 and 11 (inset) for a *rigid surface* and *dynamic surface*, respectively.

2.1. Rigid surface

For a rigid surface, we considered the model system shown in Fig. 6, and studied the effect of rotation on the dissociative adsorption (associative desorption) process. Because normal energy scaling is observed for Cu(111) [32,94], we only considered the reaction of a hydrogen molecule — with a *center-of-mass* (CM) distance Z above the equilibrium position of the surface oscillator, an internuclear distance or bond-length r and a molecular axis orientation θ with respect to the surface normal — incident perpendicular to a flat metal surface.

2.1.1. One-dimensional activation barrier

From earlier experiments [10,11,20,24,28,29,31–33], using seeded molecular-beam scattering and state-resolved TOF measurements of desorption, done to study the detailed dependence of the dissociation probability on the translational, vibrational, and rotational DOF, and on the surface temperature, we now know that the dissociation of hydrogen on the low-index surfaces of Cu is hindered by a considerable energy barrier. This suggests that we can think of the dissociation of

hydrogen on the low-index surfaces of Cu as a 1D scattering problem, with a potential barrier of the form

$$V(s) = \frac{E_a}{\cosh^2(\alpha s)}, \quad (2)$$

where E_a is the activation barrier/potential barrier height ($E_a = 0.54$ eV, this is based on parameters used by previous dynamical calculations) [34,66], α is the width parameter and s the reaction coordinate. The analytical solution [95] of the corresponding Schrödinger equation gives the functional form for the transmission coefficient T , which corresponds to the sticking/adsorption probability in the gas–surface interaction problem. The dependence of T on the incidence energy E_t is shown in Fig. 7. The ‘S’-shaped SP vs. energy curve results from previous dynamical calculations [34,68,69,73] and experiments [10], done to study the associative desorption/dissociative adsorption process of H_2/Cu systems, are qualitatively reproduced here. Note that the plot can be divided into two regions: (1) $E_t < E_a$, where the mechanism for transmission is through tunneling and (2) $E_t > E_a$, where the mechanism for transmission is through the utilization of the available translational/kinetic energy to overcome the barrier. Another point to note is that the width of the potential barrier (manipulated through the parameter α) determines the width of the transition region, where the SP value changes from 0 to 1.

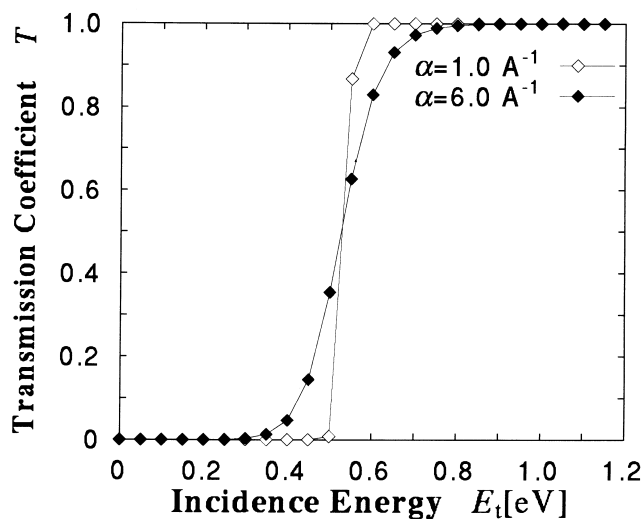


Fig. 7. Comparison of transmission coefficient T vs. incidence energy E_t curves for a wide ($\alpha = 1.0 \text{ \AA}^{-1}$) and a narrow ($\alpha = 6.0 \text{ \AA}^{-1}$) $\cosh^2(x)$ -type potential. Activation energy was taken to be $E_a = 0.54$ eV. From Ref. [36].

2.1.2. Orientationally anisotropic potential barrier and effective molecular bond-length for rigid surface

Electron-energy calculations [51–57,59–61,63], as well as experiments [26], show that the form of relevant the PES is strongly dependent on the orientation of the hydrogen molecular axis with respect to the metal surface. We again show a typical example of this dependence in Fig. 8, for the case when the molecular axis is artificially kept parallel ($\theta = \pi/2$, Fig. 8(a)), and when the molecular axis is artificially kept perpendicular ($\theta = 0$, Fig. 8(b)) to the surface. Two things are immediately evident. First, there is a ‘well’ after the potential barrier for the $\theta = \pi/2$ orientation, whereas, no such ‘well’ exists for the $\theta = 0$ orientation, which means that, a molecule with a $\theta = 0$ orientation is most likely not to be adsorbed. Second, there is a distinct difference in the curvature of the reaction path (indicated by the dashed line in Fig. 8(a)) for the two orientations. Assuming that the curvature of the reaction path changes as the molecular orientation changes from $\theta = 0$ to $\theta = \pi/2$, an appropriate molecular orientation dependent potential barrier is (Fig. 9) [36]

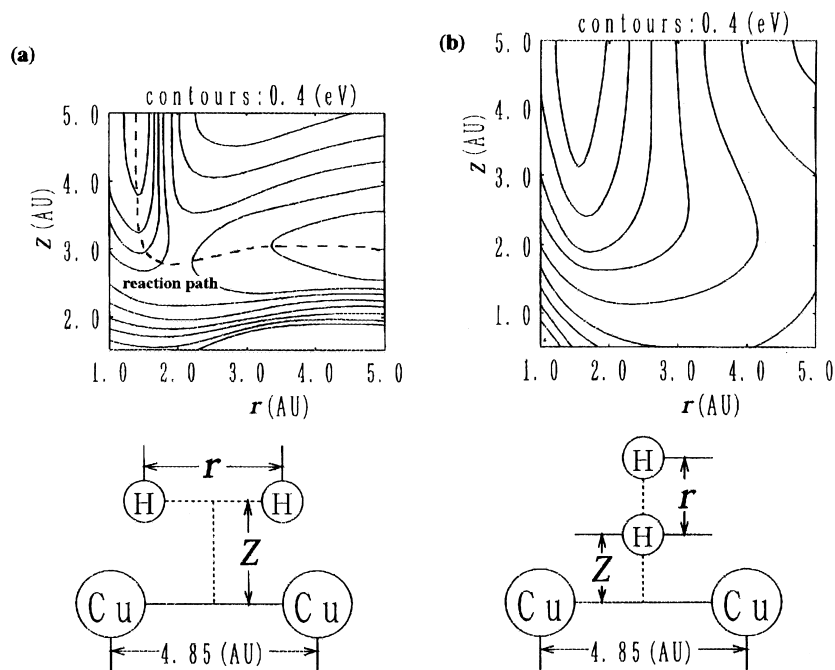


Fig. 8. Results of ab-initio potential energy calculation (GAUSSIAN88) [58] for H₂/Cu showing (a) parallel, and (b) perpendicular orientations of the H₂ molecule relative to the Cu surface. Contour spacing is 0.4 eV and barrier height in (a) is approximately 1.6 eV. The dashed line connecting the potential minimum in (a) represents the *reaction path*. 1 AU (atomic unit) \approx 0.5 Å. From Ref. [36].

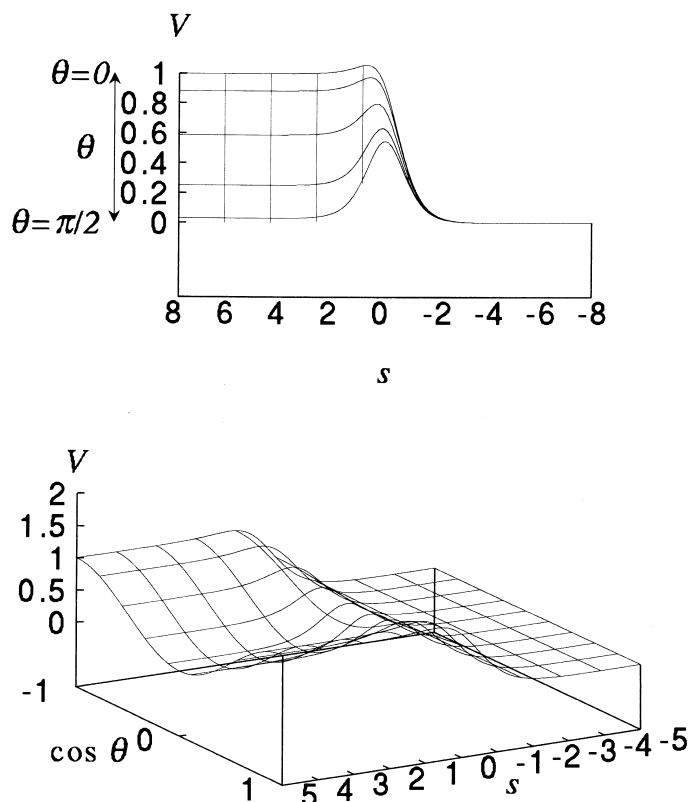


Fig. 9. A molecular orientation dependent activation barrier $V(s, \theta)$ ($E_a = 0.54$ eV, $V_1 = 1.0$ eV, $\beta = 0.25$ and in this figure $\alpha = 1.0 \text{ \AA}^{-1}$). The $+s$ -region corresponds to the surface side. The upper figure shows how the activation barrier changes with the molecular orientation. From Ref. [36].

$$V(s, \theta) = \frac{E_a}{\cosh^2(\alpha s)}(1 - \beta \cos^2 \theta) + V_1 \cos^2 \theta \frac{[1 + \tanh(\alpha s)]}{2}, \quad (3)$$

where β is an additional parameter that determines the degree of anisotropy of the activation barrier.

A typical potential is shown in Fig. 9, where a molecule incident with an orientation parallel to the surface $\theta = \pi/2$ encounters a $\cosh^2(s)$ -type potential. On the other hand, a molecule with an orientation perpendicular to the surface $\theta = 0$ will encounter a rather smooth step potential with a finite, non-zero peak after the transition region. Thus, a molecule with a parallel orientation relative to the surface will most likely be adsorbed onto the surface as compared with a molecule with a perpendicular orientation relative to the surface.

Returning to Fig. 8, it is obvious from the PES plots that each point along the reaction path (corresponding to a particular value of s or Z) corresponds to a particular molecular bond-length r . Thus, we have $r(s)$ or $r(Z)$. At distances Z

sufficiently far from the surface (corresponding to a range of values of s from $s = -\infty$), r takes the value r_0 , the gas-phase equilibrium internuclear distance. Upon reaching some distance Z sufficiently close to the surface, i.e. near the onset of the curved region, r begins to increase rapidly (almost exponentially) with s . In this region, we assumed the bond-length has the following s -dependence

$$r(s) = r_0 \sqrt{1 + \exp(\alpha s)}. \quad (4)$$

2.1.3. Model Hamiltonian for rigid surface

The Hamiltonian for the model system corresponding to a rigid surface described above (Fig. 6) has the form

$$H(Z, r, \theta) = -\frac{\hbar^2}{2\mu} \partial_r^2 - \frac{\hbar^2}{2M} \partial_Z^2 + \frac{\hbar^2}{2\mu r^2} L^2 + V(Z, r, \theta), \quad (5)$$

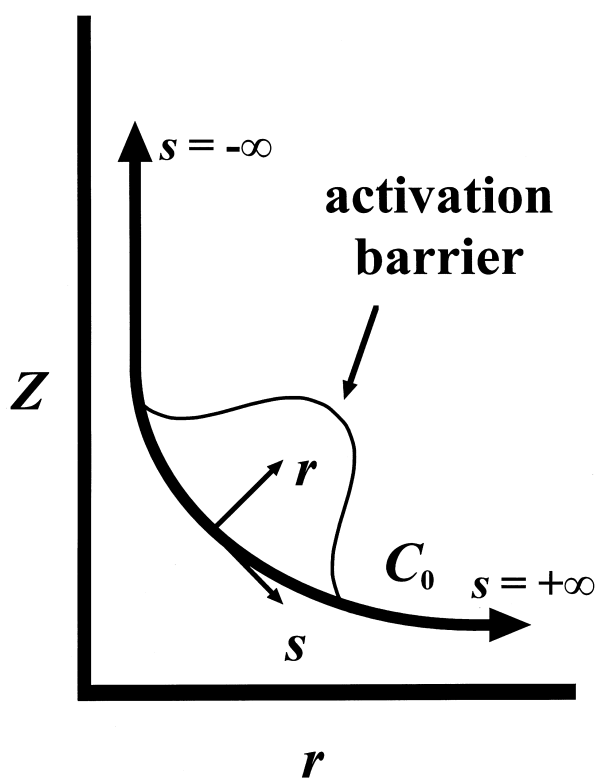


Fig. 10. A typical reaction path curve C_0 , which corresponds to the dashed line in Fig. 8(a). With this curve C_0 , we can derive for the relation between the coordinates (Z, r) and (s, ρ) . Far from the surface, the reaction path coordinate s , along C_0 , corresponds to the center-of-mass coordinate Z . Near the surface, s corresponds to the intramolecular distance r . The ρ -coordinate is always perpendicular to s , as r is perpendicular to Z .

where

$$M = m_D + m_D = 2m_D, \quad (6)$$

$$\mu = \frac{m_D m_D}{m_D + m_D} = \frac{1}{2} m_D, \quad (7)$$

$$L^2 = - \left[\frac{1}{\sin \theta} \partial_\theta (\sin \theta \partial_\theta) + \frac{1}{\sin^2 \theta} \partial_\phi^2 \right], \quad (8)$$

and $V(Z, r, \theta)$ is the relevant PES, which, in this case, is the ground-state energy of the electron system. For convenience, advantage was taken of by using a new coordinate system in terms of (s, ρ, θ) (Fig. 10), derivable from the concept of a reaction path or path of least potential [58,65,66,93,96–100], which is based on contour plots of available PES (e.g. Fig. 8). The variable s stands for the reaction path coordinate along the least potential on the PES. Far from the surface, it corresponds to the Z coordinate. The reference point is the position where the peak of the activation barrier is, and far from the surface s takes on negative values. The variable ρ is the reaction vibration coordinate orthogonal to s at every point on s . The polar angle θ gives the molecular-axis orientation with respect to the surface normal. This coordinate is normal to the plane defined by s and ρ . (For more discussion regarding the change in coordinate system see Refs. [65,66,93,97–100].) Due to the difference in time scales of molecular vibration and rotation, it is possible to decouple molecular vibration from rotation, as a first approximation [96]. The model Hamiltonian, after transformation using a mass-weighted reaction path coordinate s , will have the form

$$H(s, \rho, \theta) = -\frac{\hbar^2}{2\mu} \partial_\rho^2 - \frac{\hbar^2}{2\mu} \left(\frac{r_0}{\rho - r_0} \right)^2 \partial_s^2 + \frac{\hbar^2}{2I(s)} L^2 + V(s, \rho, \theta), \quad (9)$$

where r_0 is the radius of curvature of the reaction path at the curved region (see Ref. [66] for a detailed derivation). If we restrict the system to its vibrational ground-state and convert back to non-mass-weighted coordinates, the model Hamiltonian takes the final form

$$H(s, \theta) = -\frac{\hbar^2}{2M} \partial_s^2 + \frac{\hbar^2}{2I(s)} L^2 + V(s, \theta), \quad (10)$$

where

$$I(s) = \mu r^2(s), \quad (11)$$

and $V(s, \theta)$ is the potential barrier that the representative point of the system encounters on its way along the reaction path. The form of the s -dependence of the internuclear distance r is discussed in Section 2.2. Numerical calculations were

done with the coupled-channel method [34,66] and using the concept of a local reflection matrix [90].

2.2. Dynamic surface

For a dynamic (non-rigid) surface, we considered the model system shown in Fig. 11 (inset) and studied the effect of rotation on the dissociative adsorption process, as well as how the adsorption probability curve will change when a dynamic surface is considered. As mentioned earlier (Section 2.1), because normal energy scaling is observed for Cu(111) [32,94], we only considered the reaction of

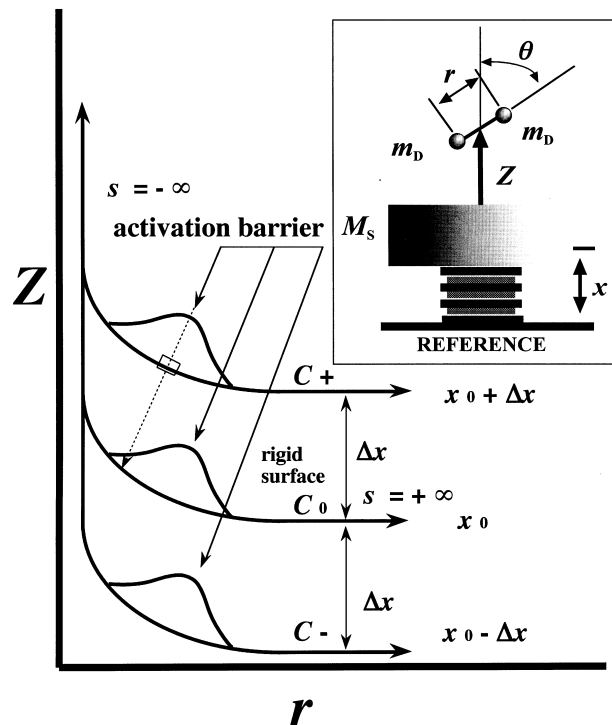


Fig. 11. A typical reaction path curve C_0 , which corresponds to the dashed line in Fig. 8(a) and the curve shown in Fig. 10, relative to the coordinates (Z, r) . Far from the surface, the reaction path coordinate along C_0 corresponds to the center-of-mass coordinate Z . Near the surface, s corresponds to the intramolecular distance r . Δx gives the relative shift of the whole reaction path curve C_0 upwards (C_+), or downwards (C_-), as the surface atom vibrates about its equilibrium position, x_0 . (Inset) The model system showing a diatomic molecule (molecular orientation with respect to the surface normal given by θ , center-of-mass (CM) to surface oscillator distance Z , and bond-length r) approaching a flat surface perpendicularly. m_D corresponds to the mass of the constituent atoms of the impinging diatomic molecule (hydrogen). Note that there is no azimuthal dependence because normal energy scaling (a flat surface) was assumed. x gives the position of the surface oscillator of mass M_S relative to some fixed reference. From Ref. [81].

a hydrogen molecule — with a CM distance Z above the equilibrium position of the surface oscillator, an internuclear distance or bondlength r and a molecular axis orientation θ with respect to the surface normal — incident perpendicular to a flat metal surface. The motion of the surface lattice is represented by an array/set of locally uncoupled *Einstein oscillators*, each having a mass M_S (≈ 63 Da, mass of one Cu atom), and an oscillator frequency ω_S given by the surface Debye temperature of copper ($\theta_D \approx 315$ K, roughly equivalent to the top of the surface phonon band). The Einstein approximation has been used extensively in surface scattering [66,101–103], and is valid provided the collision energies and energy transfers involved are large compared with the phonon band width. Furthermore, due to the relatively small size of our impinging molecule (hydrogen) compared with each individual surface atom, most scattering processes occur between an impinging molecule and a single surface atom, further justifying our choice of adopting the Einstein approximation.

2.2.1. Orientationally anisotropic potential barrier and effective molecular bond-length for dynamic surface

We treat the coupling between the rotational DOF of the impinging molecule and the vibrational DOF of the surface lattice (modeled as independent Einstein oscillators) by attaching the orientationally anisotropic PES of [36] rigidly, via the CM coordinate Z , to the Einstein oscillators (taken as harmonic oscillators) [101–108]. Then the PES has the form

$$V(Z, r, \theta, x) = V(Z - x, r, \theta) + \frac{1}{2}M_S\omega_S^2x^2, \quad (12)$$

where $V(Z, r, \theta)$ is the relevant PES seen by the representative point of the system for a particular orientation θ of the impinging molecule relative to the normal to the rigid surface. r is the internuclear distance or bond-length of the impinging molecule. x gives the position of the surface oscillator relative to some fixed reference (cf. inset, Fig. 11). (The difference between the results obtained using a rigid surface and a dynamic surface is then due solely to the dynamics and not to changes in the barrier height or shape when the oscillator is excited.)

Again, we adopt the new coordinate system (s, ρ, θ) (Section 2.1.3). The variable s stands for the reaction-path coordinate along the path of least potential on the PES. Far from the surface, it corresponds to the Z -coordinate. The reference point is the position where the peak of the activation barrier is and, far from the surface, s takes on negative values. In Fig. 11, we show a typical reaction-path curve for a given orientation of the impinging molecule, say, parallel to the surface (curve C_0 , rigid surface). The variable ρ is the reaction vibration coordinate orthogonal to s at every point along curve C_0 . The polar angle, θ , still gives the molecular axis orientation with respect to the surface normal. This coordinate is normal to the plane defined by s and ρ .

If we restrict the surface oscillator (surface atom) to move up and down normal to its equilibrium position (as described above), then the corresponding reaction paths of the resulting PES will move up and down (curves C_+ and C_- ,

respectively, in Fig. 11) normal to the equilibrium position of the reaction path of the PES for a rigid surface (curve C_0 in Fig. 11). (Because we assumed a flat surface, vibrations along the surface plane do not influence the reaction.) We can immediately see that the projections of the positions of the activation barrier peaks of curves C_+ and C_- along curve C_0 do not land on the same point along C_0 . If the variation (Δx) in the position of the surface atoms relative to its equilibrium position (x_0) is small enough, the coupling (12) results in a virtual motion of the activation barrier along the reaction path described by C_0 without a change in barrier height. We can then make the approximate transformation

$$(Z - x, r, \theta) \implies (s - x, \rho - x, \theta). \quad (13)$$

In carrying out the coupling described in (12), we considered the orientationally anisotropic model PES for a rigid surface, expressed in terms of s and θ , given in Ref. [36]. Using the approximate transformation (13), we have the final potential given by

$$V(s - x, \theta) = \frac{E_a}{\cosh^2[\alpha(s - x)]} (1 - \beta \cos^2 \theta) + V_1 \cos^2 \theta \frac{\{1 + \tanh[\alpha(s - x)]\}}{2}, \quad (14)$$

where α is the width parameter [36]. In addition, for a rigid surface, we know that each point along the reaction path (of the PES) corresponds to a particular value of r (the bond-length). Thus, we have $r(s)$. Following the arguments proposed in Refs. [36,76], we assumed that, upon applying the approximate transformation (13), the bond-length has the following s -dependence

$$r(s - x) = r_0 \sqrt{1 + \exp[\alpha(s - x)]}, \quad (15)$$

where r_0 is the gas phase equilibrium internuclear distance.

2.2.2. Model Hamiltonian for dynamic surface

The Hamiltonian for the model system described above has the form

$$H(Z, r, \theta, x) = -\frac{\hbar^2}{2\mu} \partial_r^2 - \frac{\hbar^2}{2M} \partial_Z^2 + \frac{\hbar^2}{2\mu r^2} L^2 + V(Z - x, r, \theta) - \frac{\hbar^2}{2M_S} \partial_x^2 + \frac{1}{2} M_S \omega_S^2 x^2, \quad (16)$$

where

$$M = m_D + m_D = 2m_D, \quad (17)$$

$$\mu = \frac{m_D m_D}{m_D + m_D} = \frac{1}{2} m_D, \quad (18)$$

$$L^2 = -\left[\frac{1}{\sin \theta} \partial_\theta (\sin \theta \partial_\theta) + \frac{1}{\sin^2 \theta} \partial_\phi^2 \right], \quad (19)$$

and $V(Z, r, \theta)$ is the relevant PES (as mentioned in Section 2.2.1), which, in this case, is the ground-state energy of the electron system. The last two terms of the model Hamiltonian (16) correspond to the Hamiltonian of the surface oscillator with mass M_S and frequency ω_S . Due to the difference in the time scales of molecular vibration and molecular rotation, as well as molecular vibration and surface vibration, it is possible to decouple molecular vibration from the other two DOF, as a first approximation. After doing the approximate transformation to the reaction-path coordinate (13), and restricting the system to its molecular-vibrational ground-state, we get the following intermediate model Hamiltonian

$$H(s, \theta, x) = -\frac{\hbar^2}{2M} \partial_s^2 + \frac{\hbar^2}{2I(s-x)} L^2 + V(s-x, \theta) - \frac{\hbar^2}{2M_S} \partial_x^2 + \frac{1}{2} M_S \omega_S^2 x^2, \quad (20)$$

where the moment of inertia is given by

$$I(s-x) = \mu r^2 (s-x), \quad (21)$$

$V(s-x, \theta)$ being the PES expressed in terms of reaction-path coordinates (14), and r the s -dependent bond-length (15). Since we restricted the system to be in its molecular-vibrational ground-state, the extra terms due to the approximate transformation (13) are reduced to mere constants, which we can accommodate into the potential term $V(s-x, \theta)$. We then define a new set of dimensionless variables (S, X), viz.

$$S = \alpha s, \quad (22)$$

$$X = \gamma^{-1} \alpha x, \quad (23)$$

where the coupling constant γ is defined as

$$\gamma^{-1} = \sqrt{\frac{M_S \omega_S}{\hbar \alpha^2}}. \quad (24)$$

The final dimensionless Hamiltonian is then given by

$$H(S, \theta, X) = -\frac{\hbar^2 \alpha^2}{2\mu} \partial_S^2 + \frac{\hbar^2}{2I(S-\gamma X)} L^2 + V(S-\gamma X, \theta) + \hbar \omega_S \left(-\frac{1}{2} \partial_X^2 + \frac{1}{2} X^2 \right), \quad (25)$$

where the relevant PES takes the final form

$$V(S - \gamma X, \theta) = \frac{E_a}{\cosh^2[\alpha(S - \gamma X)]} (1 - \beta \cos^2 \theta) + V_1 \cos^2 \theta \frac{[1 + \tanh[\alpha(S - \gamma X)]]}{2}, \quad (26)$$

and the moment of inertia is given as

$$I(S - \gamma X) = \mu r^2 (S - \gamma X) = \mu r_0^2 [1 + \exp(S - \gamma X)]. \quad (27)$$

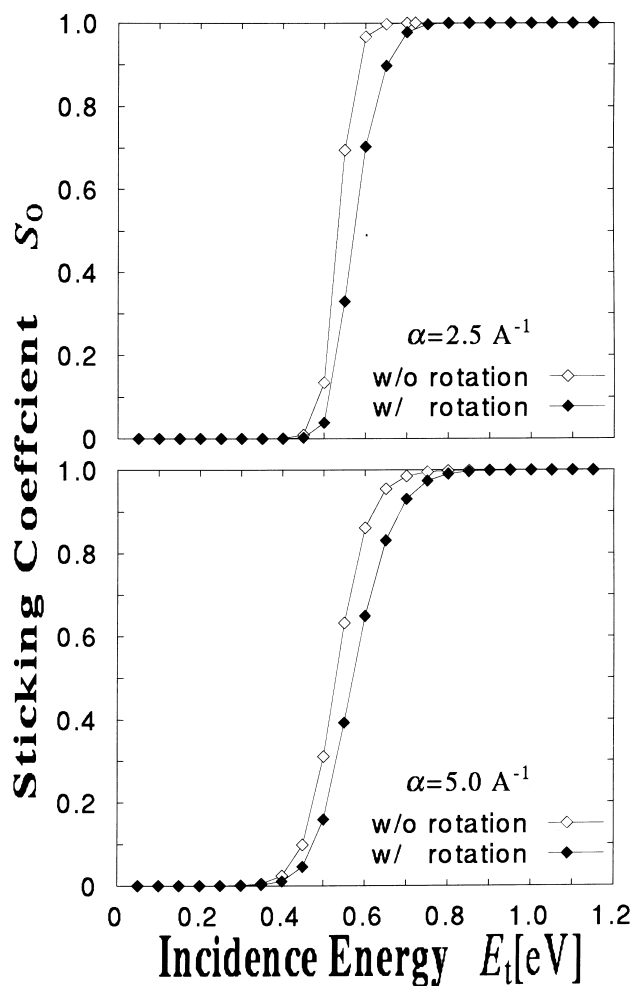


Fig. 12. Comparison of the corresponding S_0 vs. E_t curves for a homonuclear diatomic molecule encountering a $\cosh^2(x)$ -type activation/potential barrier with different widths (given by $\alpha = 2.5 \text{ \AA}^{-1}$ and $\alpha = 5.0 \text{ \AA}^{-1}$) for the case when the rotational degree of freedom is not considered (\diamond), and when it is considered (filled \diamond). Activation energy was taken to be $E_a = 0.54 \text{ eV}$. From Ref. [36].

3. Rotational effects in dissociative adsorption and inelastic scattering dynamics of $D_2/Cu(111)$

3.1. Rigid surface

3.1.1. Steering and energy transfer effects

In Fig. 12, we see that the general effect of putting part of the available energy of the incident molecule² into its rotational DOF is to decrease the corresponding SP S_0 (SP for initial rotational state $j=0$). This came about as a result of the anisotropic PES reorienting (rotating) the molecule, steering it to different regions of the PES. Thus, there is a decrease in the amount of available energy to overcome the barrier to dissociation. Such a reorientation of the molecule by the anisotropic potential is called steering effect (SE). The prominent ‘S’-shape of the S_0 vs. E_t curve, characteristic of activated systems, agrees qualitatively with the initial results of Kasai and Okiji [34] for low incidence translational energies. There was a general increase in S_0 as a function of E_t .

The particular form of the potential $V(s, \theta)$ results in a selection rule where molecules in even (odd) initial rotational states end up in even (odd) final rotational states, i.e. even (odd) rotational states are coupled only to even (odd) rotational states. In Fig. 13, we show a comparison between the reflection probabilities R_{j0} of a molecule, initially in the rotational state $j=0$, with different incidence energies and barrier widths encountered. In general, for a given width of the activation barrier (determined by fixing the value of α in (2) and (3)), molecules prepared with higher incidence translational energies exhibited higher probabilities of rotational excitations (final j states reaching higher values). This implies that, on its way towards the surface, the high sensitivity of the molecule to the anisotropy of the potential causes it to reorient (rotate) out of its initially prepared orientation, seeking the *path of least resistance (path with the least potential)*, corresponding to the best orientation for adsorption). For a given incidence energy, molecules encountering a wider barrier (smaller α) will exhibit higher probabilities of rotational excitations, which, in turn, implies that a wider potential is more effective in reorienting the molecule.

In Fig. 14(a), we show how the S_0 vs. E_t curve depends on the initial rotational state j of the impinging molecule, suppressing the SE ($\beta=0$, $V_1=0$, no potential anisotropy) in the PES (3). Only the *rotational to translational energy transfer effect* (RTETE) is present through the coupling of the rotational motion with the motion along the reaction path. There is a pronounced enhancement of the dissociative adsorption probability as the initial rotational state j increases (shown by the leftward shift of the S-shaped curve for increasing j).

In Fig. 14(b), we show the effect of turning on the SE ($\beta \neq 0$, $V_1 \neq 0$, with potential anisotropy) in the PES (3). We can clearly see that the enhancement of

²We will be using the term molecule here to refer to homonuclear diatomic molecules like H_2 and D_2 .

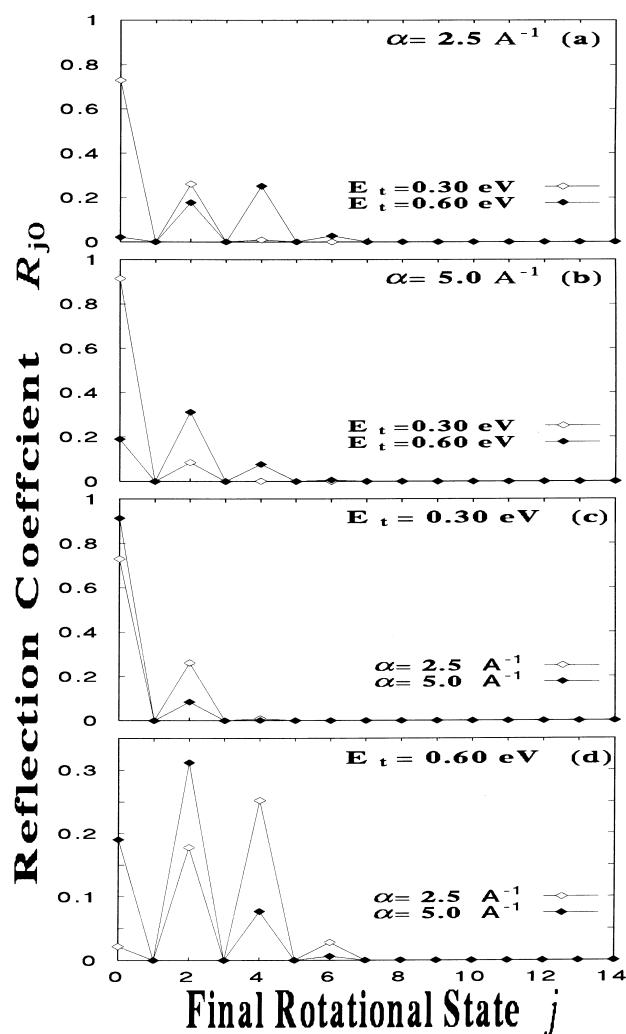


Fig. 13. Comparison of the corresponding R_{j0} vs. j curves (a)–(b) for a molecule encountering a potential barrier with a fixed barrier width, and with different incidence energies; (c) and (d) for a molecule encountering a potential barrier with different barrier widths (determined by α [\AA^{-1}]) and a fixed incidence energy E_t . Activation energy was taken to be $E_a = 0.54 \text{ eV}$. From Ref. [36].

the adsorption probability as the initial rotational state j increases seen before is considerably decreased.

To get a clearer picture of what the SE does, we show in Fig. 15(a) the m -resolved initial rotational state dependence of the dissociative adsorption probability for a constant translational energy of 0.6 eV. If we interpret m as one of the $2j + 1$ possible Z -components of the total angular momentum \mathbf{j} , then each m represents one particular orientation of the molecule. $m \approx 0$ corresponds to

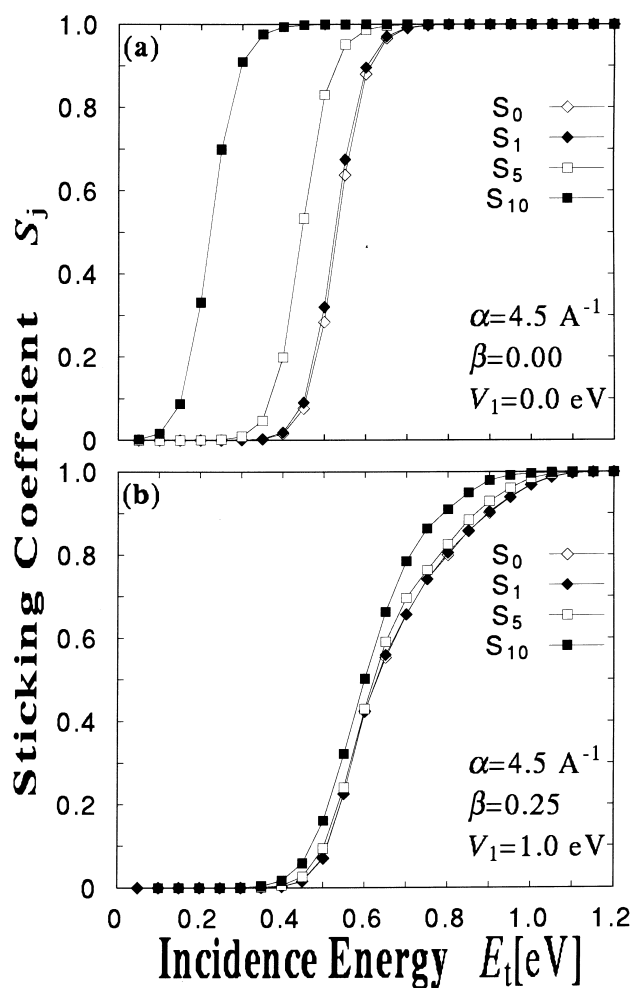


Fig. 14. Initial rotational state j -dependent adsorption probabilities for a homonuclear diatomic molecule in the vibrational ground-state encountering (a) an orientationally isotropic potential barrier ($\beta = 0.0$, $V_1 = 0.0$ eV) and (b) an orientationally anisotropic potential barrier ($\beta = 0.25$, $V_1 = 1.0$ eV). Width of the potential barrier (determined by $\alpha = 4.5 \text{ \AA}^{-1}$) is the same for the two cases. Activation energy was taken to be $E_a = 0.54$ eV. The homonuclear diatomic molecule was assumed to be D_2 , with a gas phase rotational constant $B \approx 3.8$ meV. From Ref. [36].

molecules doing cartwheel-like rotations, i.e. molecular orientation is predominantly perpendicular to the surface, and $m \approx j$ corresponds to molecules doing helicopter-like rotations, i.e. molecular orientation is predominantly parallel to the surface. Consider one particular initial rotational state, say $j = 1$, in Fig. 15(a). Note the big difference in the corresponding SP for $|m| = 0$ (perpendicular orientation) and $|m| = j = 1$ (parallel orientation). This SE would, however, be dominated by the RTETE at initial rotational states that are high enough. In this

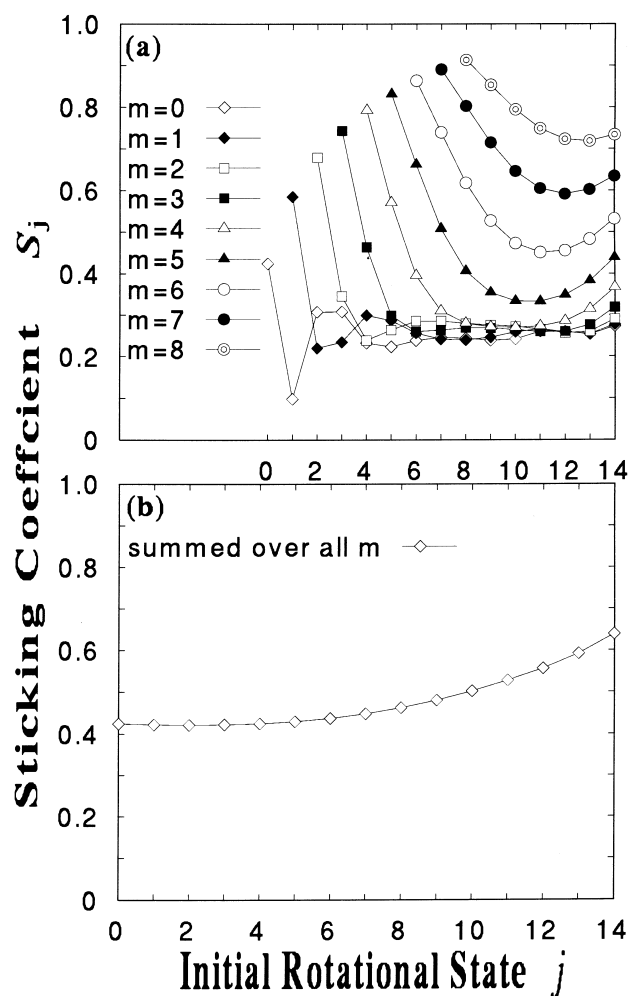


Fig. 15. Sticking coefficient S_j for a homonuclear diatomic molecule as a function of its initial rotational state j . (a) m -resolved (b) summed over all m ($\alpha = 4.5 \text{ \AA}^{-1}$, $\beta = 0.25$, $E_a = 0.54 \text{ eV}$, $V_1 = 1.0 \text{ eV}$, $E_t = 0.60 \text{ eV}$). The homonuclear diatomic molecule was assumed to be D_2 , with a gas phase rotational constant $B \approx 3.8 \text{ meV}$. From Ref. [36].

region (region of high initial rotational states), the SP for different m values (different orientations) would almost be the same. With high initial rotational states, the surface cannot distinguish one orientation from the other, and since the rotational energy is now large enough to contribute to the translational energy, the molecule can easily overcome the activation barrier, regardless of orientation.

In Fig. 15(b), we show the combined effect on the total SP. We can see that there is a very slight initial decrease in the SP (cf. value of S_j for $j=0$ and $j=1$) and then a gradual increase in the SP for $j > 1$.

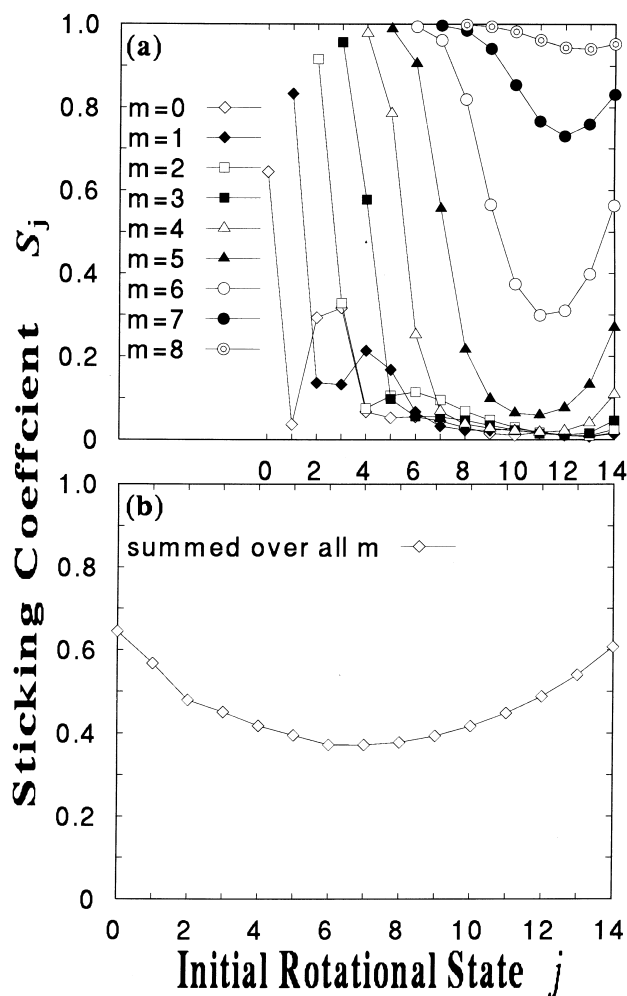


Fig. 16. Sticking coefficient S_j of a D_2 impinging a Cu(111) as a function of its initial rotational state j . (a) m -resolved (b) summed over all m ($\alpha = 1.5 \text{ \AA}^{-1}$, $\beta = 0.25$, $E_a = 0.54 \text{ eV}$, $V_1 = 1.0 \text{ eV}$, $E_t = 0.60 \text{ eV}$). The gas phase rotational constant of D_2 is $B \approx 3.8 \text{ meV}$. From Ref. [36].

Increasing the potential barrier range/width (through the parameter α) changes the SP curve (cf. Figs. 15 and 16). This change is particularly noticeable at the low initial rotational state region ($j < 8$), where a wider potential allows more time for an initially unfavorably oriented molecule to reorient to a more favorable one. Thus, the corresponding SP increases. On the other hand, there is a corresponding decrease in the SP for an initially favorably oriented molecule. The total effect is an initial decrease, and then a final increase in the SP (Fig. 16(b)).

Comparing Figs. 2 and 16(b), we see that we were able to reproduce the experimental observation of an initial decrease and then a final increase of the SP

as a function of the initial rotational state j of D_2 at a particular incidence translational energy $E_t = 0.60$ eV. In order to compare Figs. 2 and 16(b), we draw an imaginary vertical line parallel to the ordinate and intersecting the abscissa of Fig. 2 at 0.6 eV. This imaginary vertical line would then intersect the S-shaped curves corresponding to $j = 0, 5, 10, 14$ approximately at relative adsorption probability values of 0.43, 0.25, 0.50 and 0.89, respectively.

Furthermore, if we imagine that the spaces between the curves corresponding to $j = 0$ and $j = 5$ are filled by curves corresponding to $j = 1, 2, 3, 4, 5$, going from left to right. Then the imaginary line intersects all points of each curve at the SP corresponding to an incidence energy of 0.6 eV. Proper choice of the parameters for the potential width α , the anisotropy β and the barrier heights E_a and V_1 give a more quantitative reproduction of experimental observations.

Based on physical arguments, our previous study [36], and earlier studies on the subject (Refs. [10,31,75,76] and references therein) there are two competing factors working for the dissociative adsorption process, viz.

1. SE or the dynamical reorientation factor and
2. RTETE or the rotational assistance via bond-length extension factor

SE pertains to reorientation of the molecule in an attempt to follow the *path of least resistance*, i.e. to assume an orientation with the least potential, which is due to the strong molecular orientation dependence of the PES. We could also say that this pertains to the capability of the orientation-sensitive PES to reorient the molecule from an initially *unfavorable* orientation (i.e. *perpendicular* to the surface) to a *favorable* orientation (i.e. *parallel* to the surface) (Fig. 17), or vice-versa. The orientation of the molecule upon encountering the surface determines the ground-state energy of the $D_2/Cu(111)$ electron system, which, in turn, serves as the effective/relevant PES that determines the dynamics of the molecule–surface

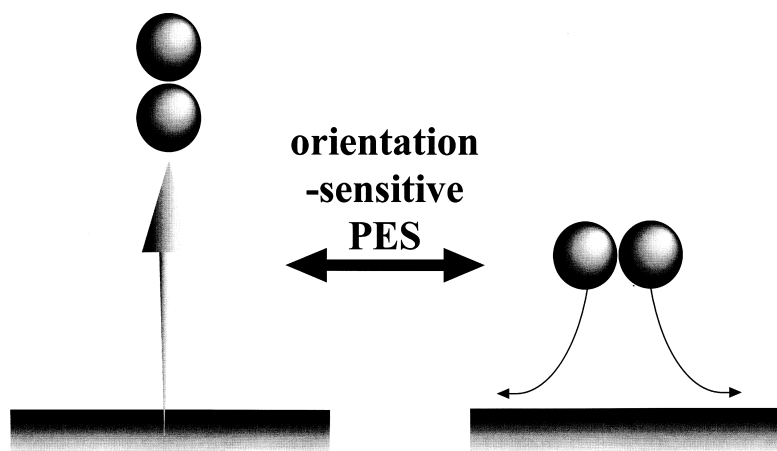


Fig. 17. A schematic diagram of the *steering or dynamical reorientation* process.

reaction. From the results of ab-initio calculations in Fig. 8, we can see that there is a big difference in the PES plot for the two molecular orientations of H_2 — parallel and perpendicular to the surface. For an orientation parallel to the surface, the molecule will encounter an activation barrier on its way towards the surface, which it could overcome by having the appropriate translational energy. On the other hand, for an orientation perpendicular to the surface, the molecule will encounter a hard-wall type potential and, thus, it might not be able to reach the surface at all. Two ways in which the SE can reduce the adsorption probability are as follows:

1. by shortening the amount of time that the molecule spends in a favorable orientation, or
2. by using up some of the translational energy needed to overcome the activation barrier to reorient a molecule approaching the surface with an initially unfavorable orientation to a favorable one.

RTETE pertains to the effective transfer of rotational energy to translational energy, which occurs due to the stretching of the molecular bond-length near the surface, and leads to a decrease in the rotational constant. This results from the coupling of the rotational motion to the translational motion along the reaction path, which is easily understood if we consider the physical problem in terms of the concept of a reaction path (*path of least resistance/hindrance or least potential*). From the two PES plots in Fig. 8, we see that, depending on the orientation of the molecule relative to the surface, there is a big difference in the form of the reaction path. Projecting the reaction path to the abscissa, each point on the reaction path corresponds to a certain H–H(D–D) internuclear distance. Since the rotational constant depends on the internuclear distance, there is coupling between rotational motion and the motion along the reaction path. In Fig. 18, we see that as the molecule approaches the surface, there is an increase in

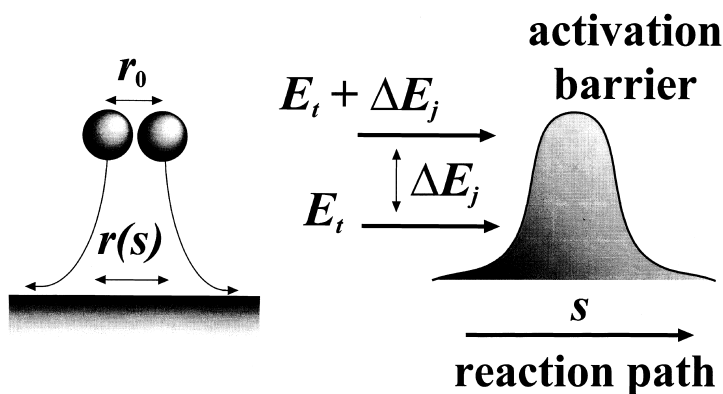


Fig. 18. A schematic diagram of the *rotational–translational energy transfer* or the *rotational assistance via bond-length extension* process.

its internuclear distance from an initial gas-phase value of r_0 to $r(s)$ (4), which leads to an increase in the moment of inertia (11), and a decrease in the rotational energy, due to a decrease in the rotational constant (10). Assuming that no rotational excitations occur, energy conservation requires that the rotational energy loss (ΔE_j in Fig. 18) be transferred to the incidence translational energy E_t (Fig. 18), which would then aid in overcoming the activation barrier.

The non-monotonic dependence of the dissociative adsorption of D_2 on Cu(111) on the initial rotational state j of the impinging D_2 , for a fixed incidence energy E_t , is due to these two factors working for and against the dissociative adsorption process. For low initial rotational states j , because of the somewhat small rotational energy, SE are dominant. As the molecule approaches the surface, it is steered to different regions of the anisotropic PES. Whether or not it will reach a point of relatively low potential on time determines whether the molecule will be adsorbed or not. In terms of the molecule, the anisotropic PES will reorient the molecule on its way towards the surface. The length of time that it stays in a favorable orientation also determines whether it will be adsorbed or not. For high initial rotational states j , the molecule has sufficient rotational energy to assist in sticking, and to the surface the molecule becomes a *blur*. (In some sense, the surface cannot distinguish in which orientation the molecule is.)

3.1.2. Incidence energy dependence

We show in Fig. 19 the calculated SP curves for the D_2 /Cu(111) system as a

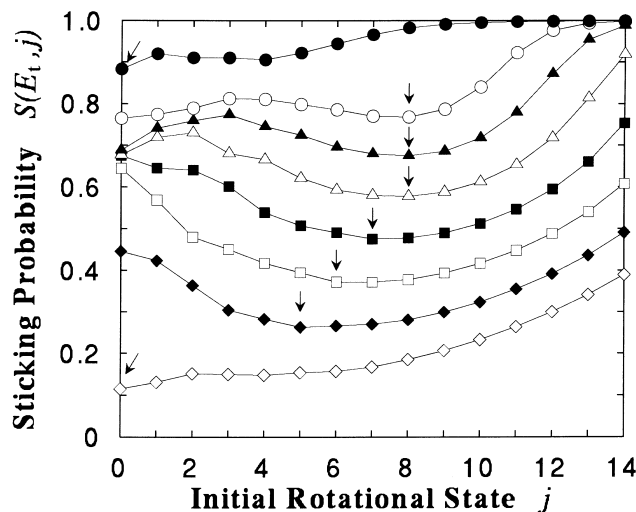


Fig. 19. Numerical results for the initial rotational state j -dependent sticking probability curves for D_2 in the vibrational ground-state and fixed incidence energies E_t . Arrows point to the corresponding minima for each curve. The gas phase rotational constant of D_2 is $B \approx 3.8$ meV. From Ref. [84]. \diamond : $E_t = 0.55$ eV, filled \diamond : $E_t = 0.575$ eV, \square $E_t = 0.60$ eV, filled \square : $E_t = 0.625$ eV, \triangle : $E_t = 0.65$ eV, filled \triangle : $E_t = 0.675$ eV, \circ : $E_t = 0.70$ eV, filled \circ : $E_t = 0.80$ eV.

function of the initial rotational state of the impinging D_2 molecule for various incidence translational energies E_t . We see in Fig. 19 that the location of the minimum for each SP curve shifts as the incidence energy is varied, i.e. when the incidence energy is comparable to or lower than the minimum energy barrier V_{\min} , *steering* will not be sufficient to aid in dissociation. Thus, RTET dominates and we see only an increase in the SP as the initial rotational state is increased for low incidence energies (cf. curves corresponding to 0.55 and 0.6 eV in Fig. 19). As the incidence energy is gradually increased, the efficacy of *steering* also increases and we see corresponding minima appearing (cf. curves corresponding to 0.575–0.625

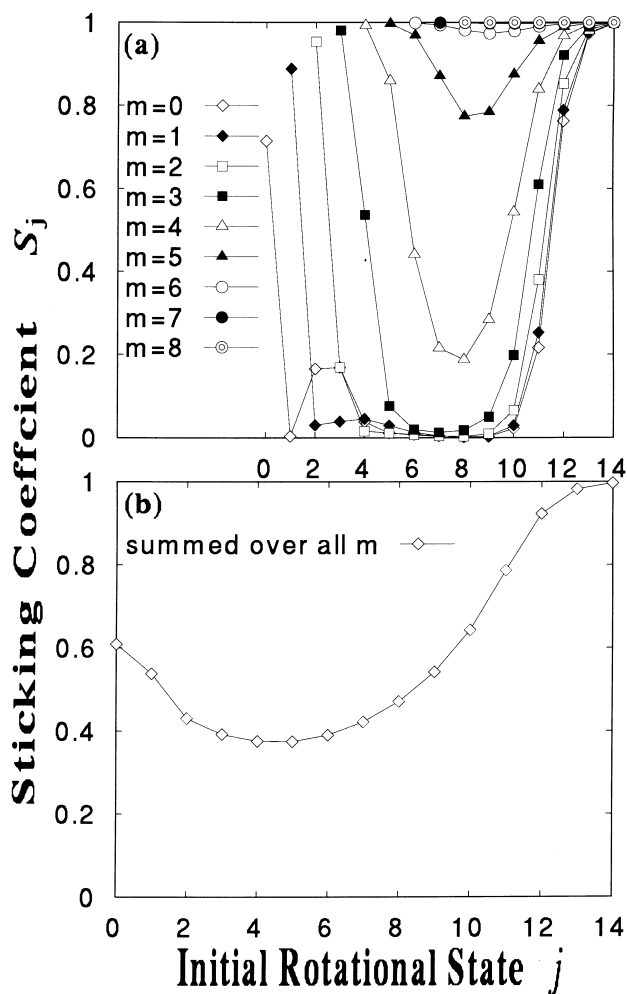


Fig. 20. Sticking coefficient S_j as a function of the initial rotational state j of a H_2 impinging a Cu(111). (a) m -resolved (b) summed over all m ($\alpha = 1.5 \text{ \AA}^{-1}$, $\beta = 0.25$, $E_a = 0.54 \text{ eV}$, $V_1 = 1.0 \text{ eV}$, $E_t = 0.60 \text{ eV}$). The gas phase rotational constant of H_2 is $B \approx 7.6 \text{ meV}$.

eV in Fig. 19), that shift towards higher initial rotational states. As the incidence energy is increased to a value that becomes comparable with the energy barrier maximum V_{\max} , the efficacy of RTET increases and we see a corresponding shift in the curve minimum towards lower initial rotational states (cf. curves corresponding to 0.80 and 0.60 eV in Fig. 19).

3.1.3. Isotope effects

In Figs. 20 and 21 we show the corresponding S_j vs. j curves for a H_2 impinging a Cu(111) with fixed incidence translational energies E_t . We immediately observe strong isotope effects, when we compare our calculated results for the dissociation of D_2 /Cu(111) (Figs. 16 and 19) with those for H_2 /Cu(111) (Figs. 20 and 21). For the same incidence energy E_t , we see that the locations of the minima for the SP curves of D_2 are shifted more towards higher rotational states ($j = 5 \rightarrow 8$) (Fig. 19), as compared with those of H_2 ($j = 4 \rightarrow 5$) (Fig. 21), with H_2 exhibiting higher SP than D_2 in the high j region. Because D_2 travels at a much lower velocity than H_2 , for the same translational energy E_t , *steering* will be more effective for D_2 than for H_2 . Thus, we see that the SP curves for D_2 , when $m = 0$, (Fig. 16(a), $m = 0$ curve) have higher values as compared with the corresponding SP curves for H_2 , when $m = 0$, (Fig. 20(a), $m = 0$ curve), which implies that, for the same translational energy E_t , the SE is more successful in reorientating an initially unfavorably oriented D_2 than a H_2 . Since H_2 travels at a much higher velocity than D_2 , it will not have as much time as D_2 to reorient to a favorable orientation

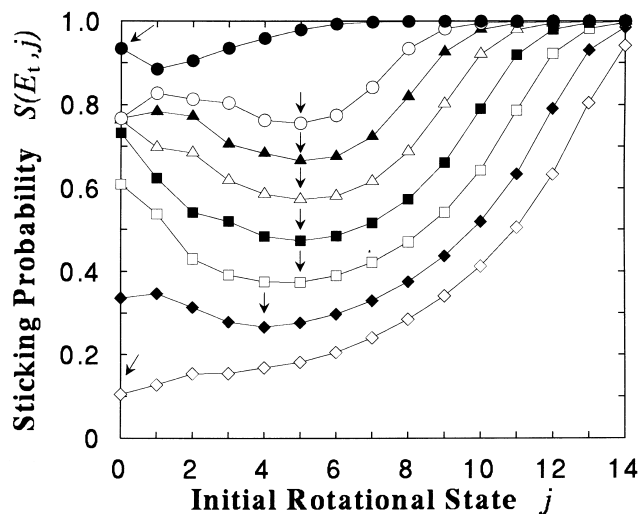


Fig. 21. Numerical results for the initial rotational state j -dependent sticking probability curves for H_2 in the vibrational ground-state and fixed incidence energies, E_t . Arrows point to the corresponding minima for each curve. The gas phase rotational constant of H_2 is $B \approx 7.6$ meV. \diamond : $E_t = 0.55$ eV, filled \diamond : $E_t = 0.575$ eV, \square $E_t = 0.60$ eV, filled \square : $E_t = 0.625$ eV, \triangle : $E_t = 0.65$ eV, filled \triangle : $E_t = 0.675$ eV, \circ : $E_t = 0.70$ eV, filled \circ : $E_t = 0.80$ eV.

and, thus, avoid the activation barrier. Furthermore, D_2 has a smaller rotational constant than H_2 and, thus, will need higher j states before the RTET can dominate and for the SP curve to increase again in the higher j region. Thus, we observe that the minima of the SP curves for D_2 (Fig. 19) are shifted more towards higher j than those for H_2 (Fig. 21).

3.2. Dynamic surface

Another interesting question is the effect of surface temperature on the dissociative adsorption process. Recent examinations [25,33,94,109] of a wide range of available experimental data for hydrogen (deuterium) on Cu systems suggest that, in order to consistently relate desorption measurements to direct adsorption experiments via the principle of detailed balance, the adsorption probabilities should show surface temperature dependence. Their results show (for fixed initial vibrational state) a SP that increases with surface temperature in the low incidence energy region, and decreases with increasing surface temperature in the high incidence energy region (Fig. 22), without a change in the energetic location of the inflection point of the corresponding adsorption/SP curve.

This surface temperature dependence of the SP is another interesting behavior which we have studied. With the aid of the model system presented in Fig. 11, we did quantal calculations using the coupled-channel method [66], the concept of a local reflection matrix [90], and considering the coupling between the rotational

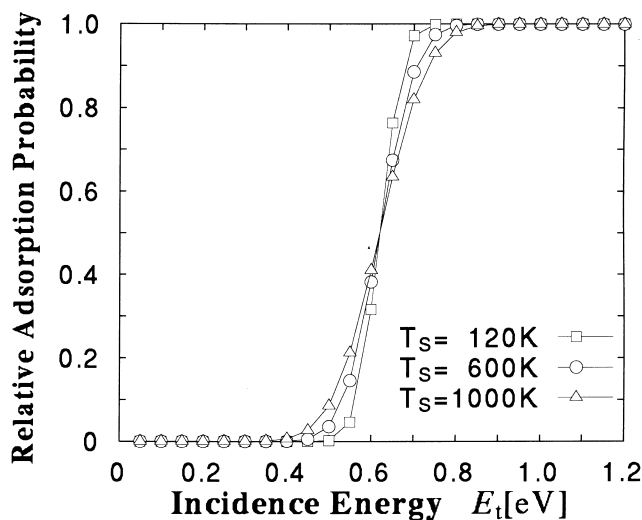


Fig. 22. Experimental surface temperature dependent adsorption probabilities for D_2 in the vibrational ground-state. The curves were obtained by plugging-in experimental data of Michelsen et al. [32,33] into their proposed functional form for the sticking coefficient, and assuming a j -independent normalization factor ($A = 1$) [32], with a surface temperature dependent transition region width [25]. From Ref. [81].

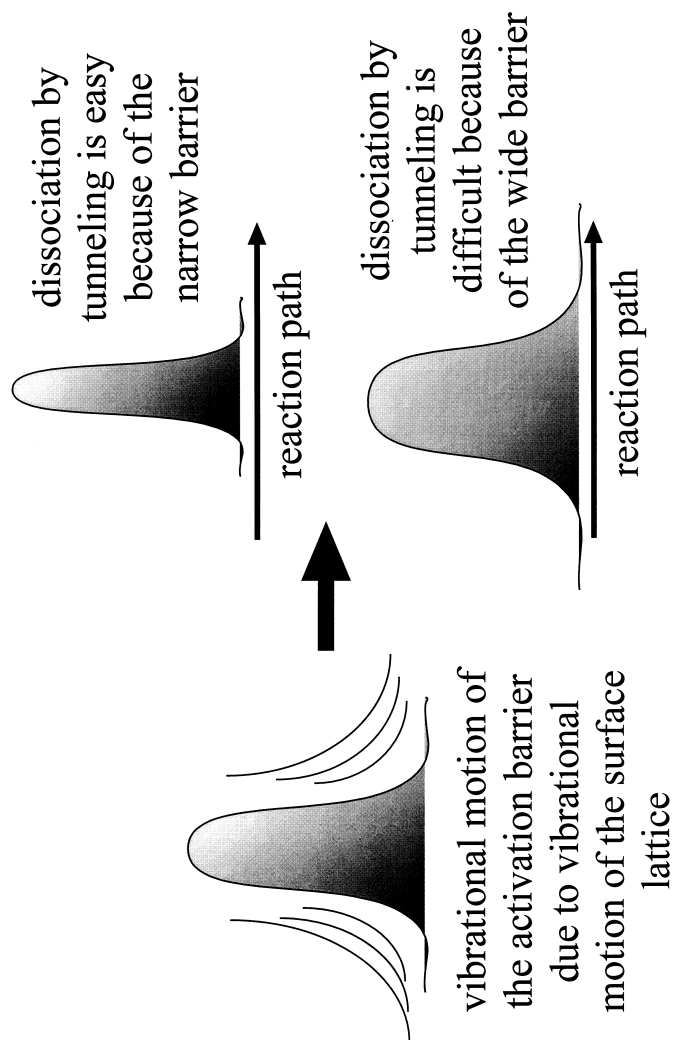


Fig. 23. A schematic diagram showing a vibrating activation barrier, which, in effect, corresponds to either a narrow activation barrier or a wide activation barrier.

DOF of the molecule and the vibrational DOF of the surface lattice. Our orientationally anisotropic model potential is again based on qualitative features of available PES plots for $H_2(D_2)/Cu$ surface systems [36,58–63], with the surface atoms modeled as locally independent Einstein oscillators. We show that this *surface recoil effect* (SRE), which allows the surface atoms to move periodically about their equilibrium position, not only changes the effective height of the activation barrier (due to a transfer/loss of available energy needed to overcome the barrier to dissociation to surface vibrations), but also changes the effective width of the activation barrier to dissociation (Fig. 23). From Section 3.1, we already know that the orientational dependence of the reaction introduces two competing factors [32,36,75,76,110] working for the dissociative adsorption process, viz. energy transfer (from translation to rotation and vice-versa) effect and SE. The SE, which is due to the anisotropic nature of the PES, dominates over the ETE for low initial rotational states j . For high j , the RTETE, which arises from the strong coupling between the rotational motion and the (translational) motion along the reaction path, dominates.

On considering the coupling between these three effects, viz. SE, ETE and SRE, we observed only a very small shift in the energetic position of the inflection point of the adsorption curves determined by using a dynamic surface, as compared with adsorption curves determined by using a rigid surface, when the impinging

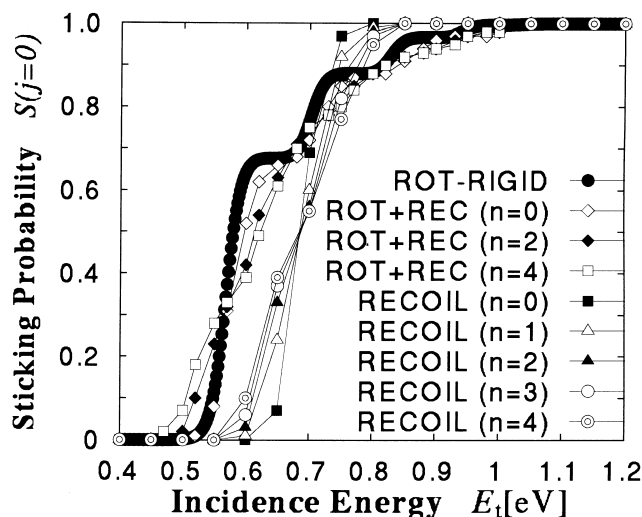


Fig. 24. Comparison between the adsorption probability curves derived from: a rigid surface and considering 5-even rotational channels (filled \circ); a dynamic surface initially in its ground-state and considering 5-even rotational channels and 20-surface vibrational channels; a dynamic surface with 1-even rotational channel and 20-surface vibrational channels. The dynamic surface is taken to be initially in its ground-state ($n = 0$) or, in its, first-, second-, third-, fourth-excited states ($n = 1, 2, 3, 4$, respectively). (Initial rotational state $j = 0$ for all curves.) ($E_a = 0.54$ eV, $V_1 = 1.0$ eV, $\beta = 0.25$ and, in this figure, $\alpha = 1.5 \text{ \AA}^{-1}$). From Ref. [81].

molecule is initially in its rotational ground-state and restricted to be in its vibrational ground-state throughout the reaction process. This differs from earlier studies [101,104–106], where the surface motion was coupled to the intramolecular vibration. They all observe a considerable shift in the energetic location of the inflection point of the adsorption curves obtained from calculations using a dynamic surface as compared with those using a rigid surface. We think this shift

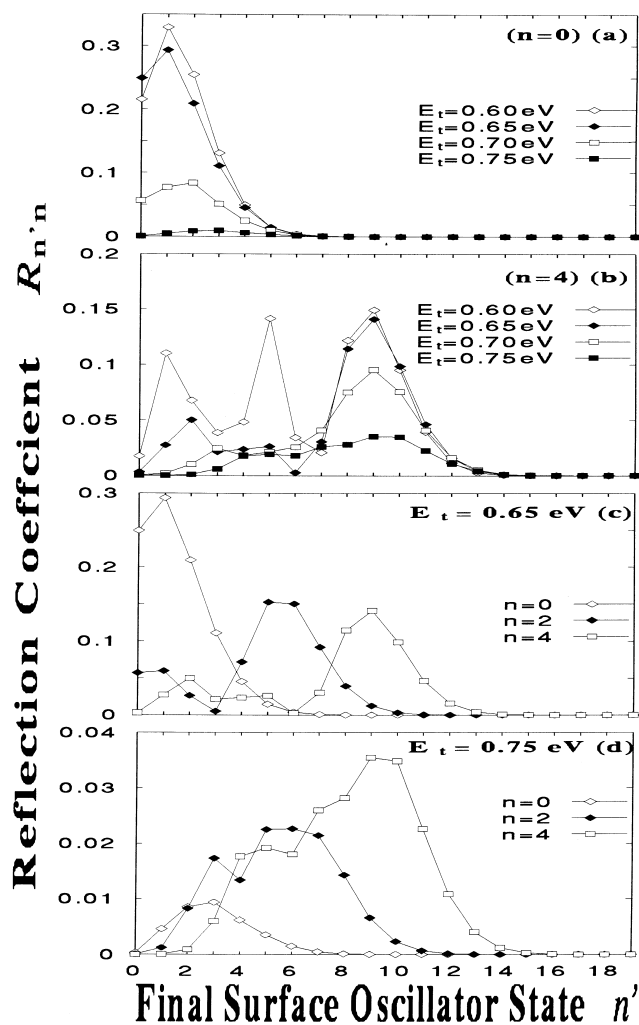


Fig. 25. Comparison of reflection coefficient R , vs. the final surface oscillator state n' , curves with (a), (b) fixed initial surface oscillator state, and different incidence energies of the impinging molecule; (c), (d) fixed incidence energy of the impinging molecule, and different initial surface oscillator state and considering 20-surface vibrational channels and only 1-rotational channel. ($E_a = 0.54$ eV, $V_1 = 1.0$ eV, $\beta = 0.25$ and, in this figure, $\alpha = 1.5 \text{ \AA}^{-1}$). From Ref. [81].

in the energetic location of the inflection point of the adsorption curve might be due to the big difference in the time scales between the intramolecular vibration and the surface-lattice vibration. As a result, the impinging molecule does not feel any effect from the motion of the surface other than an effective increase in the barrier height (or a loss of available translational energy, needed to overcome the activation barrier, to surface motion). Furthermore, we ascribe the broadening of the transition region (where the adsorption probability changes from 0 to 1) of the adsorption curve, with increasing surface temperature, to the narrowing of the effective width of the activation barrier. (Although the SRE results in a change in the effective width of the activation barrier to dissociation, as shown in Fig. 23, only the narrowing part will qualitatively account for the experimental results.)

3.2.1. Surface recoil effect

In Fig. 24, we show a comparison between the adsorption/sticking probability curves for different situations. At the leftmost (filled \circ s), we show the adsorption probability curve for the case when an impinging molecule reacts with a rigid surface. Relative to this curve (filled \circ s) is a cluster of curves in the rightmost part (marked by filled \square s, \triangle s, filled \triangle s, \circ s, and concentric \circ s). These are the resulting curves when an impinging molecule reacts with a dynamic surface (introducing the SRE) with different initial surface oscillator states (given by the n s), and suppressing the coupling between the different rotational states of the impinging molecule. (This was done by choosing a single effective activation barrier height, which is the average of all potentials corresponding to all possible orientations.) We immediately see that, regardless of the initial state of the surface oscillator, the energetic location of the inflection point of this cluster of adsorption curves (rightmost part of Fig. 24) does not change. Furthermore, in the low incidence energy region, impinging molecules hitting surface oscillators with high initial states have higher SP as compared with those hitting surface oscillators with lower initial states. On the other hand, in the high incidence energy region, impinging molecules hitting surface oscillators with low initial states have higher SP as compared with those hitting surface oscillators with higher initial states.

Fig. 25 depicts the corresponding reflection coefficients for the cluster of adsorption curves mentioned above. For fixed initial surface oscillator states (Fig. 25(a) and (b)), we see a decrease in the number of reflected molecules (proportional to the area under the corresponding reflection curve) as the incidence energy is increased, because the molecules gain more translational energy to overcome the activation barrier to dissociation. For fixed incidence energy and varying initial oscillator states (Fig. 25(c) and (d)), in the low incidence energy region, high initial surface oscillator states result in more impinging molecules being adsorbed. On the other hand, in the high incidence energy region, high initial surface oscillator states result in fewer impinging molecules being adsorbed, which can be ascribed to the narrowing of the effective width of the activation barrier (Fig. 23). Because of SRE, part of the available translational energy needed to overcome the barrier to dissociation is lost to surface oscillator

excitations, resulting in motion of the activation barrier along the reaction path. This (virtual) motion of the activation barrier causes its effective width to increase and decrease. In the low incidence energy region, where, classically, the impinging molecules cannot overcome the activation barrier, the narrowing of the activation barrier, during part of the time that the reaction takes place, increases the chance for the impinging molecules to tunnel through the barrier. In the intermediately high incidence energy region (region where the difference between the translational energy of the impinging molecules and the activation barrier height is small), where, classically, the impinging molecules are sure to overcome the activation

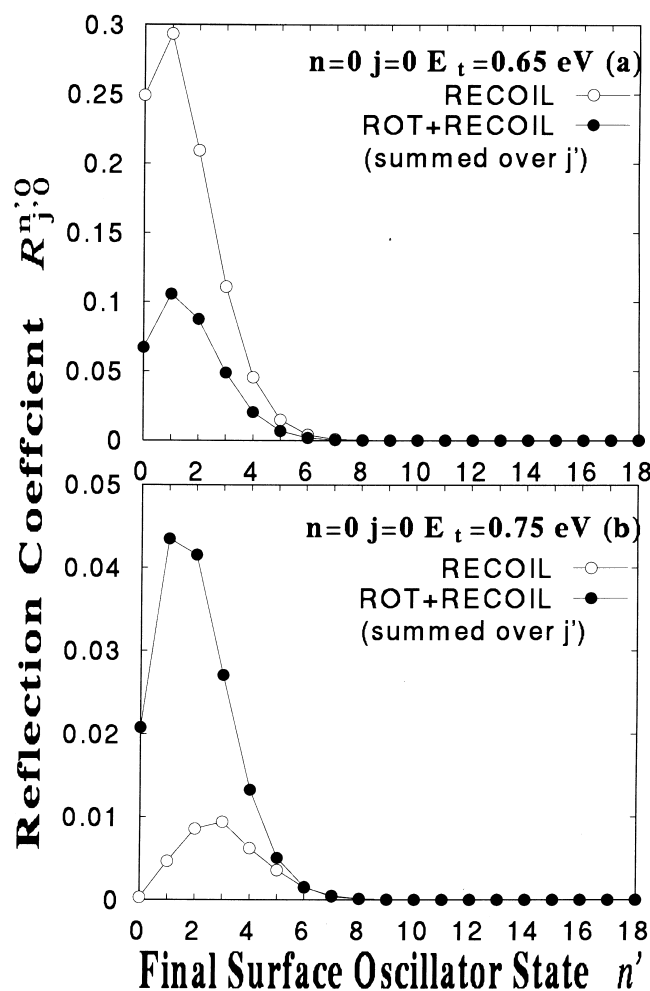


Fig. 26. (a) and (b) Comparison between the reflection coefficient R vs. final surface oscillator state n' . Curves derived from a dynamic surface and neglecting (\circ) rotation or (filled \circ) considering rotation. ($E_a = 0.54$ eV, $V_1 = 1.0$ eV, $\beta = 0.25$ and, in this figure, $\alpha = 1.5 \text{ \AA}^{-1}$). From Ref. [81].

barrier, the narrowing of the activation barrier, during part of the time that the reaction takes place, decreases the chance that there is an integral number of half-wavelengths of the wave (representing an impinging molecule) that is inside the region of influence of the activation barrier (a quantal condition for full transmission); and this results in a decrease in the adsorption/sticking probability. For even higher incidence energies, apart from a continuous loss of translational energy to excite the surface, the impinging molecules will not feel the motion of the surface.

The adsorption curve of the impinging molecules, derived from a dynamic

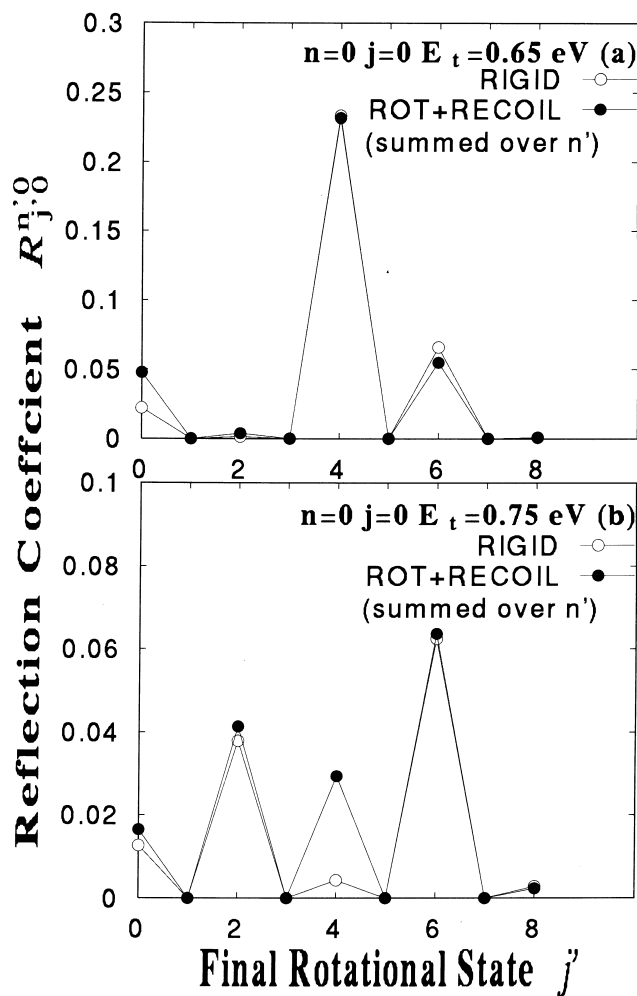


Fig. 27. (a) and (b) Comparison between the reflection coefficient R vs. final rotational state of reflected molecules j' . Curves derived from (○) a rigid surface and a (filled ○) dynamic surface. ($E_a = 0.54 \text{ eV}$, $V_1 = 1.0 \text{ eV}$, $\beta = 0.25$ and, in this figure, $\alpha = 1.5 \text{ \AA}^{-1}$). From Ref. [81].

surface with fixed initial rotational state ($j = 0$), do not show as much shift in the energetic location of the inflection point as compared with the adsorption curve derived from the same dynamic surface, but with the rotational DOF of the impinging molecules suppressed (Fig. 24), which indicates that the inclusion of the rotational DOF of the impinging molecules suppresses the SRE. This is shown in Fig. 26(a) (Fig. 26(b)) as a decrease (increase) in the area under the reflection curve (filled \odot) (for the case when the molecular–rotational DOF is coupled to the surface vibrational DOF) compared with that of the reflection curve (\odot) (for the case when the molecular–rotational DOF is suppressed). Eventually (cf. Figs. 24 and 26(b)), the SP derived from a dynamic surface, with the inclusion of molecular rotation, approaches the adsorption curve derived from a rigid surface, because, apart from a feeding of translational energy to the surface oscillator (resulting in a virtual increase in activation barrier height), inclusion of molecular rotation allows for a further increase in the activation barrier height, depending on the ability of the PES to reorient the impinging molecules. On the other hand, the SRE has negligible effect on the rotational excitation of the reflected molecules as shown by the same position of the reflection peaks along the abscissa (Fig. 27(a) and (b), \odot): rigid surface (filled \odot):dynamic surface).

3.3. Steering, energy transfer and surface recoil effects

Based on physical arguments, our numerical results and earlier studies on the subject, we conclude that, to properly consider the SRE, it is necessary to take into account the coupling between the internal rotational DOF of the impinging molecule and the surface vibrational DOF. This is contrary to conventional belief that, because of the time scale difference between the internal rotational DOF and the internal vibration DOF of the impinging molecule, it is a good simplification to neglect the internal rotational DOF when studying SRE.

We already know that, as a molecule approaches the metal surface, it encounters a PES that is orientation-dependent [26,36,59–61]. In order for the molecule to dissociate and be adsorbed on the metal surface, it must be able to find the path of least resistance (path of least potential), and have enough energy to reach the surface. This process depends on what the initial state of the impinging molecule is, what its incidence energy is and how long it stays under the influence of the anisotropic PES [36]. Thus, the rotational DOF plays a vital role in the dissociative adsorption process. In the case of rotation, there are two competing factors working for the dissociation process, viz. SE and ETE. The first, SE, pertains to the orientational dependence of the reaction. The second, ETE, pertains to the effective transfer of rotational energy to translational energy. This results from the coupling of the rotational motion to the translational motion along the reaction path [36,76]. The non-monotonous behavior [32] of the rotational dependence of the translational dependence of dissociative adsorption of D_2 on Cu(111) can be ascribed to these two competing factors working for the dissociative adsorption process. For low initial rotational states, because of the somewhat small rotational energy, SE dominates. For high initial rotational states,

because the molecule has sufficient rotational energy to assist in sticking, RTETE dominates.

(In this study, where we considered the impinging molecule to be initially in its rotational ground-state, the SE dominates. Thus, most of the difference we find between results obtained by suppressing or including rotational motion can be ascribed to the SE.)

The coupling of the translational DOF of the impinging molecule with the vibrational DOF of the surface introduces the SRE. We have shown (Section 2.2.1) that the vibration of the surface oscillators normal to the surface plane causes the projections of the activation barrier peaks positions (for the different PES curves corresponding to different positions of the surface oscillators relative to a fixed reference, Fig. 11) to the reaction path curve for a rigid surface C_0 , to move along C_0 . Thus, the impinging molecule encounters an activation barrier that is periodically moving towards and away from it. As a result, the effective width of the activation barrier, which is also an important factor in considering the rotational DOF of the impinging molecule [36], changes. Comparison of the surface temperature-dependent SP, shown in Fig. 22 with results of our previous studies (cf. Fig. 25 of Ref. [36]), show that the widening of the transition region of the adsorption probability curve, as the surface temperature increases, can be ascribed to a narrowing of the effective activation barrier width, with higher surface temperatures corresponding to narrower activation barriers. In the low energy region, where, classically, the impinging molecule will not stick, a narrow activation barrier increases the chances of the impinging molecule to tunnel through the activation barrier. In the high energy region, where, classically, the impinging molecule is sure to stick, a narrowing of the activation barrier decreases the chance that there is an integral number of half-wavelengths (of the wave representing the impinging molecule) that is inside the region of influence of the activation barrier (a quantal condition that should be satisfied for full transmission).

As for the big shift in the energetic location of the inflection point of the adsorption curve, derived from a dynamic surface compared with that derived from a rigid surface, observed by previous studies [101,104–106] we think this is due to the incompatibility between the two DOF considered, viz. internal vibrational DOF of the impinging molecule and the vibrational DOF of the surface. Incompatibility, in the sense that, because of the big difference in the time scales of the molecular vibration and the surface vibration, there is a continuous feeding of translational and vibrational energy to the surface oscillators without the impinging molecule noticing any change in the activation barrier other than a relative increase in the height of the activation barrier. In the case of a coupling between the rotational DOF of the impinging molecule and the vibrational DOF of the surface, the time scales are comparable. Hence, even though there is still a continuous feeding of energy to the surface oscillators (as can be noted by a slight shift in the resulting adsorption curve towards higher incidence energies, Fig. 24), because of the comparable time scales, the impinging molecule notices the change in the position of the activation barrier, which changes the effective width of the

activation barrier. For surface oscillators with low initial vibrational states and impinging molecules with initially unfavorable orientations, the previous gain, due to the SE, which is able to reorient the impinging molecule to a favorable orientation, will be lost, because the effective widening of the activation barrier provides enough time for the PES to reorient the impinging molecule to an unfavorable orientation. The reverse can be said for surface oscillators with high initial vibrational states, and impinging molecules with initially favorable orientations. For very high initial rotational states of the impinging molecule, this SRE is expected to be very noticeable again, such that, once more, there will be a considerable shift in the adsorption curve results derived from a dynamic surface relative to one derived from a rigid surface. We consider this in our succeeding studies. Another interesting question is: “Why is normal energy scaling observed despite recent total energy calculations suggesting a very corrugated Cu surface?” Recent ab-initio energy calculations [59–61] report a change in the height of the activation barrier and its position along the reaction path, depending on the surface sites approached by the impinging molecule. This change in height and position of the activation barrier along the reaction path is of the same magnitude as the change introduced, if we consider the rotational DOF of the impinging molecule and allow for surface motion. Thus, if we neglect the rotational DOF of the impinging molecule, as well as the effect of surface temperature, there will be a considerable difference in the adsorption curves derived from a corrugated and a flat surface. (Similar to that observed for the effect of neglecting molecular rotation in considering surface vibration, as shown above.) However, with the inclusion of the rotational DOF of the impinging molecule, the difference in the adsorption curves derived from a corrugated and a flat surface would again be made negligible. Thus, providing us with the probable answer to the above question.

4. Rotational effects in associative desorption dynamics of D₂/Cu(111)

4.1. Consistency between dissociative adsorption and associative desorption results

When the adsorption probability of molecules colliding with a surface is independent of the distribution of molecular internal states, orientations and velocities, equilibrium statistical mechanics predicts that the molecular quantum state distributions in the corresponding reverse process of desorption will be determined solely by the surface temperature T_S . However, this is often not the case, as we have here for the hydrogen on Cu system. Thus it would also be interesting to study how the desorption probability (the probability that D atoms initially chemisorbed on the Cu surface come together and detach from the surface as D₂ molecules) will behave, as such studies could elucidate the nature of those special forces and configurations experienced by the desorption flux, when we relate them to the adsorption probabilities.

We performed quantal calculations [34–36,81,84,90] of the desorption

probability, independent of the adsorption probability results, by invoking the principle of *microscopic reversibility* [34,35] and solving the time-independent Schrödinger equation for a D_2 molecule moving along the reaction path, and under the influence of an orientationally anisotropic PES based on the *qualitative features* of available PES plots for the H_2 on Cu(111) surface system [36,58,59]. As described in Section 2, the dynamical variables we considered were the translational and vibrational coordinates of the desorbing molecule, which are represented by the reaction coordinates s and r , respectively, and the polar and azimuthal angular orientation of the molecule with respect to the surface, represented by θ and φ , respectively. The energy barrier for a parallel-oriented D_2 molecule was set at $V_{\min} = V_{\parallel} \approx 0.5$ eV, and gradually increased to a value $V_{\max} = V_{\perp} \approx 0.9$ eV for a perpendicular-oriented molecule. The form of our orientation-dependent PES results in a *selection rule*, where molecules in even (odd) initial rotational states will end up in even (odd) final rotational states. Furthermore, the

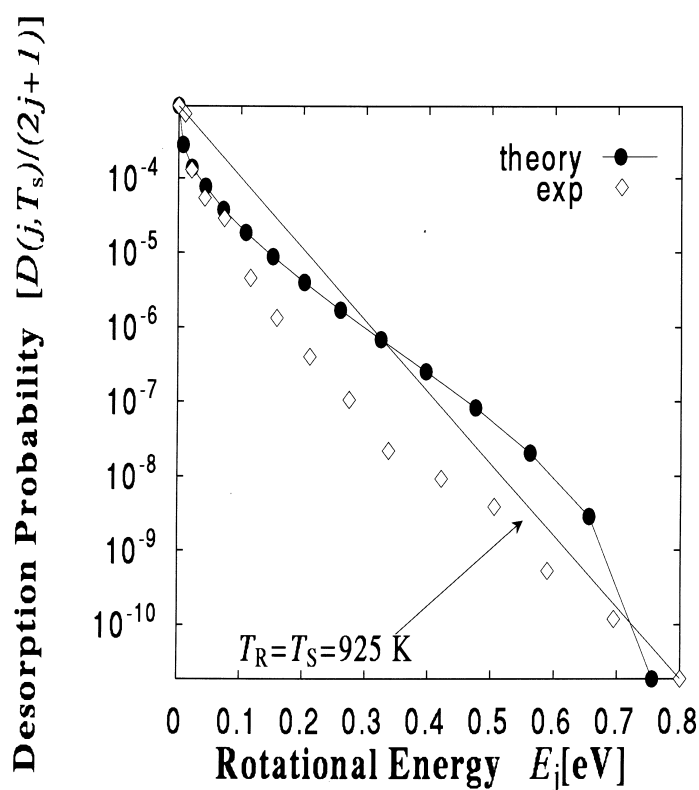


Fig. 28. Boltzmann plot of the D_2 desorption probability vs. rotational energy E_j of the state. The line $T_R = T_S = 925$ K is plotted for reference. The \diamond 's correspond to experimental data [32]. The gas phase rotational constant of D_2 is $B \approx 3.8$ meV. From Ref. [84].

azimuthal quantum numbers m_j are conserved. (See Section 2 and Refs. [34–36,81,90] for more details regarding the calculation method, and the actual form of the model potential adopted.) We then calculated the probability $D(j, T_S)$ that the molecule desorbs with a final rotational state j from a surface at the surface temperature T_S , by taking the Boltzmann average of the raw, numerical desorption probability results over the initial energy distribution at surface temperature T_S . Fig. 28 provides a Boltzmann plot of the resulting desorption probability of D_2 molecules as a function of the rotational energy. A Boltzmann distribution would appear as a straight line (cf. Fig. 28). However, the calculated desorption probability result shown in Fig. 28 is not represented by a single temperature, and the mean rotational energy is less than T_S [35]. These qualitative features have also been observed experimentally [28,29,31–33].

In order to relate the desorption results in Fig. 28 to the adsorption probability results in Fig. 19, we show, in Fig. 29, a Boltzmann plot of our numerical results for the desorption probability of D_2 molecules as a function of the rotational

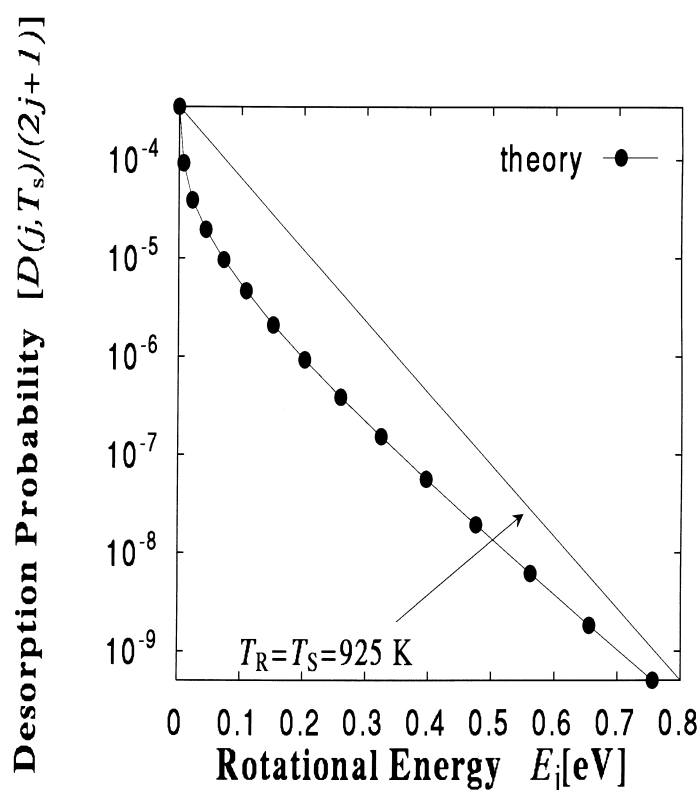


Fig. 29. Boltzmann plot of the D_2 desorption probability vs. rotational energy E_j of the state j ($v = 0$), for fixed translational energy $E_t = 0.60$ eV. The line $T_R = T_S = 925$ K is plotted for reference. The gas phase rotational constant of D_2 is $B \approx 3.8$ meV. From Ref. [84].

energy for a fixed incidence energy. Recall from the principle of microscopic reversibility, and the conservation of energy [34,35], that the dynamic behavior of the adsorption probability is reflected in the distribution of molecular quantum states in desorption by

$$D(E_t, j) \propto S(E_t, j) \exp\left(-\frac{E_t + E_j}{k_B T_S}\right), \quad (28)$$

where E_t is the translational energy of the molecule, and j is its rotational state with a corresponding rotational energy E_j . The initial decrease in the SP curve corresponding to an incidence energy of $E_t = 0.6$ eV in Fig. 19 is reflected as a decrease in the rotational temperature in desorption (Fig. 29). The final increase in the SP curve is reflected as an increase in the rotational temperature relative to the former decrease. Note that the increase in rotational temperature is not as dramatic as that expected from the corresponding SP curve in Fig. 19, because the Boltzmann factor in (28) decreases much more rapidly compared with the increase in the SP. If we then sum over all the incidence energies, we obtain the Boltzmann plot shown in Fig. 28, where the initial decrease in the rotational temperature, with respect to the surface temperature for low rotational energies, $E_j \leq 0.05$ eV, is due to an initial mean decrease in the SP for low initial rotational states, and the mild increase in the rotational temperature for higher rotational energies, 0.05 eV $\leq E_j \leq 0.5$ eV, is due to a mean increase in the SP for higher initial rotational states (cf. Figs. 19 and 28). The final decrease again of the rotational temperature can be understood by considering the result shown in Fig. 29 and the relation between the SP and the desorption probability (28). As the rotational energy E_j , appearing in the Boltzmann factor, increases, the only relevant contributions come from the SP corresponding to those incidence energies $E_t \ll V_{\min}$. In this energy region, the SP are not much different from 0, even for $j = 14$. As a result, we observe this final decrease in the rotational temperature for the desorption probability of hydrogen molecules in their vibrational ground-state ($v = 0$).

4.2. Rotational alignment and dynamical quantum filtering

To demonstrate how surfaces that adsorb hydrogen can act as *rotational quantum state filters*, and cause desorbing hydrogen molecules to exhibit rotational alignment, we again consider the reaction of a D_2 molecule with a Cu(111) surface and calculate the corresponding desorption probability, as described in Sections 2 and 4.1. For a given total kinetic energy E_{tot} (defined as the sum of the final translational energy E_t and the final rotational energy E_j of the molecule after desorption, $E_{\text{tot}} = E_t + E_j$), we calculated for the m_j -resolved probability $D_{jm_j}(E_{\text{tot}})$ that the molecule desorbs with final rotational state (j, m_j) , where molecules with azimuthal quantum number $|m_j| = j$ have their rotational axes oriented, predominantly, perpendicular to the surface (helicopter-type rotation), molecules with $m_j = 0$ have their rotational axes oriented, predominantly, parallel to the surface (cartwheel-type rotation), and molecules with $0 < |m_j| < j$ have their

rotational axes oriented intermediate between the two former ones. From these calculated desorption probabilities $D_{jm_j}(E_{\text{tot}})$, we find the corresponding quadrupole alignment factors

$$A_0^{(2)}(j, E_{\text{tot}}) = \frac{\sum_{m_j} [3m_j^2 - j(j+1)] D_{jm_j}(E_{\text{tot}})}{j(j+1) \sum_{m_j} D_{jm_j}(E_{\text{tot}})}, \quad (29)$$

which yield an insight as to the degree of alignment and orientation preference of the desorbing D_2 molecules for assumed values in the range $[-1, 3j/(j+1)-1]$. For molecules exhibiting cartwheel-type rotations ($|m_j| \approx 0$) with respect to the surface normal $\hat{\mathbf{n}}$, $A_0^{(2)}(j) < 0$, while those exhibiting helicopter-like rotations ($|m_j| \approx j$) have $A_0^{(2)}(j) > 0$, with perfect alignment given by $A_0^{(2)}(j) = 3j/(j+1) - 1$, and as $j \rightarrow \infty$, $A_0^{(2)}(j) \rightarrow 2$. A spatially isotropic distribution of the angular momentum \mathbf{j} -vector is described by $A_0^{(2)}(j) = 0$.

In Fig. 30, are the calculated $A_0^{(2)}(j)$ results for D_2 molecules desorbing in the vibrational ground-state ($\nu = 0$) from Cu(111), with total kinetic energy $E_{\text{tot}} = 0.40 \rightarrow 1.00$ eV. For total kinetic energies lower than the minimum translational barrier height ($E_{\text{tot}} < V_{\text{min}} = V_{\parallel} \approx 0.5$ eV, Fig. 30), there is a general preference for cartwheel-type rotations. As E_{tot} increases, there is eventually an emerging preference for helicopter-type rotations ($E_{\text{tot}} \geq V_{\text{min}} = V_{\parallel} \approx 0.5$ eV, Fig. 30). Also apparent is that, for a particular total kinetic energy E_{tot} , $A_0^{(2)}(j)$ is a *non-monotonic* function of the detected final rotational state j . Furthermore, this non-monotonic behavior is strongly dependent on the translational energy E_t (cf. Figs.

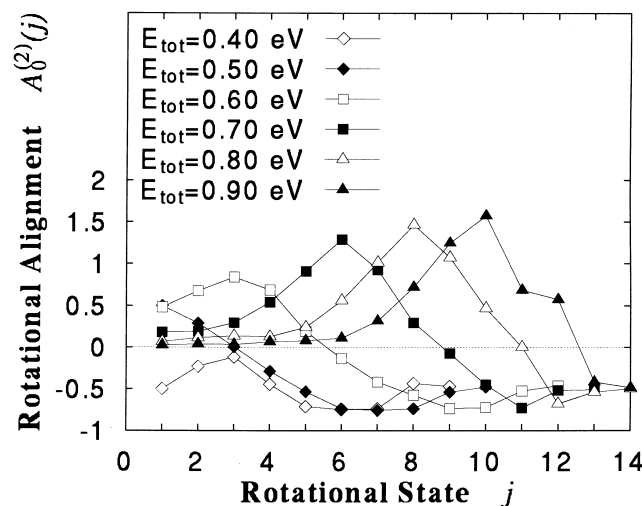


Fig. 30. Rotational alignment for D_2 molecules desorbing in the state ($\nu = 0, j, E_{\text{tot}}$) from Cu(111) as a function of the final rotational state j . Total kinetic energy $E_{\text{tot}} = 0.40 \rightarrow 0.90$ eV.

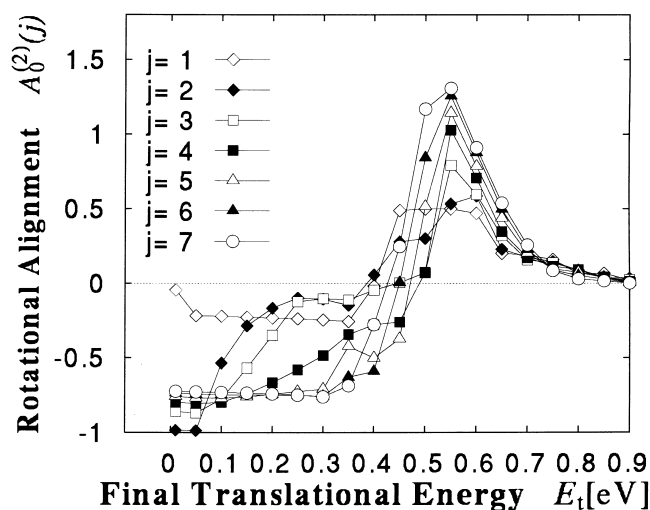


Fig. 31. Rotational alignment for D_2 molecules desorbing in the state $(\nu = 0, j, E_t)$ from Cu(111) as a function of the final translational energy E_t . Final rotational state $j = 1 \rightarrow 7$. Surface temperature $T_S = 950$ K. From Ref. [88].

31 and 32). These observations are quite understandable, if we keep three things in mind. First, associative desorption is a strongly orientation-dependent process, where molecules oriented parallel to the surface are favored to perpendicular-

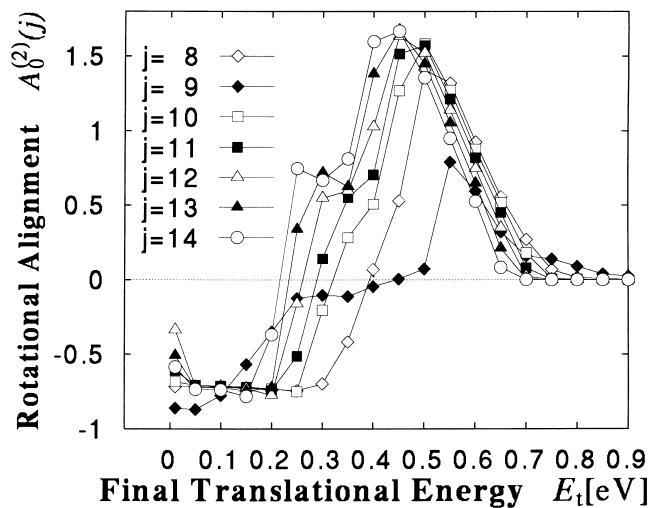


Fig. 32. Rotational alignment for D_2 molecules desorbing in the state $(\nu = 0, j, E_t)$ from Cu(111) as a function of the final translational energy E_t . Final rotational state $j = 8 \rightarrow 14$. Surface temperature $T_S = 950$ K. From Ref. [88].

oriented molecules. Second, when hydrogen molecules are found adsorbed on the surface, there is essentially no such thing as a rotational state, nor does an initial orientation have any meaning. Third, the maximum final rotational state j_{\max} , accessible to the desorbed molecules, is limited by the available total kinetic energy E_{tot} (Table 1).

On the way towards the gas phase, desorbing molecules are bound to follow the *path of least resistance* (path of least potential). Since the initial rotational state j_{ad} of molecules about to form from adsorbed atoms may take any value, and we may assume that these molecules are then initially oriented parallel to the surface ($|m_{\text{ad}}| \approx j_{\text{ad}}$), all molecules will try to desorb. However, on crossing the transition region towards desorption, the metal surface, via the orientation-dependent PES, acts as a sort of *rotational quantum state filter/sieve*, and filters out all rotational states j_{des} greater than some critical rotational state j_{crit} , which depends on the relative value of E_{tot} with respect to V_{min} . As a result, upon desorption, only those molecules with rotational state $j_{\text{des}} \leq j_{\text{crit}}$ will survive. Given V_{min} and E_{tot} , we can roughly estimate j_{crit} and j_{\max} by calculating for the corresponding energies $E_{j_{\text{crit}}}$ and $E_{j_{\max}}$. (When $[E_{\text{tot}} - V_{\text{min}}] > 0$, $E_{j_{\text{crit}}} \approx [E_{\text{tot}} - V_{\text{min}}]$, otherwise $E_{j_{\text{crit}}} = 0$. $E_{j_{\max}} \approx E_{\text{tot}}$). For D_2 , the approximate values of j_{crit} and j_{\max} for a particular value of E_{tot} are listed in Table 1. Furthermore, it should be noted that, since the *path of least resistance* (path of least potential) will be favored over all other possible paths, as $j_{\text{des}} \rightarrow j_{\text{crit}}$, a majority of those molecules that did survive the attempt to desorb will exhibit helicopter-like rotations (i.e. $|m_{\text{des}}| \approx j_{\text{des}}$). This is easily understood if we recall that a sufficient translational energy is required to, at least, overcome the barrier minimum V_{min} . Suppose a molecule that survives an attempt to desorb assumes a rotational state $j_{\text{des}} \approx j_{\text{crit}}$ upon desorption. With a fixed total energy E_{tot} , it will only have just enough translational energy to overcome the barrier minimum V_{min} , which requires that the desorbing molecule exhibits helicopter-like rotation ($|m_{\text{des}}| \approx j_{\text{des}}$).

Table 1

The list shows the estimated maximum final rotational state j_{\max} accessible to the desorbed D_2 molecules and the corresponding rotational energy $E_{j_{\max}} = B_{j_{\max}}(j_{\max} + 1)$ for fixed final total kinetic energies E_{tot} . Also shown are the corresponding estimated critical rotational states j_{crit} . The rotational constant of D_2 in the gas phase is taken to be $B \approx 3.8$ meV and $V_{\text{min}} = V_{\parallel} \approx 0.5$ eV. From Ref. [88]

E_{tot} (meV)	$E_{j_{\max}}$ (meV)	j_{\max}	j_{crit}
100	76	4	0
200	160	6	0
300	274	8	0
400	342	9	0
500	418	10	1
600	593	12	3
700	692	13	6
800	798	14	8
900	798	14	10
1000	921	15	10

Upon desorption, we find the molecules in the state $(j_{\text{des}}, m_{j_{\text{des}}})$, where $|m_{j_{\text{des}}}| \leq j_{\text{des}} \leq j_{\text{crit}} \leq j_{\text{max}}$. The desorbed molecules then assume a final rotational state (j, m_j) by undergoing either rotational excitations ($j > j_{\text{des}}$) or de-excitations ($j < j_{\text{des}}$), or by remaining in the same rotational state ($j = j_{\text{des}}$). Those that assume final rotational states $j < j_{\text{crit}}$ ($j > j_{\text{crit}}$) are more inclined to exhibit helicopter-like (cartwheel-like) rotations. For a fixed total kinetic energy E_{tot} , those that undergo rotational excitation do so at the expense of the translational energy E_t . By undergoing rotational excitation upon desorption, the molecule assumes a final rotational state (j, m_j) with $j > j_{\text{des}} \geq |m_{j_{\text{des}}}| = |m_j|$ and, thus, we would most likely find these molecules exhibiting cartwheel-like rotations. On the other hand, those that undergo rotational de-excitation will do so with a gain in translational energy E_t . By undergoing rotational de-excitation, the molecule assumes a final state (j, m_j) with $j < j_{\text{des}} \geq |m_{j_{\text{des}}}| = |m_j|$ and, since $j \geq |m_j|$ always, we would most likely find these molecules exhibiting helicopter-like rotations. Those that undergo neither rotational excitations nor de-excitations retain the same translational energy E_t and, as mentioned earlier, we would most likely find these molecules exhibiting helicopter-like rotations, with $|m_j| = |m_{j_{\text{des}}}| \approx j$.

When the total kinetic energy E_{tot} is small ($E_{\text{tot}} \leq V_{\text{min}}$), $j_{\text{crit}} \approx 0 \ll j_{\text{max}}$ and, since only those states $j > j_{\text{crit}}$ are accessible as final rotational states, rotational excitations are more likely to occur. Thus, we find the desorbed molecules exhibiting cartwheel-like rotations ($E_{\text{tot}} = 0.4 \rightarrow 0.5$ eV in Fig. 30). As the total kinetic energy E_{tot} increases, j_{crit} also increases. Now both $j > j_{\text{crit}}$ and $j < j_{\text{crit}}$ are possible final rotational states. If the desorbed molecules assume final rotational states $j < j_{\text{crit}}$, we find them more inclined to do helicopter-like rotations (cf. low j region, in Fig. 30, with $E_{\text{tot}} > V_{\text{min}}$). As the final rotational state j increases ($j \rightarrow j_{\text{crit}}$), $A_0^{(2)}(j) \rightarrow 3j/(j+1) - 1$ (perfect alignment), and the rotation becomes more helicopter-like. Where desorbed molecules assume final rotational states $j > j_{\text{crit}}$, they prefer to do cartwheel-like rotations (cf. high j region, in Fig. 30, with $E_{\text{tot}} > V_{\text{min}}$). When E_{tot} is large enough ($E_{\text{tot}} \gg V_{\text{min}}$), $j_{\text{crit}} \rightarrow j_{\text{max}}$ and rotational excitations as well as de-excitations are equally possible. We then find the molecules exhibiting an almost orientationally isotropic \mathbf{j} -vector distribution, i.e. $A_0^{(2)}(j) \rightarrow 0$ (cf. $A_0^{(2)}(j = 1 \rightarrow 14)$ for $E_{\text{tot}} = 1.00$ eV in Fig. 30).

Because the quadrupole alignment factors $A_0^{(2)}(j)$ (29) are defined for a particular final rotational state j , corresponding to a particular rotational energy E_j , we can also define the corresponding translational energy (E_t -) dependent quadrupole alignment factors $A_0^{(2)}(j)$, the results of which appear in Figs. 31 and 32. As expected, from previous discussions, D_2 molecules desorbing with translational energies lower than the minimum barrier height ($E_t < V_{\text{min}}$) have correspondingly low total kinetic energies E_{tot} , and exhibit cartwheel-like rotational preference (cf. $E_t < 0.5$ eV region in Fig. 31, and $E_t \leq 0.2$ eV region in Fig. 32). As the E_t increases, corresponding to an increase in E_{tot} , the rotational preference becomes more helicopter-like (cf. $0.5 \leq E_t < 0.6$ eV region in Fig. 31, and $0.2 \leq E_t \leq 0.5$ eV region in Fig. 32). For sufficiently large translational energies ($E_t > V_{\text{min}}$), the D_2 molecules exhibit an almost orientationally isotropic \mathbf{j} -vector distribution ($A_0^{(2)}(j) \rightarrow 0$) regardless of the final rotational state (cf.

$A_0^{(2)}$ ($j = 1 \rightarrow 14$) for $E_t = 0.80 \rightarrow 0.90$ eV in Figs. 31 and 32). It should be noted that the same general features, as those presented here, occur even for other strongly orientation-dependent reactions between hydrogen molecules and other surfaces. An example is the desorption of D_2 from a Pd-surface [41], which, although it requires an altogether different corresponding set of values for V_{\min} and V_{\max} [40], is also strongly orientation dependent.

So far, we have presented alignment factor results without considering the surface temperatures. In Fig. 33, the results of our calculation for $A_0^{(2)}(j)$ are shown, averaged over the Boltzmann distribution of total kinetic energies E_{tot} of the desorbing molecules at the surface temperature $T_S = 920$ K, i.e.

$$A_0^{(2)}(j, T_S) = \left\langle \frac{3j_z^2 - \mathbf{j}^2}{\mathbf{j}^2} \right\rangle_j = \frac{\int dE_t \sum_{m_j} [3m_j^2 - j(j+1)] D_{jm_j}(E_{\text{tot}}) e^{-E_{\text{tot}}/k_B T_S}}{j(j+1) \int dE_t \sum_{m_j} D_{jm_j}(E_{\text{tot}}) e^{-E_{\text{tot}}/k_B T_S}}, \quad (30)$$

in which a majority of the contribution to this average will come from desorbing molecules with total kinetic energies that are comparable with the barrier minimum, i.e. $E_{\text{tot}} \approx V_{\min}$. Upon averaging over the Boltzmann distribution of the total kinetic energies of the desorbing molecules at the surface temperature relevant to existing experiments ($T_S \approx 920$ K for Cu [47,48]), we find an alignment factor of $A_0^{(2)}(j, T_S) \approx 0.3 \rightarrow 0.7$ for $j = \rightarrow 14$, corresponding to a small preference for helicopter-like rotation, which qualitatively agrees with experimental results [48]. The small helicopter-like rotation preference is to be expected, because,

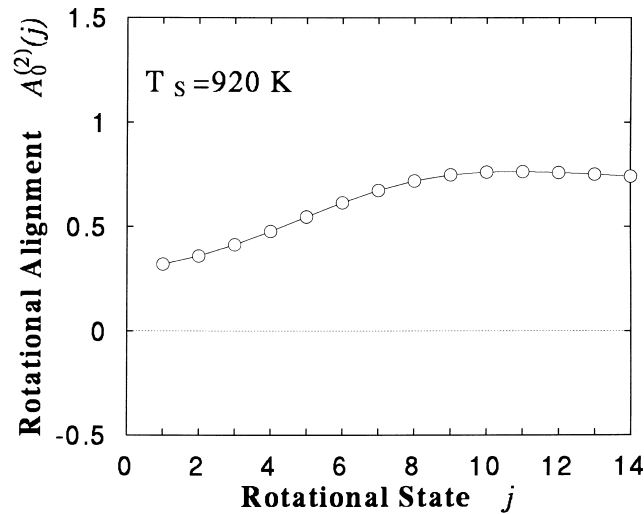


Fig. 33. Rotational alignment for D_2 molecules desorbing in the state ($v = 0, j$) from Cu(111), averaged over the Boltzmann distribution of total kinetic energies at the surface temperature $T_S = 920$ K.

although there are many possible paths to desorption, the *path of least resistance* (path with the lowest energy requirement), corresponding to a parallel orientation (helicopter-like motion), will be strongly preferred over other paths. In terms of an m_j -resolved desorption probability, because of the Boltzmann factor, only events corresponding to a particular range of E_{tot} , wherein there is only a slight difference between the results for $|m_j| = j$ and $m_j = 0$, are chosen to contribute to the desorption at the surface temperature T_S . However, as we have shown here, strong orientational preference in the desorption of hydrogen molecules should be observable with state (j -) and energy (E_{tot} - or E_t -) resolved measurements.

It would also be interesting to see how a higher-dimensional description, which includes surface corrugations and surface oscillations, will affect the results presented here. However, given the relatively high surface temperatures considered in experimental measurements [31,32,41,47,48], we expect to see only slight surface corrugation effects. Furthermore, as mentioned above, the desorbing molecules are bound to follow the *path of least resistance* (path with the lowest energy requirement), and thus, we believe that a high-dimensional description will still show the same general features presented here.

We have shown that the metal surface, via the orientation-dependent PES, can act as a *rotational quantum state filter*, and cause desorbing hydrogen molecules to exhibit rotational alignment. We have also shown that the resulting alignment of the desorbed molecules, as determined by the value of the quadrupole alignment factors $A_0^{(2)}(j)$, exhibits a non-monotonic j - and E_t -dependence, similar to the

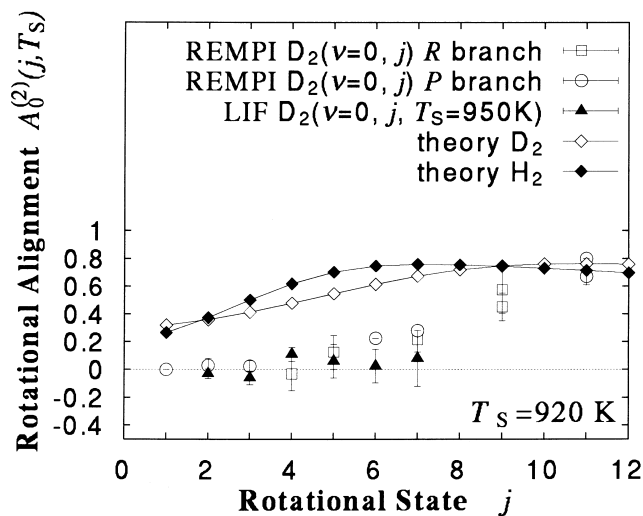


Fig. 34. Comparison between the rotational alignments of D_2 (\diamond) [87] and H_2 (filled \diamond) desorbing in the state ($\nu = 0, j$) from Cu(111), averaged over the Boltzmann distribution of total kinetic energies at the surface temperature $T_S = 920\text{ K}$. \square and \circ : experimental results for D_2 ($\nu = 0, j, T_S = 920\text{ K}$) using REMPI detection with P and R branch transitions, respectively [48]. Filled \triangle : experimental results for D_2 ($\nu = 0, j, T_S = 950\text{ K}$) using LIF detection [47]. From Ref. [89].

dependence of the adsorption probability of a hydrogen molecule, impinging a Cu(111) surface, on its initial rotational state [31,32,36] and initial translational energy [84]. Thus, we could, e.g. permeate H(D) atoms through the bulk of a copper single crystal and use the Cu(111) surface as a DQF to produce oriented H₂(D₂) molecules. As shown in Figs. 31 and 32, all we have to do is devise a means to either select only slow desorbing ($E_t \ll V_{\min}$) molecules or fast desorbing ($E_t > V_{\min}$) molecules, and get, respectively, either perpendicular-oriented or parallel-oriented molecules.

4.3. Isotope effects

Fig. 34 displays the calculated $A_0^{(2)}(j, T_S)$ results for H₂ and D₂ desorbing in the vibrational ground-state ($\nu = 0$) from Cu(111), averaged over the Boltzmann distribution of total kinetic energies at the surface temperature $T_S = 920$ K. For reference, the experimental results of Zacharias' [47] and Auerbach's [48] groups, are replotted for D₂ desorbing in the vibrational ground-state ($\nu = 0$) from Cu(111), with surface temperatures $T_S = 950$ and 920 K, respectively. The slightly lower results of Zacharias et al. [47] may, in part, be due to surface temperature T_S effects. Earlier studies (cf. Section 3.2 Ref. [81] and references therein) have demonstrated that, for a particular initial rotational state and low collision energies, an increase in T_S results in an increased dissociation, which can be associated with a decrease in effective dissociation barrier and, in turn, a decrease in the orientational anisotropy of the PES. Applying the principle of microscopic reversibility [34,35], an increase in T_S will result in decreased alignments (Fig. 34).

Within the limits of the experimental error bars, our results qualitatively agree with experiments, and show small preference for helicopter-like rotation. We got $A_0^{(2)}(j = 1 \rightarrow 14, T_S = 920 \text{ K}) \approx 0.3 \rightarrow 0.7$, as compared with experimental measurements of $A_0^{(2)}(j = 1 \rightarrow 7, T_S = 950 \text{ K}) \approx 0 \rightarrow 0.1$ [47] and $A_0^{(2)}(j = 1 \rightarrow 11, T_S = 920 \text{ K}) \approx 0 \rightarrow 0.8$ [48]. For low final rotational states j , the spatial distribution of the angular momentum \mathbf{j} -vector of desorbing H₂ is more helicopter-like (has greater $A_0^{(2)}(j, T_S)$ values) compared with desorbing D₂. As j increases further, we eventually observe that the \mathbf{j} -vector distribution of desorbing H₂ becomes more

Table 2

The list shows the corresponding estimated critical rotational states j_{crit} , the maximum final rotational state j_{max} accessible to the desorbed H₂(D₂), and the corresponding rotational energy $E_{j_{\text{max}}} = B_{j_{\text{max}}}(j_{\text{max}} + 1)$ for fixed final total kinetic energies E_{tot} . The rotational constant of H₂(D₂) in the gas phase is taken to be $B \approx 7.6(3.8)$ meV, and $V_{\min} = V_{\parallel} \approx 0.5$ eV. From Ref. [89]

	E_{tot} (meV)	\approx	500	600	700	800	900	1000
H ₂	$E_{j_{\text{max}}}$ (meV)	\approx	425	547	684	684	836	836
	j_{max}	\approx	7	8	9	9	10	10
	j_{crit}	\approx	1	2	4	6	7	8
D ₂	$E_{j_{\text{max}}}$ (meV)	\approx	418	593	692	798	798	912
	j_{max}	\approx	10	12	13	14	14	15
	j_{crit}	\approx	1	3	6	8	10	10

isotropic (has smaller $A_0^{(2)}(j, T_S)$ values) compared with desorbing D_2 . To explain this, we recall [87,88] that the initial rotational state j_{ad} of molecules about to form from adsorbed atoms may take any value. We may then suppose that these molecules are most likely initially oriented parallel to the surface ($|m_{jad}| \approx j_{ad}$). Upon introducing a certain amount of energy to the system, e.g. by increasing T_S , all molecules will try to desorb, but not all will necessarily succeed. On their way towards the gas phase, these molecules have to cross a transition region, where a sufficient amount of translational energy is necessary to, at least, overcome the barrier minimum V_{min} . Thus, the metal surface, via the orientation-dependent PES, will act as a sort of *rotational quantum state filter/sieve*, and filter out all rotational states j_{des} greater than some critical rotational state j_{crit} . As a result, only those molecules with rotational state $j_{des} \leq j_{crit}$ will survive and desorb with final rotational states $j \leq j_{max}$ (maximum accessible final rotational state, vide infra). Given V_{min} and E_{tot} , we can roughly estimate j_{crit} and j_{max} by calculating for the corresponding energies $E_{j_{crit}}$ and $E_{j_{max}}$ (cf. Table 2, when $[E_{tot} - V_{min}] > 0$, $E_{j_{crit}} \approx [E_{tot} - V_{min}]$, otherwise $E_{j_{crit}} = 0$, $E_{j_{max}} \approx E_{tot}$). For a fixed E_{tot} , suppose a molecule survives the attempt to desorb, and had a rotational state $j_{des} \approx j_{crit}$ upon desorption. It would mean that the molecule had only just enough translational energy to overcome the barrier minimum V_{min} , which requires that the molecule exhibits helicopter-like rotation ($|m_{j_{des}}| \approx j_{des}$) upon desorption. Thus, as $j_{des} \rightarrow j_{crit}$, a majority of those molecules that did survive the attempt to desorb will exhibit helicopter-like rotations, i.e. $|m_{j_{des}}| \approx j_{des}$. Upon desorption, we find the molecule in the state (j_{des}, m_{des}) , where $|m_{j_{des}}| \leq j_{des} \leq j_{crit} \leq j_{max}$. The molecule will then assume its final rotational state (j, m_j) by either

1. undergoing rotational excitation ($j > j_{des} \geq |m_{j_{des}}| = |m_j|$) at the expense of its

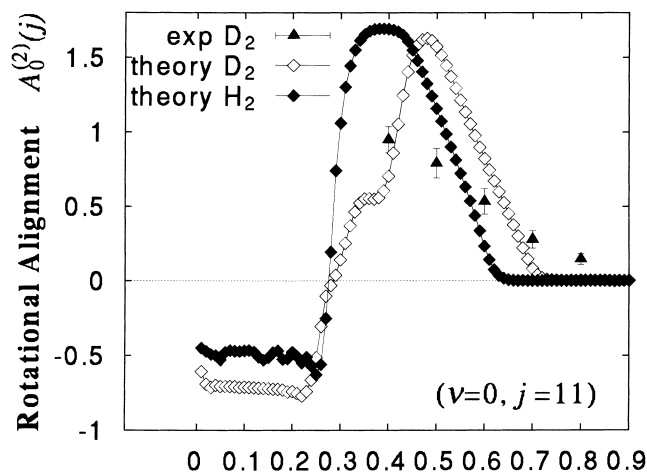


Fig. 35. Comparison between the rotational alignments of D_2 (\diamond) [88] and H_2 (filled \diamond) desorbing in the state $(v=0, j=11, E_t)$ from Cu(111) as a function of the final translational energy E_t . Filled \triangle : experimental results for D_2 ($v=0, j=11$) using REMPI detection [111]. From Ref. [89].

- translational energy E_t , or
2. undergoing rotational de-excitations ($j < j_{\text{des}} \geq |m_{j_{\text{des}}}| = |m_j|$) with a gain in E_t , or
 3. by remaining in the same rotational state ($j = j_{\text{des}} \approx |m_{j_{\text{des}}}| = |m_j|$) and retaining the same E_t .

Thus, those that assume final rotational states $j \leq j_{\text{crit}}$ are more helicopter-like (have greater $A_0^{(2)}(j)$) compared to those that assume final rotational states $j > j_{\text{crit}}$. Because the rotational constant of H_2 is greater than that of D_2 , for the same total kinetic energy E_{tot} , H_2 has lower j_{crit} compared with D_2 (Table 2). As a consequence, Fig. 34 reveals that, upon averaging over the Boltzmann distribution of total kinetic energies at the surface temperature $T_S = 920$ K, the spatial distribution of the angular momentum \mathbf{j} -vector of desorbing H_2 is more helicopter-like (has slightly greater $A_0^{(2)}(j, T_S)$ values) compared with desorbing D_2 , for low j . Furthermore, when j is sufficiently large ($j > 9$), the \mathbf{j} -vector distribution of desorbing H_2 becomes more isotropic (has smaller $A_0^{(2)}(j, T_S)$ values) compared with desorbing D_2 .

As stated earlier, because the quadrupole alignment factors $A_0^{(2)}(j)$ (29) are defined for a particular final rotational state j , corresponding to a particular rotational energy E_j , we can also define the corresponding translational energy (E_t -) dependent quadrupole alignment factors $A_0^{(2)}(j)$. In Fig. 35 we show the calculated $A_0^{(2)}(j)$ results for $\text{H}_2(\text{D}_2)$ desorbing in the state ($\nu = 0, j = 11$) from Cu(111). For reference, also replotted are the experimental results of Auerbach's group [111], for D_2 desorbing in the state ($\nu = 0, j = 11$) from Cu(111). As expected from previous discussions [87,88], $\text{H}_2(\text{D}_2)$ desorbing with translational energies lower than the minimum barrier height ($E_t < V_{\text{min}}$) have correspondingly low total kinetic energies E_{tot} and exhibit cartwheel-like rotational preference (cf. $E_t < 0.3$ eV region in Fig. 35). As E_t increases, corresponding to an increase in E_{tot} , the rotational preference becomes more helicopter-like (cf. $0.3 \leq E_t < 0.6$ eV region in Fig. 35). When the translational energy is sufficiently large ($E_t > V_{\text{min}}$), the desorbing $\text{H}_2(\text{D}_2)$ exhibits an almost orientationally isotropic \mathbf{j} -vector distribution ($A_0^{(2)}(j) \rightarrow 0$), regardless of the final rotational state [86]. For translational energies comparable to the barrier minimum (i.e. $E_t \approx V_{\text{min}}$), the \mathbf{j} -vector distribution of desorbing H_2 is more helicopter-like (has greater $A_0^{(2)}(j)$ values) compared with desorbing D_2 , as expected. As E_t increases, the corresponding \mathbf{j} -vector distribution of desorbing H_2 eventually becomes more spatially isotropic (has smaller $A_0^{(2)}(j)$ values) than does the corresponding \mathbf{j} -vector distribution of desorbing D_2 . It should be noted that we also obtained the same general features as that presented here even for the desorption of $\text{H}_2(\text{D}_2)$ from a Pd-surface [41], which, although it requires an altogether different corresponding set of values for V_{min} and V_{max} (cf. Section 5 Ref. [40] and references therein), is also strongly orientation-dependent.

The discrepancy in magnitude between our results and those of experimental measurements may, in part, be due to our flat-surface model. However, considering the relatively high surface temperatures in actual experiments

[47,48,111], we expect to see only slight corrugation effects, and a higher-dimensional description that takes into account *all* DOF will still exhibit the qualitative features presented here. Furthermore, aside from the relatively large experimental error bars, background signals arising from molecules that reenter the detection volume after undergoing collisions, which are unpolarized and may decrease measured alignments, may not have been sufficiently accounted for [48,112,113], indicating a need for further experimental verifications [112,113].

5. Rotational effects in dynamics of hydrogen on Pd-surface

5.1. Rotational effects in dissociative adsorption dynamics

Upto now, we have considered the activated $\text{H}_2(\text{D}_2)/\text{Cu}(111)$ system, which we can associate with an ‘S’-shaped dissociation probability vs. translational energy curve. However, as expected, not all systems are activated, nor will they show this ‘S’-shaped dissociation curve. A typical example of such a (non-activated) system is $\text{H}_2(\text{D}_2)/\text{Pd}(111)$. In this section, we treat the dissociative adsorption and associative desorption dynamics of $\text{H}_2(\text{D}_2)/\text{Pd}(111)$, and see how the dynamics of such a non-activated system compares with the activated $\text{H}_2(\text{D}_2)/\text{Cu}(111)$ system discussed earlier.

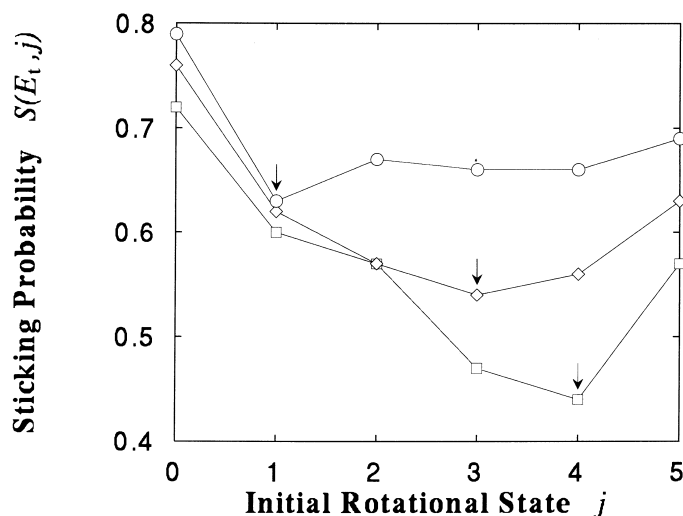


Fig. 36. Experimental results for the j -dependent sticking probability curves for H_2 on Pd(111) for fixed translational energies, E_t . Arrows point to the corresponding minimum for each curve. The curves were obtained by replotting the experimental data of Gostein and Sitz (Table 2 of Ref. [39]). The statistical uncertainties for the sticking probabilities were omitted in the figure for clarity. The corresponding incidence energies E_t , and the location of the minimum for each curve, j_{\min} , are as follows: \square : $E_t = 55 \pm 2$ meV, $j_{\min} = 4$; \diamond : $E_t = 73 \pm 3$ meV, $j_{\min} = 3$; \circ : $E_t = 94 \pm 5$ meV, $j_{\min} = 1$.

More recent advances in molecular-beam-scattering techniques have made it possible to determine the initial rotational state of hydrogen molecules prior to being adsorbed on metal surfaces [37–39]. For the $\text{H}_2/\text{Pd}(111)$ system, Gostein and Sitz [39] directly observed, for the first time, that the sticking (dissociation) coefficient¹ of H_2 on $\text{Pd}(111)$ has a non-monotonic dependence on the initial rotational state of the impinging H_2 (Fig. 36), i.e. first decreasing with increasing initial rotational state ($j = 0 \rightarrow 3$), for low j , then increasing again for higher j ($j = 4, 5$). This interesting feature of the sticking coefficient of $\text{H}_2/\text{Pd}(111)$ as a function of the initial rotational state j of the impinging H_2 reminds us of the SP results inferred from rotationally state-resolved TOF distribution results of Michelsen et al. [31] for D_2 molecules associatively desorbing from $\text{Cu}(111)$. We show in this section that the mechanism behind the non-monotonic j -dependence observed here can be understood by again taking into account the two competing factors working for the dissociative adsorption process, viz. SE or the *dynamical*

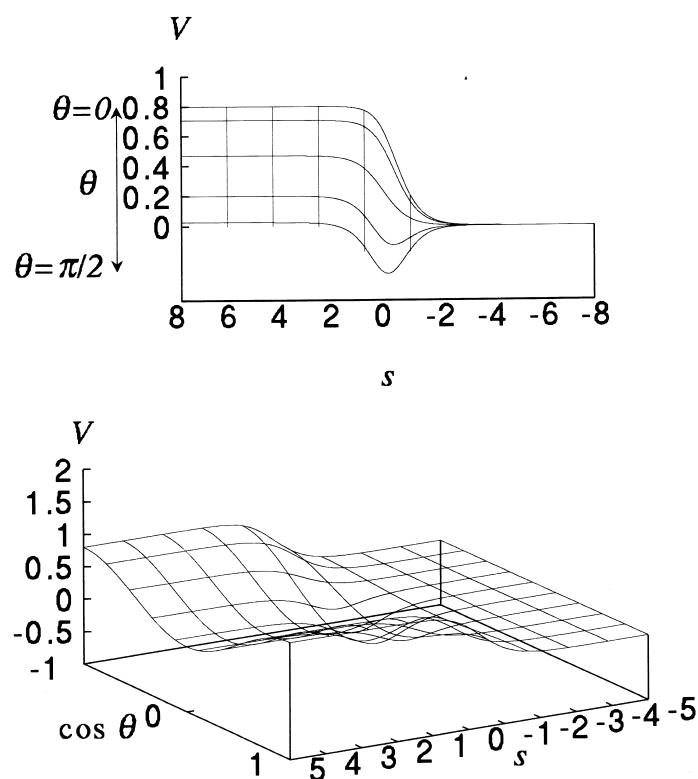


Fig. 37. A molecular orientation dependent activation barrier $V(s, \theta)$ ($E_a = -0.35$ eV, $V_1 = 0.80$ eV, $\beta = 0.25$, and in this figure $\alpha = 1.0 \text{ \AA}^{-1}$). The $+s$ -region corresponds to the surface side. The upper figure shows how the activation barrier changes with the molecular orientation. Notice the corresponding attractive well for a parallel ($\theta = \pi/2$) orientation. From Ref. [36].

reorientation factor, and RTETE or the *rotational assistance via bond-length extension* factor. These factors are similar to the ones observed for the hydrogen on copper system, and come about as a consequence of the orientational dependence of the hydrogen–surface reaction. Another interesting aspect, directly observed from the results of Gostein and Sitz for the sticking coefficients of $H_2/Pd(111)$ (Fig. 36), are the shifts in the SP curve minima, when the incidence energy of H_2 is varied, which, in turn, reminds us of our prediction for the hydrogen on Cu(111) system regarding the shifts in the SP curve minima, when the incidence energy is varied (Section 3.1.2 and Ref. [84]). This stresses the general importance of the incidence energy (velocity) of the impinging hydrogen molecule. Furthermore, we will also show here that considerable isotope effects should be observed for the j -dependence of the adsorption probability of hydrogen on Pd.

To account for the non-monotonic dependence of the SP of H_2 on Pd(111) on the initial rotational state j of the impinging H_2 molecule and to show the significance of the incidence energy E_t in accounting for this interesting behavior, we investigated the reaction of a H_2 molecule impinging a *flat* Pd-surface at *normal incidence* [36,81,84]. Quantal calculations of the SP were carried out by solving the time-independent Schrödinger equation for a H_2 molecule moving under the influence of an orientation-dependent PES corresponding to the H_2/Pd -system [91,92], using the coupled-channel method [34,35] and the concept of a

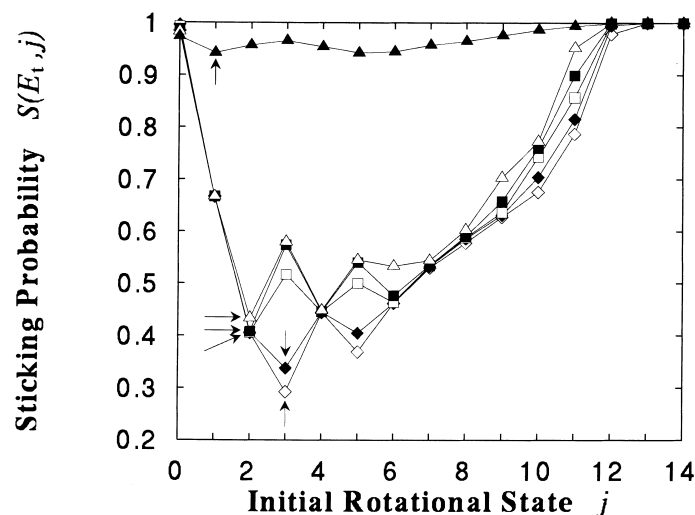


Fig. 38. Numerical results for the j -dependent SP curves for H_2 on Pd(111) in the vibrational ground-state and fixed incidence energies, E_t . Arrows point to the corresponding minimum for each curve. ($H_2/Pd(111)$: $V_{max} = V_{\perp} \approx 0.80$ eV, $V_{min} = V_{\parallel} \approx -0.35$ eV.) The corresponding incidence energies, E_t and the location of the minimum for each curve, j_{min} are as follows: \diamond : $E_t = 45$ meV, $j_{min} = 3$; filled \diamond : $E_t = 55$ meV, $j_{min} = 3$; \square : $E_t = 65$ meV, $j_{min} = 2$; filled \square : $E_t = 75$ meV, $j_{min} = 2$; \triangle : $E_t = 85$ meV, $j_{min} = 2$; filled \triangle : $E_t = 350$ meV, $j_{min} = 2$.

local reflection matrix [90]. The dynamical variables considered are the CM distance of the molecule from the surface Z , and the polar and azimuthal angular orientation of the molecule with respect to the surface, θ and φ , respectively. Our orientationally anisotropic, vibrationally adiabatic, model potential is based on *qualitative features* of available PES plots for H_2/Pd -surface system [91,92] (Fig. 37). The energy barrier for a perpendicular-oriented H_2 molecule was set at $V_{\max} = V_{\perp} \approx 0.80$ eV, and gradually decreased to a value $V_{\min} = V_{\parallel} \approx -0.35$ eV (an *attractive* potential) for a parallel-oriented molecule. The final SP data result from a sum over *all* the contributions from all possible types of rotation (helicopter-type, with the rotational axis of the molecule oriented predominantly perpendicular to the surface, cartwheel-type, with the rotational axis of the molecule oriented predominantly parallel to the surface, or a rotation with the rotational axis oriented intermediate between the two former ones). Section 2 provides more details regarding the calculation method and the actual form of the model potential adopted.

5.1.1. Steering and energy transfer effects

Fig. 38 gives the SP results for H_2 . Aside from the structure in the range $3 \leq j \leq 5$, which is discussed later, good agreement with the experimental trend is found, in that the SP initially decreases with increasing initial rotational state ($j = 0 \rightarrow 3$), for low j , then increases again for higher j ($j > 4$). There is also a general shift of the SP curve minimum towards lower j as the incidence energy increases. The discrepancy in magnitude between our results and experiment is most likely due to our reduced dimensionality. Some sites along the Pd(111) surface have higher barriers to dissociation, or less attractive wells than the one we have considered, which will then reduce the dissociation. Previous studies concerning with the dissociation of H_2 on Cu [59–61,78,114], Pd(100) [77,78,89,90], W(100) [115], and Rh(100) [92,116,117], have shown the importance of surface corrugation and, for a perfect quantitative explanation of the process, a multidimensional description is, of course, required. However, we believe that our basic picture, in which, qualitatively, the non-monotonic dependence of the SP on the initial rotational state j of the impinging hydrogen molecule, and the strong dependence on its incidence energy are general features of an orientation dependent reaction, such as the dissociative adsorption of hydrogen on metal surfaces, will not change. Furthermore, we found the same general features for the j - and E_i -dependence of the SP of H_2 using other values for V_{\max} and V_{\min} .

When a hydrogen molecule approaches a metal surface, it encounters an orientation-dependent PES [59–62,91,92]. In order for the molecule to dissociate and be adsorbed on the surface, it must be able to find the *path of least resistance* (path of least potential), and have enough energy to reach the surface. This process depends on what the initial rotational- and vibrational-states of the impinging hydrogen molecule are, what its incidence energy is, and how long it stays under the influence of the anisotropic PES [36,81,84]. As mentioned earlier (Section 3), in the case of rotation, there are two competing factors working for the dissociation process, viz. the SE (dynamical reorientation) and RTET (via

bond-length extension). The SE, which originates from the orientational dependence of the dissociative adsorption process, pertains to a dynamical reorientation of the impinging molecule towards a more favorable orientation (a predominantly parallel orientation). However, there are two ways by which the SE can reduce the adsorption probability:

1. by shortening the amount of time that the molecule spends in a favorable orientation, or
2. by consuming some translational energy needed for dissociation, in an attempt to reorient molecules that approach the surface with an initially unfavorable orientation to a favorable one.

The SE dominates when the impinging molecule does not have sufficient rotational energy to assist in its adsorption. The RTETE, which originates from the strong coupling between the rotational and translational DOF, pertains to the effective transfer of rotational energy to translational energy. As the molecule approaches the surface, a considerable stretching of the molecular bond-length (*bond-length extension*) occurs, which in turn increases the moment-of-inertia of the molecule, which leads to a corresponding decrease in the rotational constant and, in effect, the rotational energy. Thus, because of the strong coupling between the rotational and translational DOF, if there is no change in the rotational state of the impinging molecule, and the conservation of energy is to be satisfied, any

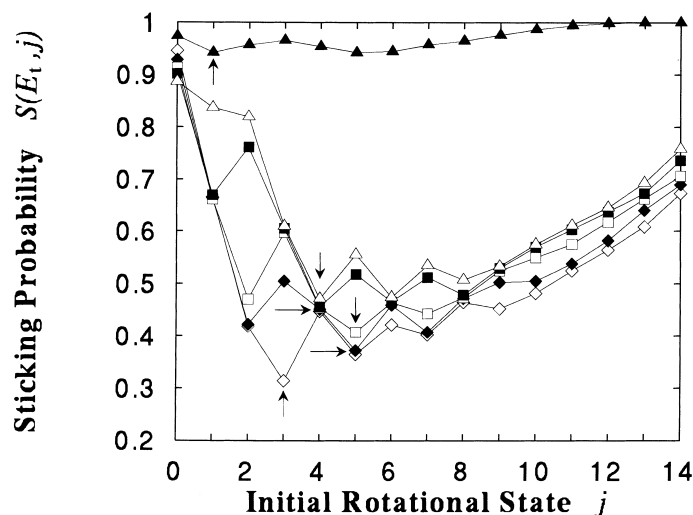


Fig. 39. Numerical results for the j -dependent sticking probability curves for D_2 on Pd(111) in the vibrational ground-state and fixed incidence energies, E_t . Arrows point to the corresponding minimum for each curve. ($D_2/Pd(111)$: $V_{\max} = V_{\perp} \approx 0.80$ eV, $V_{\min} = V_{\parallel} \approx -0.35$ eV.) The corresponding incidence energies, E_t and the location of the minimum for each curve j_{\min} are as follows: \diamond : $E_t = 45$ meV, $j_{\min} = 3$; filled \diamond : $E_t = 55$ meV, $j_{\min} = 5$; \square : $E_t = 65$ meV, $j_{\min} = 5$; filled \square : $E_t = 75$ meV, $j_{\min} = 4$; \triangle : $E_t = 85$ meV, $j_{\min} = 4$; filled \triangle : $E_t = 350$ meV, $j_{\min} = 1$.

decrease in the rotational energy, due to bond-length extension, will be efficiently transferred to the translational energy and assist in the dissociation. RTET dominates when the impinging hydrogen molecule has sufficient rotational energy to assist in its adsorption.

For low initial rotational states, because of the rather small rotational energy, the SE will be dominant. As the molecule approaches the surface, it is steered to different regions of the anisotropic PES. Whether it will reach a point of relatively low potential on time determines whether the molecule will be adsorbed.

For high initial rotational states, the molecule has sufficient rotational energy to assist in dissociation. Furthermore, to the surface the molecule becomes a blur. (In some sense, the surface cannot distinguish in which orientation the molecule is.) Thus, RTET will be dominant.

The combined effect of these two factors leads to an initial decrease and then, eventually, an increase in the SP as the initial rotational state of the impinging molecule is increased for a fixed incidence energy (cf. curve corresponding to 55 meV in Figs. 36 and 38). Because any positive incidence energy given to the impinging hydrogen molecule will be greater than the minimum barrier, as the incidence energy is increased, even a slight contribution from the rotational energy will be sufficient to assist in dissociation. Thus, the efficacy of RTET increases with increasing incidence energy and we see a corresponding shift in the curve minimum towards lower initial rotational states (cf. curves corresponding to 55 and 75 meV in Figs. 36 and 38).

5.1.2. Isotope effects

In addition, we can also observe strong isotope effects when we compare our calculation results for the dissociation of $\text{H}_2/\text{Pd}(111)$ (Fig. 38) with those for $\text{D}_2/\text{Pd}(111)$ (Fig. 39). For the same incidence energy E_t , we can immediately see that the locations of the minima for the SP curves of D_2 are shifted more towards higher rotational states ($j = 5 \rightarrow 8$) (Fig. 39) as compared with those of H_2 ($j = 4 \rightarrow 5$) (Fig. 38), with the H_2 molecules exhibiting higher SP than D_2 molecules in the high j region. Because a D_2 molecule is much slower than a H_2 molecule, even for the same incidence energy E_t , the SE will be more effective with the D_2 molecules than the H_2 molecules. Furthermore, the D_2 molecules have a lower rotational constant compared with H_2 molecules, and we will need higher j states for D_2 before the RTET could dominate and for the SP curve to increase again in the higher j region. Thus, we observe that the minima of the SP curves for D_2 molecules are shifted more towards higher j than those for H_2 molecules.

With regard to the structure in Figs. 38 and 39, because of the form of the PES we have adopted, some trapping processes may occur where the molecules cannot escape and dissociate, because of too much rotation, nor can they be reflected back, because there is not enough translational energy (rotationally mediated selective adsorption). Because these resonances are quantized, the structures in Figs. 38 and 39 could occur, if the total energy coincides with a resonance energy. As we can see, these structures disappear at high rotational states ($j > 10$) and high incidence energies ($E_t = 300$ meV).

5.2. Rotational effects in associative desorption dynamics

5.2.1. Rotational alignment and dynamical quantum filtering

As a *rotational quantum state filter*, how effective is the Pd-surface compared with the Cu surface? To consider this, we again calculated the alignment factors $A_0^{(2)}(j)$ corresponding to each final rotational state j that a D_2 molecule assumes after desorbing from a Pd-surface. (The calculation is as described in Sections 2 and 4.2.) In Fig. 40, we show the calculated E_t -dependent alignment factor $A_0^{(2)}(j)$ results for D_2 molecules desorbing in the vibrational ground-state ($v = 0$) from a Pd-surface, with final rotational states $j = 8 \rightarrow 14$. Unlike the desorption of D_2 from Cu(111) (Fig. 32), there are no molecules doing cartwheel-like rotations, which is to be expected. At the final translational energies E_t , considered in Fig. 40, the corresponding total kinetic energies E_{tot} are small, and the maximum final rotational states j_{max} accessible to the desorbing D_2 molecules are almost the same as the final rotational state j the desorbing D_2 molecules assume, i.e. $j \approx j_{\text{max}}$. Because of the very small barrier minimum for the D_2 /Pd-surface system ($V_{\text{min}} \approx -0.35$ eV), the corresponding critical rotational states j_{crit} are approximately the same as the maximum final rotational state j_{max} accessible to the desorbing D_2 molecules, i.e. $j_{\text{crit}} \approx j_{\text{max}}$. From earlier arguments (Section 4.2), the desorbing molecules are bound to follow the *path of least resistance*, which corresponds to an orientation parallel to the surface and, as a result, the desorbing D_2 molecules will show a helicopter-like rotational preference. Thus, to answer the question we have posed earlier in this section, with low energies

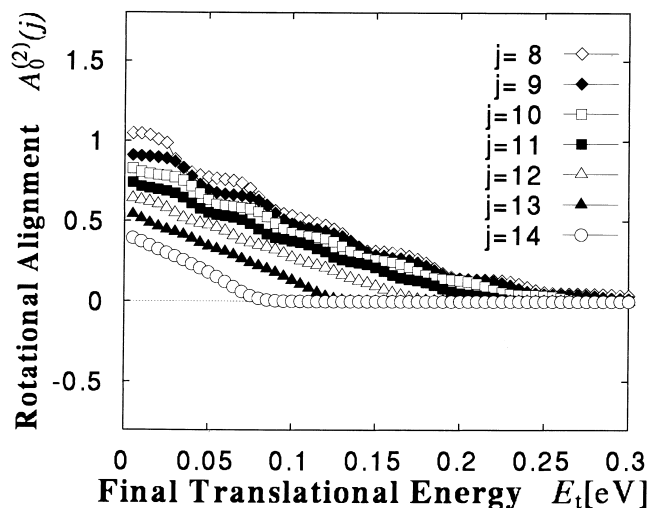


Fig. 40. Rotational alignment for D_2 molecules desorbing in the state ($v = 0, j, E_t$) from a Pd-surface as a function of the final translational energy E_t . Final rotational state $j = 8 \rightarrow 14$. Surface temperature $T_s = 690$ K.

($E_t < 0.25$ eV), as a filter, Pd-surfaces are more effective in producing helicopter-like rotating D_2 molecules, and Cu surfaces are more effective in producing cartwheel-like rotating D_2 molecules (cf. Fig. 32).

6. Conclusions and discussion

The present review is based, in part, on earlier and ongoing studies [36,40,81–88] of orientational effects on the activated [36,81–86] and non-activated [40] dissociation of hydrogen molecules on metal surfaces and the reverse process of association and then desorption from metal surfaces [82–88]. Throughout this study, we have tried to answer the following general questions: What is the role of the molecular orientation on the dynamics of hydrogen-surface reactions? How can this be understood based on the model we have adopted? How can they be verified experimentally? How are they related to earlier experimental results? What further experiments do we need to perform? How feasible are the ideas we have proposed and what immediate use do we have for them?

In Section 2, we gave a full description of the model adopted to study the dynamics of hydrogen on copper and palladium surfaces, and considered both a *rigid* and a *dynamic* surface. We did quantal model calculations using the coupled-channel method [34,66] and the concept of a local reflection matrix [90]. Our model potential was based on the qualitative features of available PES plots for the H_2/Cu surface [36,58–63] (e.g. ab-initio PES calculation results of Ref. [57] shown in Fig. 8) and H_2/Pd -surface [91,92] systems. We also availed ourselves of the reaction-path concept [66].

Section 3 discussed results concerning the rotational effects on the dissociative adsorption dynamics and inelastic scattering dynamics of $H_2(D_2)$ on Cu(111). Our theoretical studies on the influence of molecular orientation on the dynamics of $H_2(D_2)/Cu(111)$, a paradigm of an *activated system*, show very interesting, surprising and general results.

For a *rigid* surface, we [36,40] showed that, due to the *inherent strong orientational dependence* of hydrogen–solid surface reactions and the coupling between the different DOF involved, there are two competing factors working for the dissociative adsorption process, viz. SE or the dynamical reorientation factor and RTET or the rotational assistance via bond-length extension factor [36]. Furthermore, we showed that the SE, which is due to the anisotropic nature of the PES, dominates over the ETE for low initial rotational states j . For high j , the ETE, which arises from the strong coupling between the rotational motion and the motion along the reaction path, dominates. We also showed that the efficacy of these two factors is strongly dependent on the incident translational energy of the impinging hydrogen molecule [84]. For molecules with incidence translational energies that are less than the activation barrier minimum V_{\min} , corresponding to a favorable (parallel) orientation, the SE will not be sufficient in aiding the impinging molecule to dissociatively adsorb on the surface. Thus, ETE will be dominant, when the incidence translational energy is less than the activation

barrier minimum. As a consequence, for a fixed incidence translational energy, the dissociative adsorption probability monotonically increases with increasing initial rotational states of the impinging molecule. As the incidence translational energy increases, the efficacy of the SE begins to increase and, for fixed incidence translational energies, we begin to observe a non-monotonic dependence of the dissociative adsorption probability on the initial rotational state of the impinging molecule. When the incidence translational energy of the molecule is comparable with the barrier maximum, corresponding to an unfavorable (perpendicular) orientation, the molecule will already be travelling at such a high speed that there will not be enough time for the molecule to reorient. As a result, the SE again loses its efficacy, and we observe a monotonic increase in the dissociative adsorption probability as a function of the initial rotational state of the impinging molecule. The two competing factors, mentioned above, seem to be general features of orientation dependent processes, as they were later directly observed for the $\text{H}_2/\text{Pd}(111)$ system [39], which, apart from exhibiting a strong orientation dependence, is described by a totally different PES, as discussed in Section 5.

For a *dynamic* surface, where the surface lattice was modeled as independent Einstein oscillators, we showed that, in addition to the two factors mentioned above (SE and RTET), we have the SRE. As a result, the incidence translational energy dependent dissociative adsorption probability shows a slight increase in magnitude with increasing surface temperatures for low incident translational energies (i.e. $E_t < V_{\min}$), and a slight decrease in magnitude with increasing surface temperatures for high incident translational energies (i.e. $E_t > V_{\min}$).

Section 4 was concerned with the discussion of the rotational effects on the associative desorption dynamics of $\text{H}_2(\text{D}_2)$ on $\text{Cu}(111)$. We were able to consistently relate the calculated adsorption results to the desorption results [84] and, for the first time, reproduce the experimentally observed initial cooling, then a mild heating, followed by a cooling again of the rotational temperature of the desorbing hydrogen molecules with respect to the surface temperature. We were also able to explain the experimentally observed surprisingly low rotational alignment [41,47,48]. Furthermore, we suggested another means by which we could estimate the effective activation barrier experimentally, i.e. by measuring the rotational alignment for different final total kinetic energies and determining the critical rotational states j_{crit} (Table 1), indicated by the peaks appearing in Fig. 30. We also suggested a means by which we could produce oriented hydrogen molecules via the so-called DQF effect [87,88], which takes advantage of the inherent nature of the desorption process to be orientation dependent. A comparison of the alignment results for D_2 molecules desorbing from Cu and Pd-surfaces at low energies indicates that the Cu surface is effective for producing cartwheeling D_2 molecules, and the Pd-surface is effective for producing helicoptering D_2 molecules.

Rotational effects on the dynamics of $\text{H}_2(\text{D}_2)$ on $\text{Pd}(111)$, an example of a *non-activated system*, were treated in Section 5. We showed that the experimental observations for the dissociative adsorption and associative desorption dynamics of H_2 on $\text{Pd}(111)$ could also be explained by considering the three factors

mentioned above, indicating that SE, ET and DQF are general, dynamical features of orientation dependent reactions [40].

So what is next? Although we successfully accounted for various experimental trends that have so far been made, and suggested some new experiments which might further our understanding of hydrogen–solid surface interaction, our task is far from complete. In fact, it would not be an exaggeration to say that the understanding of surface dynamics is far from complete [118]. On the contrary, it can be said that we have just begun. So far, our study concerning the hydrogen–solid surface reaction concentrated on the effects of the molecular orientation of the impinging and/or desorbing hydrogen molecules, and although it has been fairly accurate in explaining recent experimental observations, a fully quantitative agreement between current experimental results and available theoretical results has not yet been achieved. To do so would require an extension of the current fully quantal dynamical calculation to take into consideration higher dimensions, and eventually all the DOF of the impinging/desorbing hydrogen molecules and that of the surface atoms would have to be considered (involving *at least* seven dimensions!). Moreover, there is a need for more ab-initio calculations (cf. Ref. [119] for a review) that would provide further information regarding the effective multidimensional PES governing the hydrogen–solid surface reaction. A list of some of the things we need to do, and are now in progress, are:

1. to consider the feasibility of extending our current fully quantal calculation to higher dimensions via some approach (e.g. Ref. [120]);
2. to study how the other DOF influence the hydrogen–solid surface reaction (e.g. Refs. [121–124]);
3. to study how we could verify and utilize further our current knowledge regarding the hydrogen–solid surface reaction by proposing new experiments and methods;
4. to consider the efficacy of semi-empirical model potentials as compared with interpolation by some functional form to match results of ab-initio calculations (e.g. Refs. [125,126]).

From these further studies, we expect to be able to extend our current fully quantum dynamical calculations to higher dimensions, which, eventually, would have to include all the DOF of the impinging/desorbing hydrogen molecule and the surface atoms. This achievement, in itself, would pave the way for a more thorough understanding of hydrogen–solid surface reactions, and making it possible for a direct quantitative comparison with current and future experimental results involving state-specific reactions.

However, regardless of how successful we are in including all the DOF in our calculation, from physical considerations, we could consider any pair, trio or other combinations of the above DOF dynamically and freeze the others, in which case we expect that we will be able:

1. to clarify how the coupling between the different DOF influences the hydrogen–solid surface reaction;

2. to identify how the total energy may be effectively distributed among the different possible motions of the impinging/desorbing hydrogen molecule;
3. to identify the efficacy of introducing a limited amount of energy to any particular DOF to promote or hinder the reaction between hydrogen molecules and solid surfaces;
4. to suggest new experiments and methods to verify, utilize and further our current knowledge regarding the hydrogen–solid surface reaction;
5. to propose a general model potential that could be easily adapted to different hydrogen–solid surface systems with barrier heights that could be chosen to match those obtained in ab-initio calculations;
6. to extend our current study to more catalytically interesting systems such as those involving alloys and utilize our current knowledge to introduce novel materials and novel means of taking advantage of the inherent nature of the reactions we have studied, that would not only benefit us academically and industrially, but would also be environment friendly.

Thus, from these and future studies, we expect to be able to make significant contributions, not only in attaining a fundamental understanding of different surface reactions, but also in the technological development of novel materials, that are not only user-friendly, but are also environment-friendly. Recently, several researchers proposed ingenious techniques [127–130] to apply combinatorial chemistry — the shotgun approach to chemical discovery, developed and applied extensively by the pharmaceutical industry, whereby researchers synthesize and test hundreds or thousands of compounds simultaneously [127,128] — to find hot novel materials, such as catalysts and superconductors. Although these techniques may succeed in finding new materials that are more efficient than those in commercial use now, the materials found may not always turn out to be ideal, neither user-wise nor environment-wise. On the other hand, it would not be a good business strategy to invest precious funds and not use these materials, just because they involve toxic materials.

What would be more desirable is a systematic theoretical study of the differences in reactivities between different classes of molecules with a surface, and the differences in reactivities between different surfaces with a class of molecules. Insights into the structure of surfaces combined with an understanding of the relation between the surface composition and reactivity could then lead to new ideas for ideal novel materials design. Only then should synthesis, characterization and tests be performed. However, if ever we are to attain a real understanding of why there is an enormous difference in reactivity of different classes of molecules with a surface and also a great difference in reactivity of different surfaces with a class of molecules, we must know the elementary steps involved in the reactions concerned and the identity of the rate-limiting reaction intermediate. Only then, with this knowledge, can we proceed to determine the structure of this reaction complex and relate its reactivity to the electronic nature of the reaction complex through theory.

Acknowledgements

We are grateful to Dr. Hiroshi Nakanishi and Dr. Yoshio Miura for helpful discussions and comments on this work. W.A.D. thanks Professor Wilhelm Brenig for helpful comments and insights during the early stages of this work, and for his continued support. Special thanks to Dr. Moritz F. Hilf, who stayed with us at Osaka University for two months as a special visiting researcher, for helpful discussions, comments and a critical reading of this manuscript. Some of the calculations presented here were done using the computer facilities of the ISSP Supercomputer Center (University of Tokyo), and the Yukawa Institute (Kyoto University). This work is partly supported by the Ministry of Education, Science, Sports and Culture of Japan through their Grants-in-Aid for Creative Basic Research (No. 09NP1201), COE Research (No. 10CE2004), and Scientific Research (No. 11640375) programs, and by the Japan Science and Technology Corporation (JST), through their Research and Development Applying Advanced Computational Science and Technology program. W.A.D. acknowledges Fellowship Grant from the Japanese Society for the Promotion of Science (JSPS), under their JPSJ Postdoctoral Fellowship Program for Foreign Researchers.

References

- [1] P.J. Feibelman, J. Harris, *Nature* 372 (1994) 135.
- [2] B. Cagnac, M.D. Plimmer, L. Julien, F. Biraben, *Rep. Prog. Phys.* 57 (1994) 853.
- [3] Y. Fukai, *The Metal–Hydrogen System*, Springer-Verlag, Berlin, 1993.
- [4] B.M. Andreev, E.P. Magomedbekov, G.H. Sicking, *Interaction of Hydrogen Isotopes with Transition Metals and Intermetallic Compounds*, Springer-Verlag, Berlin, 1996.
- [5] H. Wipf, *Hydrogen in Metals III*, Springer-Verlag, Berlin, 1997.
- [6] M.S. Daw, M.I. Baskes, *Phys. Rev. Lett.* 50 (1983) 1285.
- [7] H. Veholf, in: H. Wipf (Ed.), *Topics in Applied Physics*, vol. 73, Springer-Verlag, Berlin, 1997, p. 215.
- [8] D.P. Gregory, *Sci. Am.* 228 (1973) 13.
- [9] P. Dantzer, in: H. Wipf (Ed.), *Topics in Applied Physics*, vol. 73, Springer-Verlag, Berlin, 1997, p. 279.
- [10] H.A. Michelsen, C.T. Rettner, D.J. Auerbach, in: R.J. Madix (Ed.), *Springer Series in Surface Science*, vol. 34, Springer-Verlag, Berlin, 1994, p. 185.
- [11] K.D. Rendulic, A. Winkler, *Surf. Sci.* 299–300 (1994) 261.
- [12] S. Holloway, *Surf. Sci.* 299–300 (1994) 656.
- [13] W. van Willigen, *Phys. Lett. A* 28 (1968) 80.
- [14] M. Balooch, M.J. Cardillo, D.R. Miller, R.E. Stickney, *Surf. Sci.* 46 (1974) 358.
- [15] M. Balooch, M.J. Cardillo, R.E. Stickney, *Surf. Sci.* 50 (1975) 263.
- [16] M. Grueble, A.H. Zewail, *Phys. Today* 43 (1990) 24.
- [17] R.B. Bernstein, *Chemical Dynamics via Molecular Beam and Laser Techniques*, Oxford University, New York, 1982.
- [18] R.D. Levine, R.B. Bernstein, *Molecular Dynamics and Chemical Reactivity*, Oxford University, New York, 1987.
- [19] G. Ehrlich, in: R. Vanselow, R. Howe (Eds.), *Chemistry and Physics of Solid Surfaces*, vol. 7, Springer-Verlag, Berlin, 1988, p. 1.

- [20] C.T. Rettner, M.N.R. Ashfold, Dynamics of Gas–Surface Collisions, Royal Society of Chemistry, Cambridge, 1991.
- [21] S. Holloway, in: C.T. Rettner, M.N.R. Ashfold (Eds.), Dynamics of Gas–Surface Collisions, Royal Society of Chemistry, Cambridge, 1991, p. 88.
- [22] B.E. Hayden, in: C.T. Rettner, M.N.R. Ashfold (Eds.), Dynamics of Gas–Surface Collisions, Royal Society of Chemistry, Cambridge, 1991, p. 137.
- [23] G.R. Darling, S. Holloway, Rep. Prog. Phys. 58 (1995) 1595.
- [24] C.T. Rettner, D.J. Auerbach, H.A. Michelsen, Phys. Rev. Lett. 68 (1992) 1164.
- [25] H.A. Michelsen, C.T. Rettner, D.J. Auerbach, Surf. Sci. 272 (1992) 65.
- [26] J.-H. Rehtien, R. Harder, G. Herrmann, K.J. Snowdon, Surf. Sci. 272 (1992) 240.
- [27] U. Heinzmann, S. Holloway, A.W. Kleyn, R.E. Palmer, K.J. Snowdon, J. Phys.: Condens. Matter 8 (1996) 3245.
- [28] G.D. Kubiak, G.O. Sitz, R.N. Zare, J. Chem. Phys. 81 (1984) 6397.
- [29] G.D. Kubiak, G.O. Sitz, R.N. Zare, J. Chem. Phys. 83 (1985) 2538.
- [30] L. Schröter, R. David, H. Zacharias, Surf. Sci. 258 (1991) 259.
- [31] H.A. Michelsen, C.T. Rettner, D.J. Auerbach, Phys. Rev. Lett. 69 (1992) 2678.
- [32] H.A. Michelsen, C.T. Rettner, D.J. Auerbach, R.N. Zare, J. Chem. Phys. 98 (1993) 8294.
- [33] C.T. Rettner, H.A. Michelsen, D.J. Auerbach, J. Chem. Phys. 102 (1995) 4625.
- [34] H. Kasai, A. Okiji, Prog. Theor. Phys. Suppl. 106 (1991) 341.
- [35] H. Kasai, A. Okiji, Prog. Surf. Sci. 44 (1993) 101.
- [36] W.A. Diño, H. Kasai, A. Okiji, J. Phys. Soc. Jpn. 64 (1995) 2478.
- [37] C.T. Rettner, D.J. Auerbach, Chem. Phys. Lett. 253 (1996) 236.
- [38] M. Beaul, M. Riedler, K.D. Rendulic, Chem. Phys. Lett. 256 (1996) 33.
- [39] M. Gostein, G.O. Sitz, J. Chem. Phys. 106 (1997) 7378.
- [40] W.A. Diño, H. Kasai, A. Okiji, J. Phys. Soc. Jpn. 66 (1997) 3344.
- [41] D. Wetzig, R. Dopheide, M. Rutkowski, R. David, H. Zacharias, Phys. Rev. Lett. 76 (1995) 463.
- [42] U. Fano, J.H. Macek, Rev. Mod. Phys. 54 (1973) 553.
- [43] C.H. Greene, R.N. Zare, Ann. Rev. Phys. Chem. 33 (1982) 119.
- [44] C.H. Greene, R.N. Zare, J. Chem. Phys. 78 (1983) 6741.
- [45] R.N. Zare, Angular Momentum, Wiley, New York, 1988.
- [46] D. Wetzig, M. Rutkowski, W. Etterich, R. David, H. Zacharias, Surf. Sci. 402–404 (1998) 232.
- [47] D. Wetzig, M. Rutkowski, R. David, H. Zacharias, Europhys. Lett. 36 (1996) 31.
- [48] S.J. Gulding, A.M. Wodtke, H. Hou, C.T. Rettner, H.A. Michelsen, D.J. Auerbach, J. Chem. Phys. 105 (1996) 9702.
- [49] E.E. Marinero, C.T. Rettner, R.N. Zare, Phys. Rev. Lett. 19 (1982) 1323.
- [50] S.L. Anderson, G.D. Kubiak, R.N. Zare, Chem. Phys. Lett. 105 (1984) 22.
- [51] P.K. Johansson, Surf. Sci. 104 (1981) 510.
- [52] A. Okiji, H. Kasai, A. Kato, J. Phys. Soc. Jpn. 51 (1982) 3291.
- [53] P. Madhavan, J.L. Whitten, J. Chem. Phys. 77 (1982) 2673.
- [54] J. Harris, S. Andersson, Phys. Rev. Lett. 55 (1985) 1583.
- [55] C. Engdahl, B.I. Lundqvist, U. Nielsen, J.K. Nørskov, Phys. Rev. B 45 (1992) 11362.
- [56] J.E. Müller, Appl. Phys. A49 (1989) 681.
- [57] J.E. Müller, Surf. Sci. 272 (1992) 45.
- [58] K. Tanada, Master thesis, Faculty of Engineering, Osaka University, Japan, 1993.
- [59] B. Hammer, M. Scheffler, K.W. Jacobsen, J.K. Nørskov, Phys. Rev. Lett. 73 (1994) 1400.
- [60] J.A. White, D.M. Bird, Chem. Phys. Lett. 213 (1993) 422.
- [61] J.A. White, D.M. Bird, M.C. Payne, I. Stich, Phys. Rev. Lett. 73 (1994) 1404.
- [62] P. Kratzer, B. Hammer, J.K. Nørskov, Surf. Sci. 359 (1996) 45.
- [63] G. Wiesnekker, G.J. Kroes, E.J. Baerends, J. Chem. Phys. 104 (1996) 7344.
- [64] A. Hanbicki, E.W. Plummer, in: K. Tanaka (Ed.), Proceedings of the Oji Seminar on Chemical Processes at Surfaces based on Atomic Scale Structure and Dynamics, WORDS Publishing House, Tokyo, 1996, p. 1.
- [65] M.R. Hand, S. Holloway, J. Chem. Phys. 91 (1989) 7209.

- [66] W. Brenig, H. Kasai, Surf. Sci. 213 (1989) 170.
- [67] J. Harris, Surf. Sci. 221 (1989) 335.
- [68] D. Halstead, S. Holloway, J. Chem. Phys. 93 (1990) 2859.
- [69] A. Okiji, H. Kasai, in: A. Yoshimori, T. Shinjo, H. Watanabe (Eds.), Springer Series in Materials Science, vol. 17, Springer-Verlag, Berlin, 1992, p. 253.
- [70] A. Gelb, M. Cardillo, Surf. Sci. 59 (1976) 128.
- [71] C.Y. Lee, A.E. DePristo, J. Chem. Phys. 87 (1987) 1401.
- [72] A. Kara, A.E. DePristo, J. Chem. Phys. 88 (1988) 5240.
- [73] S. Holloway, J. Phys.: Condens. Matter 3 (1991) S43.
- [74] J. Sheng, J.Z.H. Zhang, J. Chem. Phys. 97 (1992) 6784.
- [75] G.R. Darling, S. Holloway, J. Chem. Phys. 101 (1994) 3268.
- [76] T. Brunner, W. Brenig, Surf. Sci. 317 (1994) 303.
- [77] A. Gross, B. Hammer, M. Scheffler, W. Brenig, Phys. Rev. Lett. 73 (1994) 3121.
- [78] A. Gross, J. Chem. Phys. 102 (1995) 5045.
- [79] A. Gross, S. Wilke, M. Scheffler, Phys. Rev. Lett. 75 (1995) 2718.
- [80] J. Dai, J.C. Light, J. Chem. Phys. 107 (1997) 1676.
- [81] W.A. Diño, H. Kasai, A. Okiji, Surf. Sci. 363 (1996) 52.
- [82] H. Kasai, W.A. Diño, A. Okiji, in: A. Okiji, H. Kasai, K. Makoshi (Eds.), Springer Series in Solid-State Science, vol. 121, Springer-Verlag, Berlin, 1996, p. 99.
- [83] H. Kasai, W.A. Diño, A. Okiji, in: K. Tanaka (Ed.), Chemical Processes at Surfaces based on Atomic Scale Structures and Dynamics, WORDS Publishing House, Tokyo, 1996, p. 223.
- [84] W.A. Diño, H. Kasai, A. Okiji, Phys. Rev. Lett. 78 (1997) 286.
- [85] H. Kasai, W.A. Diño, A. Okiji, Butsuri 52 (1997) 824 (in Japanese).
- [86] A. Okiji, H. Kasai, W.A. Diño, in: J.L. Moran-Lopez (Ed.), Current Problems in Condensed Matter: Theory and Experiments, Plenum Press, New York, 1998, pp. 275–282.
- [87] W.A. Diño, H. Kasai, A. Okiji, J. Phys. Soc. Jpn. 67 (1998) 1517.
- [88] W.A. Diño, H. Kasai, A. Okiji, Surf. Sci. 418 (1998) L39.
- [89] W.A. Diño, H. Kasai, A. Okiji, Surf. Sci. 427–428 (1999) 358.
- [90] W. Brenig, T. Brunner, A. Groß, R. Russ, Z. Phys. B 93 (1993) 91.
- [91] S. Wilke, M. Scheffler, Phys. Rev. B 53 (1996) 4926.
- [92] A. Eichler, G. Kreese, J. Hafner, Surf. Sci. 397 (1998) 116.
- [93] S. Goldstone, K.J. Laidler, H. Eyring, The Theory of Rate Processes, McGraw-Hill, New York, 1941.
- [94] H.A. Michelsen, D.J. Auerbach, J. Chem. Phys. 94 (1991) 7502.
- [95] L.D. Landau, E.M. Lifshitz, Quantum Mechanics, 3rd ed., Pergamon Press, Oxford, 1977 (§25, Problem 4).
- [96] H. Kasai, A. Okiji, Surf. Sci. 242 (1991) 394.
- [97] R.A. Marcus, J. Chem. Phys. 41 (1964) 603, 610, 2614.
- [98] R.A. Marcus, J. Chem. Phys. 45 (1966) 4493, 4500.
- [99] C.C. Rankin, J.C. Light, J. Chem. Phys. 51 (1969) 1701.
- [100] G. Miller, J.C. Light, J. Chem. Phys. 54 (1971) 1635, 1643.
- [101] M.R. Hand, J. Harris, J. Chem. Phys. 92 (1990) 7610.
- [102] W. Brenig, H. Kasai, H. Müller, Surf. Sci. 161 (1985) 608.
- [103] W. Brenig, H. Kasai, H. Müller, in: A. Yoshimori, M. Tsukada (Eds.), Springer Series in Solid-State Physics, vol. 50, Springer-Verlag, Berlin, 1985, p. 2.
- [104] A. Groß, Surf. Sci. 314 (1994) L843.
- [105] A. Groß, Surf. Sci. 320 (1994) L68.
- [106] G.R. Darling, S. Holloway, Surf. Sci. 321 (1994) L189.
- [107] J. Harris, J. Simon, A.C. Luntz, C.B. Mullins, C.T. Rettner, Phys. Rev. Lett. 67 (1991) 652.
- [108] A.C. Luntz, J. Harris, Surf. Sci. 258 (1991) 397.
- [109] D.J. Auerbach, C.T. Rettner, H.A. Michelsen, Surf. Sci. 283 (1993) 1.
- [110] C. Engdahl, B.I. Lundqvist, Chem. Phys. Lett. 215 (1993) 103.
- [111] H. Hou, S.J. Gulding, C.T. Rettner, A.M. Wodtke, D.J. Auerbach, Science 277 (1997) 80.
- [112] H. Zacharias, private communications.

- [113] D.J. Auerbach, private communications.
- [114] J. Dai, J.Z.H. Zhang, *J. Chem. Phys.* 102 (1995) 6280.
- [115] M. Kay, G.R. Darling, S. Holloway, J.A. White, D.M. Bird, *Chem. Phys. Lett.* 245 (1995) 311.
- [116] P.J. Feibelman, *Phys. Rev. Lett.* 67 (1991) 461.
- [117] A. Eichler, G. Kresse, J. Hafner, *Phys. Rev. Lett.* 77 (1996) 1119.
- [118] R.J. Madix, in: R.J. Madix (Ed.), *Springer Series in Surface Science*, vol. 34, Springer-Verlag, Berlin, 1994, p. 1.
- [119] G.P. Brivio, M.I. Trinio, *Rev. Mod. Phys.* 71 (1999) 231.
- [120] W. Brenig, R. Brako, M.F. Hilf, *Z. Phys. Chem.* 197 (1996) 237.
- [121] A. Gross, *Surf. Sci. Rep.* 32 (1998) 291.
- [122] G.J. Kroes, *Prog. Surf. Sci.* 60 (1999) 1.
- [123] Y. Miura, H. Kasai, W.A. Diño, A. Okiji, *J. Phys. Soc. Jpn.* 68 (1999) 887.
- [124] Y. Miura, H. Kasai, W.A. Diño, A. Okiji, *Surf. Sci.*, 438 (1999) 254.
- [125] D.E. Makarov, H. Metiu, *J. Chem. Phys.* 108 (1998) 590.
- [126] A. Gross, M. Scheffler, M.J. Mehl, D.A. Papaconstantopoulos, *Phys. Rev. Lett.* 82 (1999) 1209.
- [127] R.F. Service, *Science* 280 (1998) 1690.
- [128] I.E. Maxwell, *Nature* 394 (1998) 325.
- [129] E. Reddington, A. Sapienza, B. Gurau, R. Viswanathan, S. Sarangapani, E.S. Smotkin, T.E. Mallouk, *Science* 280 (1998) 1735.
- [130] S.M. Senkan, *Nature* 394 (1998) 350.



PERGAMON

Progress in Surface Science 72 (2003) 53–86

Progress in
SURFACE
SCIENCE

www.elsevier.com/locate/progsurf

Surface science-based reaction design: increasing the *ortho*–*para* hydrogen conversion yield via molecular orientation, a case study

Hideaki Kasai ^{*}, Wilson Agerico Diño, Rifki Muhida

Department of Applied Physics, Osaka University, Suita, Osaka 565-0871, Japan

Abstract

One of the ultimate goals of surface science is to be able to design and control reactions as they progress on surfaces. This entails an atomic-level understanding of the fundamental principles (elementary processes) underlying the bond-making and bond-breaking at surfaces. Our current understanding has gained significantly from systematic experimental and theoretical studies on such benchmark systems as the interaction of hydrogen with metal surfaces. Yet, fundamental, examples of surface science-based reaction design are extremely few. Here, we consider the *ortho*–*para* (*o*–*p*) H₂ conversion as a case study. We invoke two processes derived from fundamental, surface science insights, based on the effect of *molecular orientation* on the hydrogen–solid surface reaction, viz., *dynamical quantum filtering* (DQF) and *Steering*, and apply them to enhance the *o*–*p* H₂ conversion yield/rate. The orientation dependence of the *o*–*p* H₂ conversion (*steric effect*, SE) dictates that cartwheel-like rotating (CLR) H₂ will have a higher rate of conversion than helicopter-like rotating (HLR) H₂. Applying DQF, we can then prepare rotationally aligned H₂, doing either HLR or CLR. This enables us to increase the *o*–*p* H₂ conversion yield.

© 2003 Elsevier Science Ltd. All rights reserved.

Keywords: Hydrogen; Deuterium; Copper; Palladium; Low index single crystal surfaces; Chemisorption; Dissociative adsorption/associative desorption; Quantum effects; Potential energy surface; Density functional theory; Vibrational excitation; Rotational excitation; Coupled channel method; Steric/steering effect(s); Dynamical quantum filter(ing); Orthohydrogen–Parahydrogen conversion; Reaction design; Hyperfine (Fermi) contact interaction

^{*} Corresponding author. Tel.: +81-6-6879-7857; fax: +81-6-6879-7859.

E-mail address: kasai@dyn.ap.eng.osaka-u.ac.jp (H. Kasai).

Contents

1. Introduction	54
1.1. Why hydrogen?	55
1.2. Why the ortho–para hydrogen conversion process?	56
2. Model system	59
2.1. The surface	59
2.2. The Hamiltonian and the <i>o</i> – <i>p</i> H ₂ conversion process	60
2.3. The wavefunctions	63
3. Orientation dependence of <i>o</i> – <i>p</i> H ₂ conversion	64
3.1. H ₂ –surface distance <i>Z</i> –dependence	68
3.2. Incident energy dependence	69
4. Steric effect on <i>o</i> – <i>p</i> H ₂ conversion	71
5. Dynamical quantum filtering via scattering	75
6. Increasing the <i>o</i> – <i>p</i> H ₂ conversion yield	81
7. Conclusions and discussion	82
Acknowledgements	83
References	84

1. Introduction

One of the ultimate goals of surface science is to be able to design and control reactions as they progress on surfaces [1]. This entails an atomic-level understanding of fundamental principles (elementary processes) underlying, among others, the bond-making and bond-breaking at surfaces. With the advent of sophisticated experimental techniques to study various dynamical processes on solid surfaces, e.g., initial molecular state preparation, energy- and state-resolved detection techniques, the study of dynamical processes occurring on solid surfaces is now at the stage where there is a more direct link between what experimental studies observe and what theory predicts. It would not be an exaggeration to say that, in surfaces we have a playground for physics, and the study of dynamical processes occurring on solid surfaces, such as the ones mentioned above, is a rich field for new discoveries and observations of novel physical phenomena, filled with many possibilities. Our current understanding has thus gained significantly from systematic experimental and theoretical studies on such benchmark systems as the interaction of hydrogen with metal surfaces (cf., e.g., [2–16]). Although several proposals (e.g., [17–20])

Nomenclature

CM	center of mass
CLR	cartwheel-like rotation
CLR H ₂	cartwheel-like rotating H ₂
DOF	degree(s) of freedom
DQF	dynamical quantum filter/dynamical quantum filtering
ETE	energy transfer effect
HLR	helicopter-like rotation
HLR H ₂	helicopter-like rotating H ₂
LIF	laser-induced fluorescence
<i>o</i> -H ₂	ortho-hydrogen
<i>p</i> -H ₂	para-hydrogen
PES	potential energy (hyper-) surface(s)
REMPI	resonance-enhanced multiphoton ionization
SE	steric/steering effect(s)

and references therein) have been made, examples (cf., e.g., [21,22]) of catalyst design on the basis of these fundamental, surface science-based insights are extremely few.

1.1. Why hydrogen?

Hydrogen is probably the most important of all elements, both for its abundance in the universe and for its theoretical interest [23]. It is the only stable neutral two-body system, and its energy levels can be calculated with an accuracy far higher than for any other element (currently of the order 10^{-11} cm⁻¹). In addition, atomic hydrogen possesses a rich spectrum of resonances ranging from radio to ultra-violet frequency and is thus a fertile ground for experimentalists. Several of its absorption resonances are particularly sharp and thus very suitable for metrology. For these reasons, the hydrogen atom has always played a central role in the development of modern physics. With hydrogen, one could, by performing measurements of its energy-level separations, make precise tests of current theories. Thus, the most natural test particle of choice is *hydrogen*.

The understanding of how hydrogen interacts with various materials is also of broad interest. From a technological point of view [24–26], the interactions of hydrogen with solids are influential in a number of industrial processes, and in energy and power systems. An outstanding technological problem concerns the degradation in the mechanical, electrical, and magnetic properties of these materials to the point of rendering them unreliable, upon interaction with hydrogen [27,28]. From an academic point of view, hydrogen is the simplest possible adsorbate. Thus, an understanding of how hydrogen behaves, when it approaches and subsequently comes

into contact with some surface, should give us the most fundamental view of gas–surface interaction.

From an environmental point of view, hydrogen has also been attracting a lot of attention. The idea of using hydrogen as a fuel is not a new one, but interest in it grew in recent years, as a result of increasing concern for the environment. With WATER as the only EMISSION from hydrogen combustion, hydrogen is being promoted as the POWER SOURCE of the future. In order to support this developing hydrogen economy [29], infrastructures have to be built. Development of efficient processes for hydrogen extraction, and efficient processes and materials for hydrogen storage [30] would also be necessary. Thus, from an economics point of view, the transition to an economy based on hydrogen (energy) could, in the long run, also serve as key to solving the problems we are currently facing.

1.2. Why the ortho–para hydrogen conversion process?

The so-called power source of the future comes with drawbacks. Among other things, the gas is so lightweight that it is tough to store enough of it for use, e.g., in a vehicle's tank. Hydrogen can be stored in liquid form, but a substantial amount of energy is needed to chill it to the extremely low temperatures required ($-253\text{ }^{\circ}\text{C}$).

Another drawback comes from H_2 having two forms (cf., e.g., [2,3,5]), viz., orthohydrogen (*o*- H_2) and parahydrogen (*p*- H_2). They differ in their relative nuclear spin orientations and, as a result of the Pauli principle, in the rotational energy levels j they occupy. The three (symmetric) nuclear spin states ($|\uparrow\uparrow\rangle$, $|\uparrow\downarrow\rangle + |\downarrow\uparrow\rangle$, $|\downarrow\downarrow\rangle$) are associated with odd j levels, to give *o*- H_2 . The one (antisymmetric) state ($|\uparrow\downarrow\rangle - |\downarrow\uparrow\rangle$) is associated with even j levels, to give *p*- H_2 . At $T = 0\text{ K}$, only the $j = 0$ rotational state is occupied, so at thermal equilibrium at low temperatures a sample of hydrogen gas is pure *p*- H_2 . At high temperatures, the gas is a mixture of both forms in the ratio of three parts *o*- H_2 to one part *p*- H_2 . The two forms have different rotational contributions to their heat capacities on account of the difference in availability of rotational states. The two forms of H_2 also differ in their magnetic properties, in addition to their difference in thermal properties [31]. The realignment of nuclear spins is slow in the absence of dissociative adsorption or paramagnetic materials, and the 3:1 mixture persists for long periods at low temperatures. However, as much as 3–4% of the hydrogen will still boil-off everyday, due to the heat released when *o*- H_2 convert to *p*- H_2 . This causes a problem. For example, although most of this boil-off will be used, e.g., by vehicles, it would be a concern for cars parked for several days between trips.

In order to limit the boil-off to low levels, it is necessary to fill the tanks with liquid hydrogen that has been processed to an equilibrium composition of almost 100% *p*- H_2 . To do this, we present here a simple, cost-effective method for increasing the *o*–*p* H_2 conversion yield, using insights from surface science. We hope that this would serve as a catalyst for further efforts to apply surface science-based insights into solving some of our more pressing needs, particularly in the design and fabrication of novel, energy-efficient, user- and environment-friendly materials and devices., esp., with recent growing concern for the environment.

There are two general methods of inducing an o - p H_2 transition. One method consists of dissociating H_2 and then inducing the two H to recombine again. When dissociated, the nuclear spin states of the two atomic nuclei are no longer orientationally restricted by the rotational states of the H_2 . Upon recombination, H_2 are formed according to the equilibrium energy distribution determined by the temperature of the system. The other method involves the interaction between an inhomogeneous magnetic field, produced by some magnetic material, and the magnetic field associated with the nuclear spin of the H_2 nuclei [5,31]. The magnetic field is produced along the axis of rotation of the nuclear spin, such that the external field causes a reversal of spin in one of the nuclei. This spin reversal is equivalent to an o - p H_2 transition [31]. In order for the catalyst to induce an o - p H_2 conversion, the H_2 must be brought close enough to the magnetic material/catalyst for the inhomogeneous magnetic field of the paramagnetic component of the catalyst to influence the H_2 [31].

Since 1933, studies on o - p H_2 conversion have been done mainly to look for the best catalyst for o - p H_2 conversion [32–38]. The materials that have been used extensively (since 1947) as catalysts for the o - p H_2 conversion are metal oxides [5,35]. Besides being good catalysts, metal oxides provide a natural framework for experimental test of the theory [35]. In 1986, it was shown that an impurity electron sitting on a metal oxide surface plays an important role in the conversion mechanism and can enhance the o - p H_2 conversion yield [35]. Recently, a new mechanism (XY process) for o - p conversion of H_2 on metal oxide surfaces was introduced [5,35–37]. Here X represents the electrostatic perturbation felt by a 3d electron on the surface of the catalyst, from the H_2 physisorbed in front of the catalyst surface, that induces a charge transfer between the H_2 and the 3d impurity of a surface. By incorporating part of the molecular orbital, the d electron reaches more easily the nucleus of hydrogen, enlarging the resulting hyperfine (Fermi) contact Y [36,39]. Recently, the XY process was applied to investigate the charge transfer process between a physisorbed H_2 and a metal oxide surface [37]. For issues related to the o - p H_2 conversion, we refer the interested readers to [2,3,5,31], and references therein. So far, the H–H bond orientation with respect to the surface normal θ has never entered into consideration.

One of the driving forces behind this idea is the already well-known inherent feature of $H_2(D_2)$ -solid surface reactions (and, in general, any reaction) to be strongly dependent on the orientation of the $H_2(D_2)$ with respect to the surface [14]. One consequence of this strong orientation dependence of the $H_2(D_2)$ -surface reaction is the concept of *Steering* [14] (and references found therein). *Steering* pertains to the dynamical reorientation of the impinging molecule, with respect to the surface components, in an attempt to follow the *path of least resistance*, i.e., to assume an orientation with the least potential, which is due to the strong molecular orientation dependence of the effective potential energy (hyper-) surface (PES). We could also say that this pertains to the capability of the orientation-sensitive PES to reorient the molecule from an initially *unfavorable* orientation to a *favorable* one, or vice versa. The orientation of the molecule upon encountering the surface determines the ground-state energy of the molecule-surface electron system, which, in turn, serves as the effective/relevant PES that determines the dynamics of the molecule-surface

reaction. By taking into account *Steering* (which allows for the dynamical reorientation [14] of the impinging $H_2(D_2)$ to a more favorable orientation, thus enabling it to undergo some desired reaction, e.g., dissociation on Cu(1 1 1)), one could explain the nonmonotonic dependence of the $H_2(D_2)$ dissociation dynamics on solid surfaces (e.g., Cu(1 1 1), on the initial rotational state of the $H_2(D_2)$) [8,11–14,40–42]. It was also shown that *Steering* is a general feature/concept, that is present regardless of whether the system is activated or not [43]. Its efficacy, however, strongly depends on the translational energy of the impinging $H_2(D_2)$ [44,45]. Later on, it was demonstrated how the concept of *Steering* could also explain the nonmonotonic initial translational energy dependence of H_2 dissociation on Pd(1 0 0) [46]. Another feature of the $H_2(D_2)$ -solid surface reaction, which can also be inferred from its inherently strong dependence on the $H_2(D_2)$ orientation, is the possibility of *dynamically quantum filtering* (DQF) [47–49] $H_2(D_2)$, so that we get rotating $H_2(D_2)$ whose rotational axes are at particular orientations with respect to the surface. Thus, in principle, it would be possible to prepare $H_2(D_2)$ such that we can have a beam of molecules all doing helicopter-like rotations (HLRs) or cartwheel-like rotations (CLRs). It was also recently shown that it is also feasible to implement DQF via $H_2(D_2)$ scattering [53].

From the discussions above, one could immediately infer that $H_2(D_2)$ is very sensitive to even the slightest variations in the *local* properties of the surface [50–52]. Thus, we can expect that such orientation dependence would also play an important role in enhancing *o-p* H_2 conversion. To implement *Surface Science-Based Reaction Design* to the above-mentioned problem, we invoke two general surface science concepts, derived as a consequence of systematic experimental and theoretical studies on the effect of *molecular orientation* on the hydrogen-solid surface reaction, viz., DQF and *Steering* (*steric effect*, SE), and apply them to enhance the *o-p* H_2 conversion yield/rate. SE (orientation dependence of *o-p* H_2 conversion) dictates that cartwheel-like rotating (CLR) H_2 will have a higher conversion rate/yield than helicopter-like rotating (HLR) H_2 . DQF enables us to separate CLR H_2 from HLR H_2 . Thus, increasing the conversion efficiency (*vide infra*).

This article is based, in part, on earlier and ongoing studies [4,6,9,17–20,40,43,44,47–49,53–57] on orientational effects on the activated [9,40,44,54–57] and the nonactivated [43] dissociation of hydrogen molecules on metal surfaces, the reverse process of association and then desorption from metal surfaces [6,9,44,47–49,55–57], and the enhancement of the *o-p* H_2 conversion yield/rate [58–62]. For a recent review of the current state of the art in experimental techniques on hydrogen interaction with surfaces, we refer the interested readers to, e.g., [7,10,15,16], and references therein. For a review on the theory, cf., e.g., [4,6,8,9,11,13,14], and references therein.

In Section 2, we give a full description of the model we adopted to study the interaction between a H_2 and a metal oxide surface [58]. For the metal oxide surface, we consider the B-terminated (0 0 1) surface of an ABO_3 perovskite, e.g., $SrTiO_3$. We assume that a 3d impurity is sitting on the metal oxide surface where there is a crystal field splitting of d orbitals. In this section also we introduce the perturbation Hamiltonian necessary to induce the *o-p* H_2 conversion based on a two-step process,

which involves the hyperfine (Fermi) contact interaction [39] and the Coulomb interaction. In Section 3 we show how the molecular orientation can influence the o - p H_2 conversion [58]. We describe the o - p H_2 conversion yield as functions of the H_2 -surface distance Z , and the H–H bond orientation angle θ , with respect to the surface normal. In this section, we also consider how it is possible to induce an o - p H_2 conversion via scattering of the H_2 , and again on how the o - p H_2 conversion yield depends on the H–H bond orientation with respect to the surface normal and the initial translational energy of the impinging H_2 [59]. In Section 4 we examine how the o - p H_2 conversion yield would differ for a HLR H_2 as compared to a CLR H_2 [60,62]. In Section 5, after briefly mentioning how DQF works in the associative desorption of $H_2(D_2)$ from surfaces [14,47–49], we demonstrate the DQF process in the scattering of H_2 on a metal surface [53]. In Section 6 we introduce a new method to enhance the o - H_2 to p - H_2 (o - p H_2) conversion yield/rate of a H_2 interacting with a solid surface. This method consists of two steps and involves the DQF process and the SE on the o - p H_2 conversion [61]. Overall conclusions, summary, and discussions appear in Section 7.

2. Model system

2.1. The surface

In 1986, it has been shown by Ilisca and Sugano that the impurity electron of metal oxide surfaces play an important role in the conversion mechanism [35]. Besides being good catalysts, metal oxides provide a natural framework for experimental test of the theory [5]. It is worth noting that this was the first time that the surface electron degrees of freedom (DOF) were made to participate, and found efficient, in enhancing the o - p H_2 conversion yield. In this context the geometry of the surface electron distribution becomes important. They found that the positions of the surface magnetic impurities with respect to the oxygen ionic planes, the surface electronic distribution and the related electric potential both above and under the surface plane, and the sharing of electrons between the magnetic impurity and the hydrogen molecule all influence the o - p H_2 conversion [5].

Here, we will consider another factor, the H_2 orientation, and show how it plays an important role in influencing the o - p H_2 conversion yield. To demonstrate this, we follow [37] and consider the B-terminated (001) surface of an ABO_3 metal oxide, such as $SrTiO_3$ [37,63–68]. We then assume that the surface ion B (e.g., Ti^{4+}) is replaced by an ion containing an open 3d shell, which we call a 3d impurity. We assume that this 3d impurity sits on the surface and surrounded by five O^{2-} ions [37,69], which give rise to a crystal field potential that quenches the orbital angular momentum by introducing the crystal field splitting of the d orbitals [69]. We also suppose [37,63] that the 3d energy levels lie in the gap of the substrate about 4 eV below the vacuum level [37,63], and coupling between the 3d orbital and the oxygen is already included in the Slater parameters we will introduce later on [37,63]. We assume that the ground state corresponds to one electron occupying either the $|xz\rangle$ or

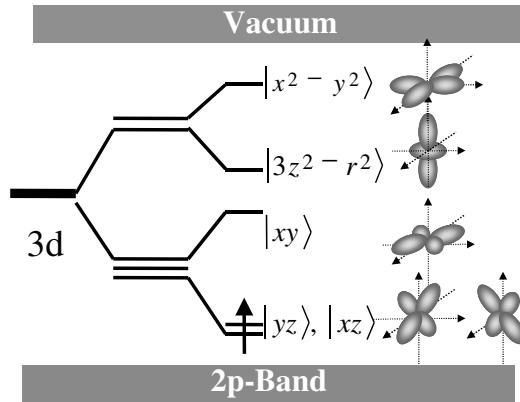


Fig. 1. 3d orbitals of a metal oxide (perovskite) surface. We supposed that the 3d energy levels lie in the gap of the perovskite substrate about 4 eV below the vacuum [37,63] and the coupling between the 3d orbital and the oxygen has already been included in the Slater parameters. We assume that, in the ground state, one electron initially occupies either the $|yz\rangle$ or the $|xz\rangle$ orbital. From [37,38,63–69].

the $|yz\rangle$ orbital. There are five d orbitals that can be listed in order of decreasing energy levels [37,38,63–69] (see Fig. 1), viz., $|x^2 - y^2\rangle$, $|3z^2 - r^2\rangle$, $|xy\rangle$, and the doubly degenerate $|xz\rangle$ and $|yz\rangle$ orbitals. The electron density in the $|x^2 - y^2\rangle$ orbital is distributed in the XY plane and overlaps with the O^{2-} ions along the X - and Y -axes, and the $|x^2 - y^2\rangle$ orbital has a high energy level. The electron density in the $|3z^2 - r^2\rangle$ orbital is distributed along the surface normal Z , avoiding the O^{2-} ion repulsion. In the $|xy\rangle$ orbital, the electron density is distributed on the XY -plane, but rotated by $\pi/4$ with respect to the X - and Y -axes. For the doubly degenerate $|xz\rangle$ and $|yz\rangle$ orbitals, the top/edge of the electron density is distributed above and below the O^{2-} ions [38,69].

In Fig. 2, we show the model system we have just described above. The molecular orientation with respect to the surface normal is given by θ , molecular center-of-mass (CM) distance from the surface is given by Z , the bond length is given by r , and the azimuthal orientation of the H–H bond with respect to the X -axis is given by ϕ . m_a and m_b correspond to the masses of H atoms a and b, respectively. \mathbf{r}_a and \mathbf{r}_b denote the position vectors of protons a and b with respect to the 3d impurity, respectively. θ_a is the angle between \mathbf{r}_a and the surface normal (Z -axis). θ_b is the angle between \mathbf{r}_b and the surface normal (Z -axis). X and Y span the surface.

2.2. The Hamiltonian and the o - p H_2 conversion process

The total Hamiltonian for the system described above, where we have H_2 interacting with a 3d impurity sitting on a metal oxide surface can be expressed as the sum [55,70,71] of the Hamiltonian corresponding to the electron system H_E (electrons) and H_2 CM motion H_{CM} , i.e., $H = H_E + H_{CM}$. The Hamiltonian for the H_2 CM motion H_{CM} can be written as

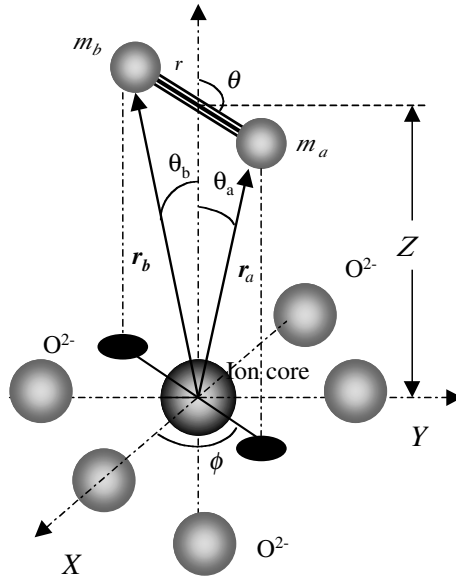


Fig. 2. Schematic diagram of a H_2 interacting with a 3d impurity sitting on a metal oxide surface. The figure shows the H_2 CM directly above the impurity. The molecular orientation with respect to the surface normal is given by θ , molecular CM distance from the surface is given by Z , the bond length is given by r , and the azimuthal orientation of the H–H bond with respect to the X -axis is given by ϕ . m_a and m_b correspond to the masses of H atoms a and b, respectively. \mathbf{r}_a and \mathbf{r}_b denote the position vectors of protons a and b with respect to the 3d impurity, respectively. θ_a is the angle between \mathbf{r}_a and the surface normal (Z -axis). θ_b is the angle between \mathbf{r}_b and the surface normal (Z -axis). The X and Y axes are parallel to the surface. From [59–62].

$$H_{CM} = -\frac{\hbar^2}{2M} \partial_Z^2. \tag{1}$$

M is the total mass of the H_2 ($M = m_a + m_b$). Z is the normal distance of H_2 CM from the surface. The Hamiltonian for the electron system can be further expanded into that for electrons of the impinging molecule $H_{M(\text{molecule})}$, that for the substrate electrons $H_{S(\text{substrate})}$, and that for the molecule–substrate interaction $H_{M(\text{molecule})-S(\text{substrate})}$, i.e., $H_E = H_M + H_S + H_{M-S}$. The Hamiltonian for the electrons of the impinging H_2 H_M is given by [70]

$$\begin{aligned} H_M = & \sum_{\sigma} \varepsilon_b C_{b\sigma}^{\dagger} C_{b\sigma} + \sum_{\sigma} \varepsilon_a C_{a\sigma}^{\dagger} C_{a\sigma} + \frac{U+J}{2} (n_{a\uparrow} + n_{b\downarrow})(n_{a\uparrow} + n_{b\downarrow}) \\ & - \frac{U-J}{2} (C_{a\uparrow}^{\dagger} C_{a\downarrow} C_{b\downarrow}^{\dagger} C_{b\uparrow} + C_{b\uparrow}^{\dagger} C_{a\downarrow} C_{b\downarrow}^{\dagger} C_{b\uparrow}) + \frac{U-J}{2} (C_{a\uparrow}^{\dagger} C_{b\uparrow} C_{a\downarrow}^{\dagger} C_{b\downarrow} \\ & + C_{b\uparrow}^{\dagger} C_{a\uparrow} C_{b\downarrow}^{\dagger} C_{b\downarrow}) + J(n_{a\uparrow} n_{b\uparrow} + n_{a\downarrow} n_{b\downarrow}), \end{aligned} \tag{2}$$

where ε_b and ε_a are the energy levels of the bonding and anti-bonding orbitals of the impinging H_2 , respectively. $C_{b\sigma}^{\dagger}$ ($C_{b\sigma}$) and $C_{a\sigma}^{\dagger}$ ($C_{a\sigma}$) are creation (annihilation)

operators for a single electron with spin σ in the bonding and anti-bonding orbitals, respectively. $n = C^\dagger C$ is the number operator. U is the intra-atomic Coulomb interaction and J is the inter-atomic Coulomb interaction.

The Hamiltonian for the substrate electron system is assumed to be that for a 3d impurity, i.e.,

$$H_S = \sum_{\sigma} \varepsilon_{xz} C_{xz\sigma}^\dagger C_{xz\sigma} + \sum_{\sigma} \varepsilon_{yz} C_{yz\sigma}^\dagger C_{yz\sigma} + \sum_{\sigma} \varepsilon_{z^2} C_{z^2\sigma}^\dagger C_{z^2\sigma}, \quad (3)$$

where ε_{xz} , ε_{yz} and ε_{z^2} are the energy levels of the $|xz\rangle$, $|yz\rangle$ and $|3z^2 - r^2\rangle$ orbitals, respectively. $C_{xz\sigma}^\dagger$ ($C_{xz\sigma}$), $C_{yz\sigma}^\dagger$ ($C_{yz\sigma}$), and $C_{z^2\sigma}^\dagger$ ($C_{z^2\sigma}$) are creation (annihilation) operators for a single electron with spin σ in the $|xz\rangle$, $|yz\rangle$ and $|3z^2 - r^2\rangle$ orbitals, respectively. Based on the model described above, we do not include the $|xy\rangle$ and $|x^2 - y^2\rangle$ orbitals in the Hamiltonian because they are lying on the surface plane and have no contribution/components along the Z direction.

We assume that the $o-p$ H_2 conversion is induced by a two-step process [35–38,58–62]. In the first step, one electron from the H_2 molecule jumps to the 3d impurity, which then occupies the $|3z^2 - r^2\rangle$ orbital of the impurity. This jump is accompanied by the Coulomb interaction. We shall consider a singlet-intermediate state for electrons in the 3d impurity, i.e., one electron from the H_2 molecule and another from the surface ($|xz\rangle$ or $|yz\rangle$ orbital). In the second step, one electron from the surface jumps to the H_2 -bonding orbital. This jump is accompanied by the hyperfine (Fermi) contact interaction [39], which induces the $o-p$ H_2 conversion. According to the two-step process described above, we can write the molecule–substrate interaction Hamiltonian H_{M-S} as the sum of the Hamiltonian corresponding to the Coulomb interaction $H_{C(\text{oulomb})}$ and the hyperfine (Fermi) contact interaction [39] H_{HC} , i.e., $H_{M-S} \propto H_C + H_{HC}$. We will give explicit expressions for these Hamiltonians below.

The Hamiltonian describing the first-step (Coulomb interaction) of the $o-p$ H_2 conversion process can be written as [58–62]

$$\begin{aligned} H_C = & \sum_{\sigma} [V_{bxz}(Z, \theta, \phi) C_{b\sigma}^\dagger C_{xz\sigma} + V_{byz}(Z, \theta, \phi) C_{b\sigma}^\dagger C_{yz\sigma} + V_{bz^2}(Z, \theta, \phi) C_{b\sigma}^\dagger C_{z^2\sigma} + \text{h.c.}] \\ & + \sum_{\sigma} [V_{axz}(Z, \theta, \phi) C_{a\sigma}^\dagger C_{xz\sigma} + V_{ayz}(Z, \theta, \phi) C_{a\sigma}^\dagger C_{yz\sigma} + V_{az^2}(Z, \theta, \phi) C_{a\sigma}^\dagger C_{z^2\sigma} + \text{h.c.}] \\ & + \sum_{\sigma\sigma'} \sum_{ijkl} U_{ijkl}(Z, \theta, \phi) C_{i\sigma'}^\dagger C_{j\sigma}^\dagger C_{k\sigma} C_{l\sigma'}, \end{aligned} \quad (4)$$

where $i, j, k, l = xz, yz, z^2, b, a$. V_{bxz} , V_{byz} , V_{bz^2} , V_{axz} , V_{ayz} , V_{az^2}, \dots , originate from the attraction of the electrons to the two protons of H_2 , and U_{ijkl} is the Coulomb repulsion between two electrons. To describe the Hamiltonian for the second-step, we consider only the anti-symmetric part of the hyperfine (Fermi) contact interaction Hamiltonian, because the symmetric part does not contribute to the $o-p$ H_2 conversion [33,34,37,58–62]. We can write the anti-symmetric part (with respect to proton interchange) of the hyperfine (Fermi) contact interaction between each electron spin and two H_2 nuclear spins as follows [58–62],

$$\begin{aligned}
 H_{\text{HC}} = & \sum_{\sigma} [A_{\text{bxz}}(Z, \theta, \phi) C_{\text{b}\sigma}^{\dagger} C_{\text{xz}\sigma} + A_{\text{byz}}(Z, \theta, \phi) C_{\text{b}\sigma}^{\dagger} C_{\text{yz}\sigma} \\
 & + A_{\text{bz}^2}(Z, \theta, \phi) C_{\text{b}\sigma}^{\dagger} C_{\text{z}^2\sigma}] + \sum_{\sigma} [A_{\text{axz}}(Z, \theta, \phi) C_{\text{a}\sigma}^{\dagger} C_{\text{xz}\sigma} \\
 & + A_{\text{ayz}}(Z, \theta, \phi) C_{\text{a}\sigma}^{\dagger} C_{\text{yz}\sigma} + A_{\text{az}^2}(Z, \theta, \phi) C_{\text{a}\sigma}^{\dagger} C_{\text{z}^2\sigma}], \tag{5}
 \end{aligned}$$

where

$$\Delta = \lambda_{\text{C}} \sum_{\alpha=1}^3 [\mathbf{S}_{\alpha} \cdot (\mathbf{I}_{\text{a}} - \mathbf{I}_{\text{b}}) [\delta(\mathbf{r}_{\text{a}} - \mathbf{r}_{\alpha}) - \delta(\mathbf{r}_{\text{b}} - \mathbf{r}_{\alpha})]]. \tag{6}$$

Here, \mathbf{I}_{a} and \mathbf{I}_{b} are operators for the nuclear spins of the two protons a and b. $\delta(\mathbf{r}_{\text{a}} - \mathbf{r}_{\alpha})$ and $\delta(\mathbf{r}_{\text{b}} - \mathbf{r}_{\alpha})$ represent the Dirac operators. \mathbf{r}_m ($m = \text{a, b}$) and \mathbf{r}_{α} ($\alpha = 1, 2, 3$) are the proton and electron coordinates respectively, as shown in Fig. 2. \mathbf{S}_{α} is the electron spin operator. λ_{C} is the hyperfine (Fermi) contact constant and has a magnitude of about 10^{-5} eV r^3 ($r = 1.41$ a.u.) [72].

2.3. The wavefunctions

To describe the dynamical process of o - p conversion when a H_2 interacts with a metal oxide surface, which is induced by the two-step process described above, we introduce the total wave function of the system, which can be represented by [58–62]

$$|\Psi_n\rangle = |\Phi_n\rangle |\chi_n\rangle |K_n\rangle, \tag{7}$$

where $|\Phi_n\rangle$, $|\chi_n\rangle$, and $|K_n\rangle$ are the wave functions for the electron system, the H_2 nuclei spins and the H_2 CM motion, respectively. The index n in (7) denotes the initial (i), intermediate (I), and final states (f).

The initial state of the system may be expressed as

$$|\Psi_i\rangle = |\Phi_i\rangle |\chi_i\rangle |K_i\rangle, \tag{8}$$

where

$$|\chi_i\rangle = \left\{ \begin{array}{c} |\uparrow\uparrow\rangle \\ \frac{1}{\sqrt{2}} (|\uparrow\downarrow\rangle + |\downarrow\uparrow\rangle) \\ |\downarrow\downarrow\rangle \end{array} \right\} \tag{9}$$

corresponds to the nuclei spins for an o - H_2 . The initial state for the electron system is described as

$$|\Phi_i\rangle = C_{\text{yz}\uparrow}^{\dagger} C_{\text{b}\uparrow}^{\dagger} C_{\text{b}\downarrow}^{\dagger} |0\rangle, \tag{10}$$

where $|0\rangle$ is the vacuum state. We represent the intermediate state as follows:

$$|\Psi_I\rangle = |\Phi_I\rangle |\chi_I\rangle |K_I\rangle, \tag{11}$$

where

$$|\Phi_I\rangle = \frac{1}{\sqrt{2}} [C_{\text{z}^2\uparrow}^{\dagger} C_{\text{yz}\downarrow}^{\dagger} C_{\text{b}\uparrow}^{\dagger} - C_{\text{z}^2\downarrow}^{\dagger} C_{\text{yz}\uparrow}^{\dagger} C_{\text{b}\uparrow}^{\dagger}] |0\rangle, \tag{12}$$

and, for H₂ nuclei spins of the intermediate state, we assume $|\chi_I\rangle = |\chi_i\rangle$. The final state of the system is given by

$$|\Psi_f\rangle = |\Phi_f\rangle|\chi_f\rangle|K_f\rangle, \quad (13)$$

where $|\chi_i\rangle$ is the expression for the nuclei spins of a *p*-H₂, which is given by

$$|\chi_i\rangle = \frac{1}{\sqrt{2}}(|\uparrow\downarrow\rangle - |\downarrow\uparrow\rangle) \quad (14)$$

with

$$|\Phi_f\rangle = C_{z\uparrow}^\dagger C_{b\uparrow}^\dagger C_{b\downarrow}^\dagger |0\rangle. \quad (15)$$

$|K_i\rangle$, $|K_I\rangle$, and $|K_f\rangle$ are the wave functions describing the H₂ CM translational motion along the *Z*-axis (which we represent by plane waves, i.e., $\langle Z|K\rangle \propto \exp(-iKZ)$) in the initial, intermediate and final states, respectively.

3. Orientation dependence of *o*-*p* H₂ conversion

We next derive the expression for the transition probability from an *o*-H₂ state (with rotational quantum number $j = 1$) to a *p*-H₂ state ($j = 0$) [58]. The transition probability for *o*-*p* H₂ conversion, obtained from time dependent perturbation theory, can be expressed as

$$W_{\Psi_f \leftarrow \Psi_i} = \frac{2\pi}{\hbar} \sum_f \left| \sum_I \frac{\langle \Psi_f | H_{\text{HC}} | \Psi_I \rangle \langle \Psi_I | H_C | \Psi_i \rangle}{E_i - E_I} \right|^2 \delta(E_i - E_f), \quad (16)$$

where

$$E_i = \frac{\hbar^2 K_i^2}{2M} + 2\varepsilon_b + \frac{U+J}{2} + \varepsilon_{\text{ortho}} + \varepsilon_{yz} \quad (17)$$

is the energy of the initial state and,

$$E_I = \frac{\hbar^2 K_I^2}{2M} + \varepsilon_b + \varepsilon_{\text{para}} + \varepsilon_{z^2} + \varepsilon_{yz} \quad (18)$$

and

$$E_f = \frac{\hbar^2 K_f^2}{2M} + 2\varepsilon_b + \frac{U+J}{2} + \varepsilon_{\text{para}} + \varepsilon_{yz} \quad (19)$$

are the energies of the intermediate and the final states of the system, respectively. After summing over all states (electron, intra-molecular motion and electron and proton spins), we can recast the *o*-*p* H₂ conversion yield as follows [58]

$$W_{\Psi_f \leftarrow \Psi_i}(Z, \theta, \phi) \propto \left| \sum_{K_I} \frac{\langle K_f | f_{\text{HC}}(Z, \theta, \phi) | K_I \rangle \langle K_I | f_C(Z, \theta, \phi) | K_i \rangle}{\frac{\hbar^2}{2M}(K_i^2 - K_I^2) + \varepsilon_b + \frac{U+J}{2} - \varepsilon_{z^2} + \Delta_{\text{op}}} \right|^2, \quad (20)$$

where Δ_{op} is the energy difference between the lowest *ortho* and *para* states ($\Delta_{\text{op}} = \varepsilon_{\text{ortho}} - \varepsilon_{\text{para}}$) and has a value of 15.08 meV. $f_{\text{HC}}(Z, \theta, \phi)$ and $f_{\text{C}}(Z, \theta, \phi)$ are the hyperfine (Fermi) contact contribution and the Coulomb contribution to the *o-p* H₂ conversion, respectively. $f_{\text{HC}}(Z, \theta, \phi)$ can be cast as follows:

$$\begin{aligned} f_{\text{HC}}(Z, \theta, \phi) &= \langle \chi_f | \langle \Phi_f | H_{\text{HC}}(Z, \theta, \phi) | \Phi_1 \rangle | \chi_1 \rangle \\ &= \frac{2}{\sqrt{2}} \lambda_{\text{C}} \sum_{\alpha=1}^3 \int g(\mathbf{r}_\alpha) [\delta(\mathbf{r}_\alpha - \mathbf{r}_a) - \delta(\mathbf{r}_\alpha - \mathbf{r}_b)] d_{z^2}(\mathbf{r}_\alpha) d\mathbf{r}_\alpha, \end{aligned} \quad (21)$$

where $g(r_\alpha)$ and $d_{z^2}(r_\alpha)$ are the bonding orbital of the hydrogen molecule and the $|3z^2 - r^2\rangle$ orbital, respectively, and have explicit expressions given by

$$g(\mathbf{r}_\alpha) = N_g \{ \exp(-\zeta|\mathbf{r}_\alpha - \mathbf{r}_a|) + \exp(-\zeta|\mathbf{r}_\alpha - \mathbf{r}_b|) \}, \quad (22)$$

and

$$d_{z^2}(\mathbf{r}_\alpha) = N_d r_\alpha^2 \exp\left(-\frac{Z_i}{3} r_\alpha\right) (3 \cos^2 \theta_\alpha - 1). \quad (23)$$

r_α denotes the length of the position vectors of the electrons. θ_α gives the angle subtended by the position vectors of the electrons and Z-axis. ϕ_α gives the angle subtended by the projection of the position vectors of electrons in the XY plane and the X-axis. N_g and N_d have explicit expressions given by

$$N_g = \frac{1 + \exp(-\zeta r)}{\sqrt{2(1 + 0.7)}}, \quad (24)$$

$$N_d = \frac{1}{\sqrt{6!}} \left(\frac{2Z_i}{3}\right)^{7/2} \sqrt{\frac{5}{16\pi}}. \quad (25)$$

Here Z_i denotes the effective nuclear charge. We use Slater type orbitals (STO) as basis functions for the 3d orbital ($Z_i = 5$ for a metal oxide surface such as SrTiO₃). For the bonding wave function of H₂ we take the Slater exponent $\zeta_1 = 1.189$ a.u. [65,68].

In Fig. 3 we show the hyperfine (Fermi) contact contribution $f_{\text{HC}}(Z, \theta, \phi)$ as functions of the H–H bond orientation θ and the azimuthal orientation of the H–H bond with respect to the X-axis ϕ . One can see that $f_{\text{HC}}(Z, \theta, \phi)$ strongly depends on θ . This strong dependence is anticipated to give rise to a substantial difference in the *o-p* H₂ conversion yield between a H₂ doing HLR and a H₂ doing CLR. We shall give a discussion on these types of H₂-rotation in *o-p* H₂ conversion later on (in Section 4).

The Coulomb contribution $f_{\text{C}}(Z, \theta, \phi)$ can be described as the sum of the Coulomb repulsion part and the Coulomb attraction part, i.e.,

$$\begin{aligned} f_{\text{C}}(Z, \theta, \phi) &= \langle \chi_1 | \langle \Phi_1 | H_{\text{C}}(Z, \theta, \phi) | \Phi_1 \rangle | \chi_1 \rangle \\ &= f_{\text{A(ttraction)}}(Z, \theta, \phi) + f_{\text{R(epulsion)}}(Z, \theta, \phi), \end{aligned} \quad (26)$$

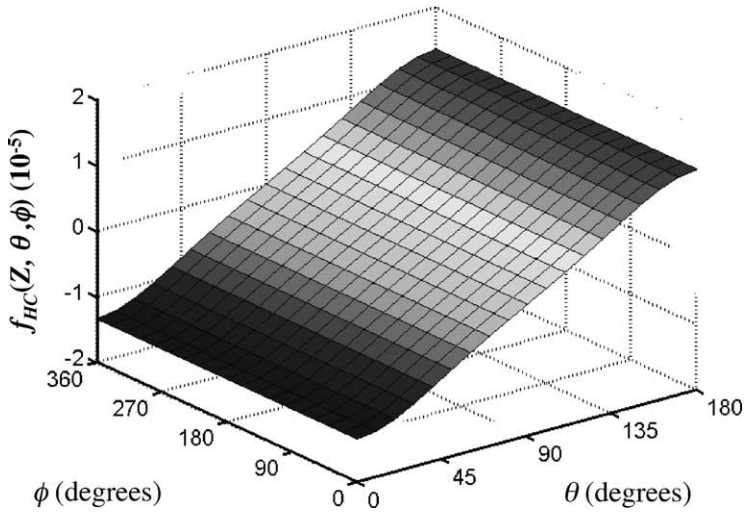


Fig. 3. The hyperfine contact contribution $f_{\text{HC}}(Z, \theta, \phi)$ for a H_2 at a CM distance $Z = 2.0$ a.u. from the surface. θ is the H–H bond orientation with respect to the surface normal. ϕ is the azimuthal orientation of the H–H bond with respect to the X -axis. From [60].

and

$$f_{\text{A}}(Z, \theta, \phi) = \frac{2}{\sqrt{2}} \sum_{\alpha=1}^3 \int g(\mathbf{r}_{\alpha}) \left\{ -\frac{1}{|\mathbf{r}_{\alpha} - \mathbf{r}_{\text{a}}|} - \frac{1}{|\mathbf{r}_{\alpha} - \mathbf{r}_{\text{b}}|} \right\} d_{z^2}(\mathbf{r}_{\alpha}) d\mathbf{r}_{\alpha}, \quad (27)$$

$$\begin{aligned} f_{\text{R}}(Z, \theta, \phi) &= \frac{2}{\sqrt{2}} \sum_{\alpha < \beta} \int \int g(\mathbf{r}_{\alpha}) g(\mathbf{r}_{\beta}) \frac{1}{|\mathbf{r}_{\alpha} - \mathbf{r}_{\beta}|} g(\mathbf{r}_{\beta}) d_{z^2}(\mathbf{r}_{\alpha}) d\mathbf{r}_{\alpha} d\mathbf{r}_{\beta} \\ &+ \frac{2}{\sqrt{2}} \sum_{\alpha < \beta} \int \int d_{yz}(\mathbf{r}_{\alpha}) g(\mathbf{r}_{\beta}) \frac{1}{|\mathbf{r}_{\alpha} - \mathbf{r}_{\beta}|} d_{z^2}(\mathbf{r}_{\beta}) d_{yz}(\mathbf{r}_{\alpha}) d\mathbf{r}_{\alpha} d\mathbf{r}_{\beta} \\ &+ \frac{2}{\sqrt{2}} \sum_{\alpha < \beta} \int \int d_{yz}(\mathbf{r}_{\alpha}) g(\mathbf{r}_{\beta}) \frac{1}{|\mathbf{r}_{\alpha} - \mathbf{r}_{\beta}|} d_{yz}(\mathbf{r}_{\beta}) d_{z^2}(\mathbf{r}_{\alpha}) d\mathbf{r}_{\alpha} d\mathbf{r}_{\beta}. \end{aligned} \quad (28)$$

$d_{yz}(\mathbf{r}_{\alpha})$ is the $|yz\rangle$ orbital and can be described as follows:

$$d_{yz}(\mathbf{r}_{\alpha}) = 2\sqrt{3}N_d r_{\alpha}^2 \exp\left(-\frac{Z_i}{3}r_{\alpha}\right) (\cos\theta_{\alpha} \sin\theta_{\alpha} \sin\phi_{\alpha}). \quad (29)$$

In Fig. 4(a) we show the numerical results of the Coulomb attraction contribution at $Z = 3.0$ a.u., as functions of the H–H bond orientation θ and the azimuthal orientation of the H–H bond with respect to the X -axis ϕ . For $\theta = 90^\circ$ (with the H–H bond of the H_2 oriented parallel to the surface) the Coulomb attraction contribution shows a maximum value, while for $\theta = 0^\circ$ and $\theta = 180^\circ$ (with the H–H bond of the H_2 oriented perpendicular to the surface) the Coulomb attraction contribution shows a minimum value. When a H_2 has a perpendicular orientation, the attraction between the two H_2 protons and the electron in the $|3z^2 - r^2\rangle$ orbital becomes stronger.

In Fig. 4(b) we show Coulomb repulsion contribution of $f_R(Z, \theta, \phi)$ at $Z = 1.0$ a.u., as functions of θ and ϕ . $f_R(Z, \theta, \phi)$ shows a strong ϕ dependence. To explain this, we should recall (28) where the electron from the $|yz\rangle$ orbital is involved. In Section 2, we mentioned that the top/edge of the electron density of the $|yz\rangle$ orbital is distributed above and below the O^{2-} ions (above and below the Y -axis). Repulsion between the H_2 electrons and the electron at the $|yz\rangle$ orbital is responsible for this behavior.

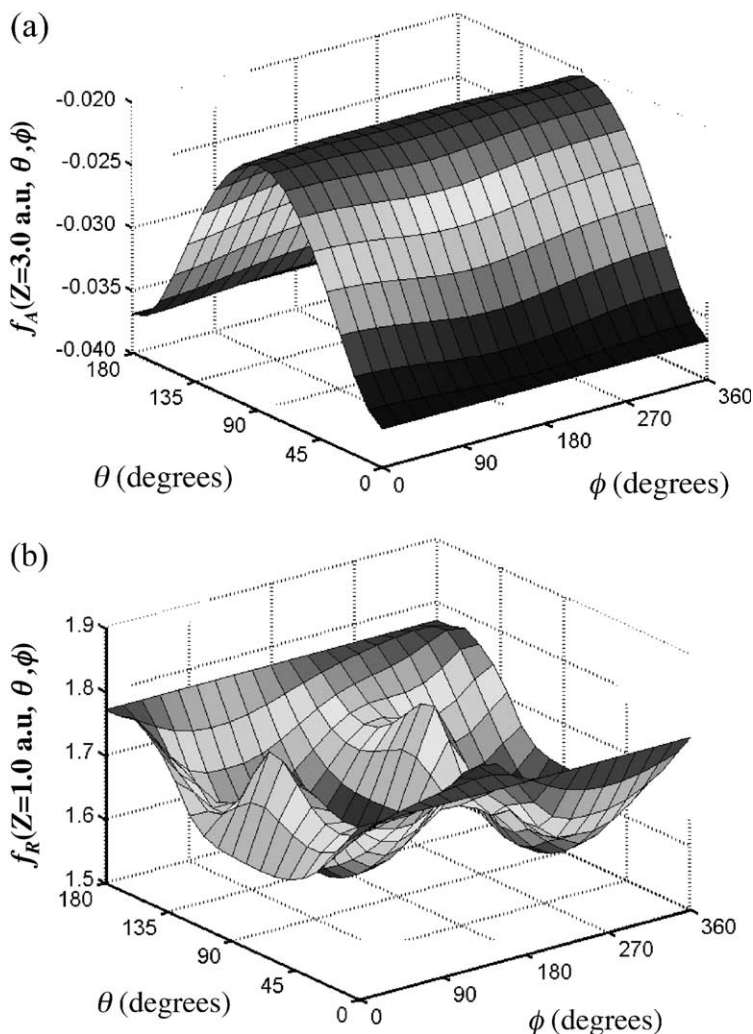


Fig. 4. (a) The Coulomb attraction contribution $f_A(Z, \theta, \phi)$ for a H_2 at a CM distance $Z = 3.0$ a.u. from the surface. (b) The Coulomb repulsion contribution $f_R(Z, \theta, \phi)$ for a H_2 at a CM distance $Z = 1.0$ a.u. from the surface. θ is the H–H bond orientation with respect to the surface normal. ϕ is the azimuthal orientation of the H–H bond with respect to the X -axis. From [60].

3.1. H₂-surface distance Z-dependence

We have shown earlier that the hyperfine (Fermi) contact contribution $f_{\text{HC}}(Z, \theta, \phi)$ strongly depends on the H–H bond orientation θ and the H–H bond azimuthal orientation with respect to the X-axis ϕ . As we have mentioned before, this strong dependence of $f_{\text{HC}}(Z, \theta, \phi)$ on θ is anticipated to give rise to a substantial difference in the *o-p* H₂ conversion yield. Here, we will see how $f_{\text{HC}}(Z, \theta, \phi)$ depends on the H₂-surface distance Z (or H₂ CM distance with respect to the surface). We express r_a , r_b , θ_a , and θ_b (as shown in Fig. 2) in terms of Z , r and θ , i.e.,

$$r_a = \sqrt{Z^2 + \frac{1}{4}r^2 + Zr \cos \theta}, \quad r_b = \sqrt{Z^2 + \frac{1}{4}r^2 - Zr \cos \theta},$$

$$\cos \theta_a = \left(Z + \frac{1}{2}r \cos \theta \right) / r_a \quad \text{and} \quad \cos \theta_b = \left(Z - \frac{1}{2}r \cos \theta \right) / r_b.$$

We can then insert these quantities (r_a , r_b , θ_a , and θ_b) to (21), calculate (21) analytically, to get

$$\begin{aligned} f_{\text{HC}}(Z, \theta, \phi) &= \langle \chi_f | \langle \Phi_f | H_{\text{HC}}(Z, \theta, \phi) | \Phi_1 \rangle | \chi_1 \rangle \\ &= \frac{2}{\sqrt{2}} \lambda_c \sum_{\alpha=1}^3 \int g(\mathbf{r}_\alpha) [\delta(\mathbf{r}_a - \mathbf{r}_\alpha) - \delta(\mathbf{r}_b - \mathbf{r}_\alpha)] d_{z^2}(\mathbf{r}_\alpha) d\mathbf{r}_\alpha \\ &= \frac{1}{2} \lambda_c N_g N_d \left\{ \left(\exp \left(-\frac{1}{3} Z_i \sqrt{Z^2 + \frac{1}{4}r^2 + Zr \cos \theta} \right) \right. \right. \\ &\quad \left. \left. - \exp \left(-\frac{1}{3} Z_i \sqrt{Z^2 + \frac{1}{4}r^2 - Zr \cos \theta} \right) \right) \left(2Z^2 + \frac{3}{4}r^2 \cos^2 \theta - \frac{1}{4}r^2 \right) \right. \\ &\quad \left. + \left(\exp \left(-\frac{1}{3} Z_i \sqrt{Z^2 + \frac{1}{4}r^2 + Zr \cos \theta} \right) \right. \right. \\ &\quad \left. \left. + \exp \left(-\frac{1}{3} Z_i \sqrt{Z^2 + \frac{1}{4}r^2 - Zr \cos \theta} \right) \right) (2Zr \cos \theta) \right\}. \quad (30) \end{aligned}$$

We can then compare (30) to the results obtained by Ilisca and Paris [37]. At distances far from the surface, for $\theta = 0^\circ$, our results agree. This is because at large Z one can expand the expression for the conversion probability with respect to r/Z and take the first term only, which is a good approximation for $r/Z \ll 1$. Then, we can reduce (30) to the results of Ilisca and Paris [37].

In Fig. 5 we show how $|f_{\text{HC}}(Z, \theta)|^2$ depends on the H₂ distance from the surface Z and the orientation of the H–H bond with respect to the surface normal θ . To see how $|f_{\text{HC}}(Z, \theta)|^2$ depends on Z and θ , we compare the corresponding results for $\theta = 0^\circ$, 50° , 70° as a function of Z . The result for $\theta = 0^\circ$ shows the largest value, followed by $\theta = 50^\circ$, and then $\theta = 70^\circ$, indicating a strong dependence of *o-p* H₂ conversion on the H–H bond orientation θ . This strong dependence on the H–H bond orientation θ is due to the anti-symmetric (with respect to proton interchange)

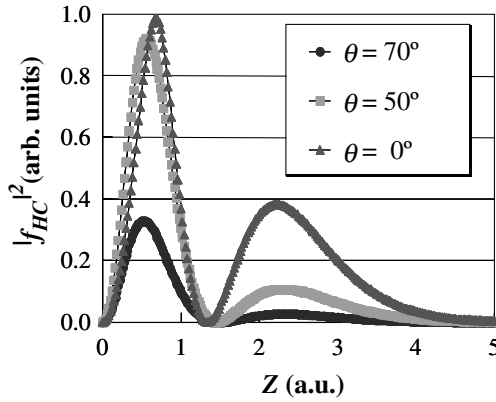


Fig. 5. Plot of the hyperfine contact contribution $|f_{\text{HC}}(Z, \theta)|^2$ as a function of the H_2 CM distance from the surface Z (in atomic units). The strong dependence on the H–H bond orientation θ is due to the anti-symmetric (with respect to proton interchange) part of the hyperfine contact interaction. These results are calculated for the case when the impinging molecule has orientations $\theta = 0^\circ$, 50° , and 70° with respect to the surface normal. We use STO as basis functions for the 3d orbitals (with 3d ion core charge $Z_i = 5$ for some metal oxide surface). For the bonding wave function of the H_2 we take the Slater exponent $\zeta_i = 1.189$. From [61].

part of the hyperfine interaction ($\delta(\mathbf{r}_a - \mathbf{r}_z) - \delta(\mathbf{r}_b - \mathbf{r}_z)$) given in (6). This strong dependence of $|f_{\text{HC}}(Z, \theta)|^2$ on the H–H bond orientation θ can be anticipated to give rise to a strong dependence of the o - p H_2 conversion yield on the H–H bond orientation θ .

3.2. Incident energy dependence

In this section, we consider a one-dimensional scattering of the H_2 along the Z direction. As shown in Fig. 2, we assume that a H_2 impinges the surface with an initial translational energy (incident energy) E_i and scattered back with a final translational energy E_f . For simplification, we just assume that the scattering event is such that the conversion yield depends only on Z and θ , and does not involve the azimuthal orientation of the H–H bond with respect to the X -axis ϕ . We then recast (20) to

$$W_{\Psi_f \leftarrow \Psi_i}(Z, \theta) \propto \left| \sum_{K_f} \frac{\langle K_f | f_{\text{HC}}(Z, \theta) | K_i \rangle \langle K_i | f_C(Z, \theta) | K_i \rangle}{\sum_{K_f} \frac{\hbar^2}{2M} (K_f^2 - K_i^2) + \varepsilon_b + \frac{U+J}{2} - \varepsilon_{z2} + \Delta_{\text{op}}} \right|^2. \quad (31)$$

In order to carry out the numerical calculation, the Coulomb contribution $f_C(Z, \theta)$ can be represented as the sum of the Coulomb repulsion contribution part and Coulomb attraction contribution part, i.e., $f_C(Z, \theta) = f_{\text{A(traction)}}(Z, \theta) + f_{\text{R(epulsion)}}(Z, \theta)$. In Fig. 6 we show the numerical results of the Coulomb repulsion contribution and Coulomb attraction contribution as functions of Z . The results are obtained for the cases when the impinging molecule has orientation $\theta = 45^\circ$, 60° and

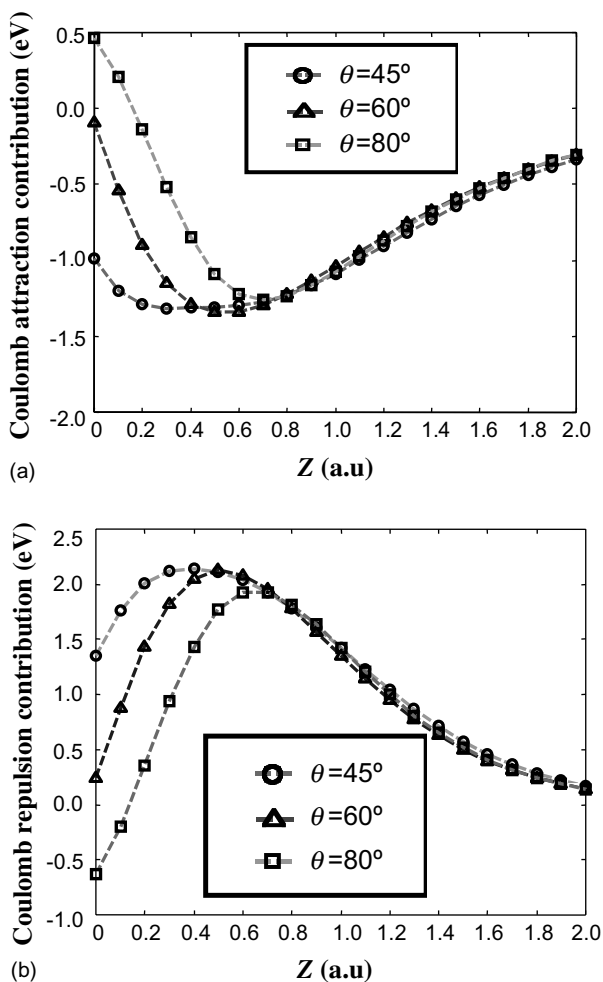


Fig. 6. The calculated results of the Coulomb attraction contribution (a) and the Coulomb repulsion contribution (b) as a function of the H₂ CM distance from the surface Z (in atomic units). These results are calculated for the case when the impinging molecule has orientations $\theta = 45^\circ$, 60° and 80° with respect to the surface normal. From [59].

80° , with respect to the surface normal. For the Coulomb attraction contribution, as shown in Fig. 6(a) when the H₂ approaches the surface, the protons of the H₂ first experience an attractive force from the 3d electron (via the wave function of the $|3z^2 - r^2\rangle$ orbital with positive sign, along the Z-axis), which results in the minima observed in Fig. 6(a). These minima correspond to the H₂-surface configuration where there is maximum 3d electron-H₂ overlap. Further attempts to bring the H₂ closer to the surface result in the repulsion of the H₂ protons by the 3d electron (via the wave function of the $|3z^2 - r^2\rangle$ orbital with negative sign, along the Z-axis). A similar argument holds to explain the results of Fig. 6(b). The H₂ at first experiences

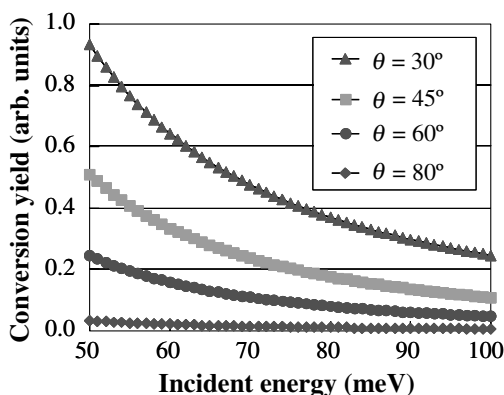


Fig. 7. The o - p H_2 conversion yield as a function of the initial translational/incident energy (in meV) of H_2 , for molecular orientations $\theta = 30^\circ, 45^\circ, 60^\circ$, and 80° . The results are obtained from (31) by, first, summing over all intermediate states K_1 , and then integrating over Z from 0 to 10 a.u. In the calculation, the following parameter values are used: $\epsilon_b = -15.7$ eV [37], $U = 16$ eV [71], $J = 8$ eV [71], and $\epsilon_{z^2} = -4$ eV [37,63]. From [59].

a repulsive force from the 3d electron (via the wave function of the $|3z^2 - r^2\rangle$ orbital with positive sign, along the Z -axis) and then an attractive force from the 3d electron (via the wave function of the $|3z^2 - r^2\rangle$ orbital with negative sign, along the Z -axis).

We next evaluate (31) numerically. Fig. 7 shows results of the o - p H_2 conversion yield for the molecular orientations $\theta = 30^\circ, 45^\circ, 60^\circ$ and 80° . One can see, as shown in Fig. 7, that the o - p H_2 conversion yield decreases exponentially with increasing translational energy. Note that an increase in translational energy corresponds to an increase in molecular velocity, which results in a decrease in interaction time between the H_2 and the 3d impurity, and thus the observed exponential decrease of the o - p H_2 conversion yield with increasing translational energy.

For $\theta = 30^\circ$ the transition probability has the largest value, followed by $\theta = 45^\circ, 60^\circ$ and 80° . This behavior is similar to the behavior of the hyperfine (Fermi) contact contribution $f_{\text{HC}}(Z, \theta)$. These results show that the strong dependence on the H–H bond orientation θ comes mainly from hyperfine (Fermi) contact interaction contribution.

4. Steric effect on o - p H_2 conversion

Next, we compare the o - p H_2 conversion yields for a CLR H_2 and a HLR H_2 [60]. We consider a H_2 in an initial rotational state $\mathbf{j} = 1$, and compare the o - p conversion yield for a H_2 doing CLR ($j = 1, m = 0$) with that for a H_2 doing HLR ($j = 1, m = \pm 1$). In Fig. 8 we show two of the different types of H_2 rotation on a solid surface. If we interpret m as one of the $(2j + 1)$ possible Z -components of the total angular momentum \mathbf{j} , then each m represents one particular orientation of molecule [14,55]. $|m| = 0$ corresponds to a H_2 doing CLR, i.e., the rotational axis of H_2 is

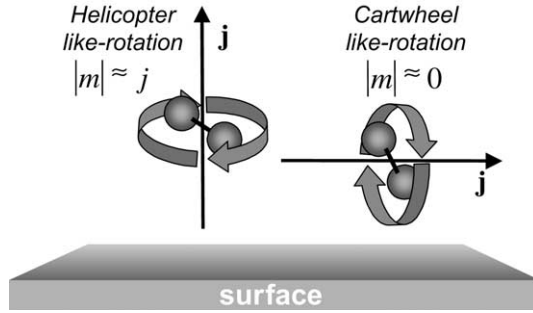


Fig. 8. Two of the different types of H_2 rotation on a solid surface. When the rotational axis of a H_2 is parallel to the surface, we have a H_2 doing cartwheel-like rotation (CLR, $|m| = 0$). When the rotational axis of H_2 is perpendicular to the surface, we have a H_2 doing helicopter-like rotation (HLR, $|m| = j$) [14,47–49,53]. Here m is one of the $(2j + 1)$ possible Z -components of the total angular momentum \mathbf{j} . From [60,61].

parallel to the surface. $|m| = j$ corresponds to a H_2 doing HLR, i.e., the rotational axis of H_2 is perpendicular to the surface [14].

The o - p H_2 conversion yield furthermore can be described as a function of the CM of H_2 , i.e.,

$$W_{\psi_f \leftarrow \psi_i}(Z) \propto \left| \frac{\langle \Theta_f | f_{\text{HC}}(Z, \theta, \phi) | \Theta_1 \rangle \langle \Theta_1 | f_{\text{C}}(Z, \theta, \phi) | \Theta_i \rangle}{\varepsilon_b + \frac{U+J}{2} - \varepsilon_{2^2} + \Delta_{\text{op}}} \right|^2, \quad (32)$$

where $f_{\text{HC}}(Z, \theta, \phi)$ and $f_{\text{C}}(Z, \theta, \phi)$ are the hyperfine (Fermi) contact contribution and the Coulomb contribution to the o - p H_2 conversion, respectively. The definitions of $f_{\text{HC}}(Z, \theta, \phi)$ and $f_{\text{C}}(Z, \theta, \phi)$ can be found in Section 3. $|\Theta_i\rangle$ is the initial rotational wave function of H_2 . The lowest energy state for an o - H_2 has a rotational quantum number $j = 1$. $|\Theta_i\rangle$ has explicit expressions given by

$$|\Theta_i\rangle = \left\{ \begin{array}{ll} \sqrt{\frac{3}{4\pi}} \cos \theta; & \text{for } m = 0 \\ \frac{3}{\sqrt{8\pi}} \sin \theta \exp(i\phi); & \text{for } m = 1 \\ \frac{3}{\sqrt{8\pi}} \sin \theta \exp(-i\phi); & \text{for } m = -1 \end{array} \right\}. \quad (33)$$

$|\Theta_1\rangle$ is the intermediate rotational wave function of H_2 and has explicit expressions given by

$$|\Theta_1\rangle = \sqrt{\frac{3}{4\pi}} \cos \theta, \quad (34)$$

and $|\Theta_f\rangle$ is the final rotational wave function for the lowest energy state of a p - H_2 ($j = 0$), which is given by

$$|\Theta_f\rangle = \frac{1}{\sqrt{4\pi}}. \quad (35)$$

In order to determine the behavior of $f_{\text{HC}}(Z, \theta, \phi)$, $f_{\text{A}}(Z, \theta, \phi)$, and $f_{\text{R}}(Z, \theta, \phi)$ with respect to Z , we can integrate them over θ and ϕ , i.e.,

$$F_{\text{HC}}(Z) = \int_0^{2\pi} \int_0^\pi f_{\text{HC}}(Z, \theta, \phi) d\theta d\phi, \quad (36)$$

$$F_{\text{A}}(Z) = \int_0^{2\pi} \int_0^\pi f_{\text{A}}(Z, \theta, \phi) d\theta d\phi, \quad (37)$$

and

$$F_{\text{R}}(Z) = \int_0^{2\pi} \int_0^\pi f_{\text{R}}(Z, \theta, \phi) d\theta d\phi. \quad (38)$$

In Fig. 9, we plot $F_{\text{HC}}(Z)$ as a function of the H_2 CM distance from the surface Z . One can see in this figure that at large distances from the surface (for instance $Z = 5$ a.u.), $F_{\text{HC}}(Z)$ show a small value as a result of the decreasing electron density of the $|3z^2 - r^2\rangle$ orbital.

In Fig. 10, we plot $F_{\text{A}}(Z)$ and $F_{\text{R}}(Z)$ as a function of Z (in atomic units). $F_{\text{A}}(Z)$ and $F_{\text{R}}(Z)$ have small values when Z is large. However, when H_2 comes closer to the surface, F_{R} increases and shows a maximum while F_{A} decreases and shows a minimum. The maximum of F_{R} and the minimum of F_{A} correspond to the H_2 -surface configuration where there is maximum 3d electron- H_2 overlap.

The matrix element $\langle \Theta_1 | f_{\text{C}}(Z, \theta, \phi) | \Theta_i \rangle$ in (32) can be calculated as follows:

$$\langle \Theta_1 | f_{\text{C}}(Z, \theta, \phi) | \Theta_i \rangle = \langle j_i, m_i | f_{\text{C}}(Z, \theta, \phi) | j_i, m_i \rangle = \langle 1, 0 | f_{\text{C}}(Z, \theta, \phi) | 1, m_i \rangle. \quad (39)$$

For $(j_i = 1, m_i = 0)$, i.e., a CLR H_2 , $\langle \Theta_1 | f_{\text{C}}(Z, \theta, \phi) | \Theta_i \rangle$ can be written as

$$\langle \Theta_1 | f_{\text{C}}(Z, \theta, \phi) | \Theta_i \rangle \propto \int_0^{2\pi} \int_0^\pi \cos \theta f_{\text{C}}(Z, \theta, \phi) \cos \theta \sin \theta d\theta d\phi, \quad (40)$$

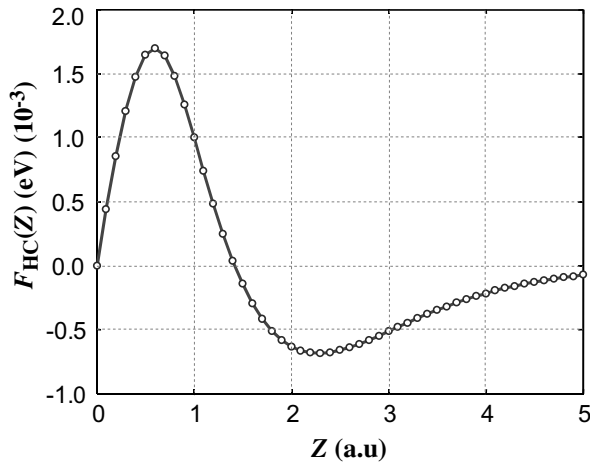


Fig. 9. The hyperfine contact contribution $F_{\text{HC}}(Z) = \int_0^{2\pi} \int_0^\pi f_{\text{HC}}(Z, \theta, \phi) d\theta d\phi$ as a function of Z . Z is the H_2 CM distance from the surface. From [60].

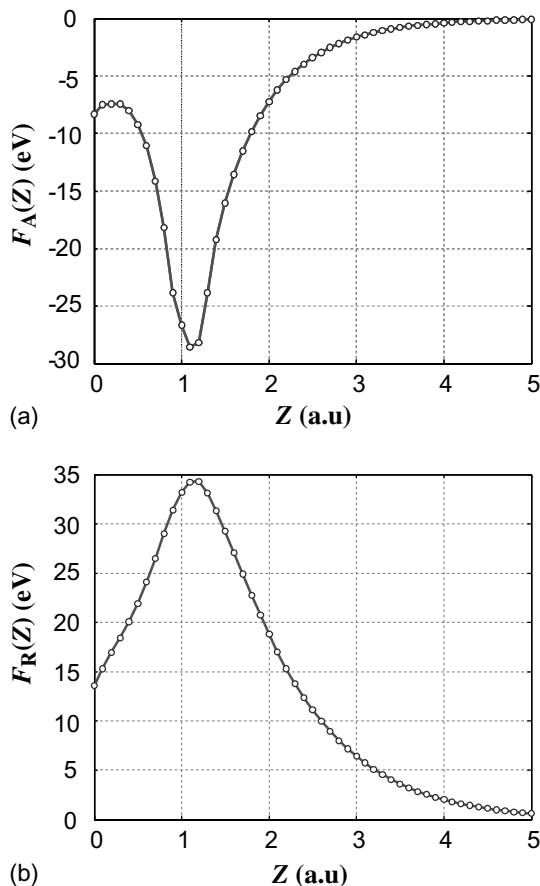


Fig. 10. The (a) Coulomb attraction contribution $F_A(Z)$ and the (b) Coulomb repulsion contribution $F_R(Z)$ as a function of Z . Z is the H_2 CM distance from the surface. From [60].

while for $(j_i = 1, m_i = \pm 1)$, i.e., a HLR H_2 , $\langle \Theta_I | f_C(Z, \theta, \phi) | \Theta_i \rangle$ can be written as

$$\langle \Theta_I | f_C(Z, \theta, \phi) | \Theta_i \rangle \propto \int_0^{2\pi} \int_0^\pi \cos \theta f_C(Z, \theta, \phi) \sin \theta \exp(\pm i\phi) \sin \theta d\theta d\phi. \quad (41)$$

The matrix elements $\langle \Theta_f | f_{HC}(Z, \theta, \phi) | \Theta_I \rangle$ can be calculated as follows:

$$\begin{aligned} \langle \Theta_f | f_{HC}(Z, \theta, \phi) | \Theta_I \rangle &= \langle j_f, m_f | f_{HC}(Z, \theta, \phi) | j_I, m_I \rangle = \langle 0, 0 | f_{HC}(Z, \theta, \phi) | 1, 0 \rangle \\ &\propto \int_0^{2\pi} \int_0^\pi f_{HC}(Z, \theta, \phi) \cos \theta \sin \theta d\theta d\phi. \end{aligned} \quad (42)$$

For the intermediate state as described in (39) and (42), we have assumed $m_I = 0$ corresponding to the molecule doing CLR. From (39) and (42) one can see that the Coulomb interaction is responsible for the change in the rotational state of H_2 , while the hyperfine (Fermi) contact interaction is responsible for the change in the nuclear

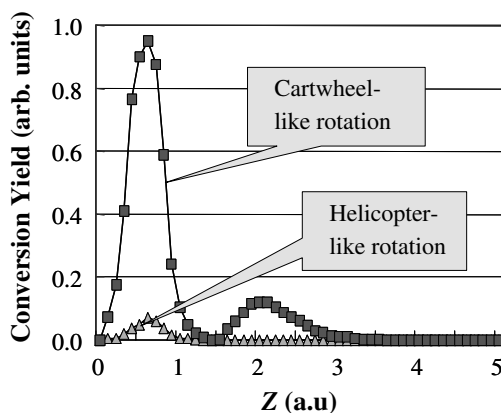


Fig. 11. The o - p H_2 conversion yield as a function of Z . In the calculation, the following parameter values are used: $\varepsilon_b = -15.7$ eV [37], $U = 16$ eV [71], $J = 8$ eV [71], $\varepsilon_{z^2} = -4$ eV [37,63] and $\Delta_{op} = 15.08$ meV. Here, U is the intra-atomic Coulomb interaction and J is the inter-atomic Coulomb interaction. ε_b is the energy level of the bonding orbital of the impinging H_2 and ε_{z^2} is the energy level of the $|3z^2 - r^2\rangle$ orbital. Δ_{op} is the energy difference between the lowest o - H_2 and p - H_2 states ($\Delta_{op} = \varepsilon_{ortho} - \varepsilon_{para}$). From [61].

spin state of H_2 . In Fig. 3 we can see that the hyperfine (Fermi) contact interaction does not influence the m value as there is no ϕ -dependence.

In Fig. 11 we show the numerical results of the o - p H_2 conversion yield (32) as a function of the H_2 CM distance from the surface Z (in atomic units) for each H_2 rotation. The behavior of these curves are similar to the behavior of the o - p H_2 conversion yield of the hyperfine (Fermi) contact contribution, indicating the dominant role of the hyperfine (Fermi) contact interaction in the conversion process. The o - p H_2 conversion yield for a H_2 doing CLR shows a larger value, compared to a H_2 doing HLR. We estimate that the o - p H_2 conversion yield for a H_2 doing CLR is around one order of magnitude higher than that for a H_2 doing HLR. This result indicates that there is a substantial difference in the o - p H_2 conversion yield between a H_2 doing HLR and a H_2 doing CLR. Furthermore, this result is consistent with our earlier results [58–60] where we considered the o - p H_2 conversion yield for fixed H–H orientations with respect to the surface. The o - p H_2 conversion yield showed that a perpendicular orientation is preferred over a parallel orientation. We expect this to be a general behavior of the o - p H_2 conversion. This result indicates that there is a promising possibility to enhance the o - p H_2 conversion by using the SE. We have recently shown that the SE is a general feature of o - p H_2 conversion by considering the same process mentioned above on a metal surface [62].

5. Dynamical quantum filtering via scattering

Earlier, we suggested that metal surfaces can, via the orientation-dependent PES, act or be utilized as rotational quantum state filters for molecules and induce, e.g.,

desorbing H_2 to exhibit rotational alignment (DQF). We showed that the resulting alignment of the desorbed molecules, as determined by the value of quadrupole alignment factor $A_0^{(2)}(j)$, exhibits a nonmonotonic dependence on the rotational quantum number j and the translational energy E_t . Molecules with $A_0^{(2)}(j) > 0$ exhibit HLR, while molecules with $A_0^{(2)}(j) < 0$ exhibit CLR [14,47–49]. Furthermore, we showed that slowly desorbing H_2 ($E_t \ll V_{\min}$, V_{\min} is the minimum activation barrier for H_2 dissociation, with the H–H bond oriented parallel to the surface. $V_{\min} \approx 0.5$ eV.) exhibit CLR, while fast desorbing H_2 ($E_t \gg V_{\min}$) exhibit HLR (cf., Fig. 12) [14,47–49].

To demonstrate and explain how we can also align the angular momentum vectors \mathbf{j} of H_2 during the scattering on metal surfaces, i.e., also observe DQF, we perform full quantum dynamics calculations of H_2 on Cu(001), taking into account all the six DOF of H_2 as dynamical variables, and using the time-independent coupled-channel method [4,6,73,74].

The dynamical variables we have considered are the perpendicular distance of the H_2 CM from the surface Z , the H_2 CM position parallel to the surface (X, Y), the H_2 bond length r , and the H_2 polar and azimuthal orientation with respect to the surface, θ and ϕ , respectively. We then make a transformation from the Cartesian coordinate system to the mass-weighted reaction path coordinate system [75]. Here, we leave the details of the derivation to [76], and show only the final form of the Hamiltonian, which is given by

$$H = -\frac{\hbar^2}{2M} \left[\frac{\partial^2}{\partial X^2} + \frac{\partial^2}{\partial Y^2} \right] - \frac{\hbar^2}{2\mu} \left[\eta^{-1} \frac{\partial}{\partial v} \eta \frac{\partial}{\partial v} \right] + \frac{\hbar^2}{2\mu} \frac{1}{r} L \frac{1}{r} + V(X, Y, s, \theta, \phi, v). \quad (43)$$

M and μ are the total and reduced masses of H_2 . s corresponds to the reaction path coordinate along the potential minimum on a PES, and v corresponds to the vibrational coordinate perpendicular to the reaction path, respectively. L is the angular

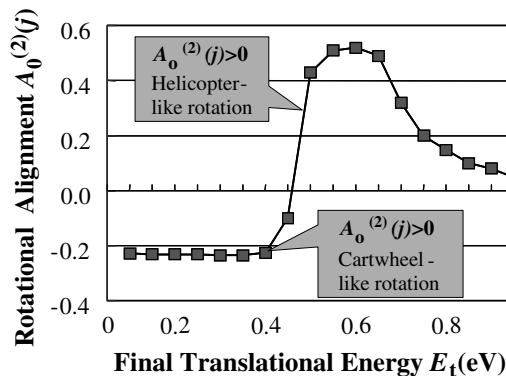


Fig. 12. Rotational alignment of H_2 ($v = 0, j = 1$) as function of the final translational energy. Molecules with $A_0^{(2)}(j) > 0$ exhibit HLRs, while molecules with $A_0^{(2)}(j) < 0$ exhibit CLR. From [48].

momentum operator. η is the Jacobian of the transformation $\eta(s, v, \theta) = 1 - v \cdot C(s, \theta)$, where $C(s, \theta)$ is the reaction path curvature. $V(X, Y, s, \theta, \phi, v)$ gives the six-dimensional (6D) PES along the reaction path for $\text{H}_2/\text{Cu}(001)$. Since the hydrogen–copper system has been studied extensively, large amounts of data are now available for the PES of hydrogen–copper system [77–80]. An analytical functional form of the 6D PES of H_2 on the $\{100\}$ face of copper fitted to the density functional theory (DFT) based PES calculation results performed for the highly symmetric sites was earlier given by Wiesenecker et al. [80] in the Cartesian coordinate system. Here, we show the corresponding functional form in the mass-weighted reaction path coordinate system,

$$\begin{aligned}
 V(X, Y, s, \theta, \phi, v) = & V_{0000}(s) + V_{0010}(s)[\cos GX + \cos GY] \\
 & + V_{0011}(s)[\cos GX \cdot \cos GY] + V_{2000}(s) \cos^2 \theta \\
 & + V_{2010}(s) \cos^2 \theta [\cos GX + \cos GY] + V_{2011}(s) \cos^2 \theta \\
 & \times [\cos GX \cdot \cos GY] + V_{2210}(s) \sin^2 \theta \cos 2\phi \\
 & \times [\cos GX - \cos GY] + \frac{1}{2} \mu \omega^2(s) v^2.
 \end{aligned} \tag{44}$$

Each $V_{jm, nm}(s)$ corresponds to the reaction path coordinate s -dependent coefficients of the expansion of the 6D PES (here, $V_{jm, nm}(s) = V_{jm, nm}(s)$). m and n are the quantum numbers for the surface parallel translational motion of H_2 , and correspond to the diffraction channels. j and m_j are quantum numbers for the rotational motion of H_2 , and j corresponds to the absolute value of the angular momentum vector \mathbf{j} , and m_j corresponds to the surface normal component of the angular momentum vector \mathbf{j} . $G = 2\pi/a$ is the reciprocal lattice constant of the surface unit cell of $\text{Cu}(001)$. $a = 2.55 \text{ \AA}$ is the nearest-neighbor distance between Cu atoms on the surface. $\omega(s)$ corresponds to the vibrational frequency of the adsorbed H ($s = -\infty$) and the vibrational frequency of the desorbing H_2 ($s = \infty$), respectively. Eq. (44) reproduces the same PES for $\text{H}_2/\text{Cu}(001)$ as those of [80]. In Fig. 13, we show each $V_{jm, nm}(s)$ in (44) as functions of the reaction path s . The wave function is expanded in terms of two dimensional plane waves dependent on X and Y , harmonic oscillator functions $\beta_v(s, v)$, and spherical harmonic functions $Y_j^{m_j}(\theta, \phi)$, i.e.,

$$\Psi(s, v, X, Y, \theta, \phi) = \sum_{mnvm_j} \phi_{mnv}^{jm_j}(s) \exp[-iG(mX + nY)] \beta_v(s, v) Y_j^{m_j}(\theta, \phi). \tag{45}$$

v is the quantum number for the vibrational motion of the product H_2 . The number of the basis set used in the coupled channel calculations is determined by the total energy of the system E_{tot} , which is defined as the sum of the kinetic energy of the surface normal translational motion, surface parallel translational motion, rotational motion, and vibrational motion of H_2 . When the maximum $E_{\text{tot}} = 0.4 \text{ eV}$, the calculation results converge with maximum quantum numbers $j_{\text{max}} = 5$, $v_{\text{max}} = 1$, and $G_{\text{max}} = 8$. We carefully checked the convergence for calculations with maximum quantum numbers $j_{\text{max}} = 7$, $v_{\text{max}} = 2$, and $G_{\text{max}} = 9$, respectively.

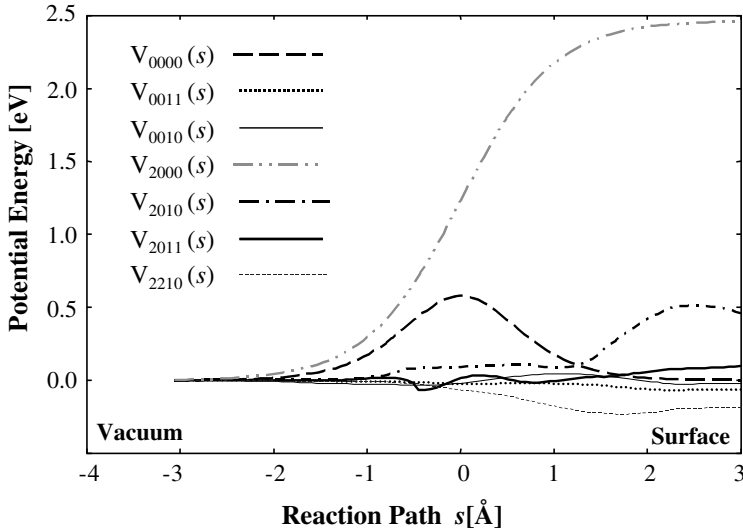


Fig. 13. Coefficients V_{mnjm_j} of the expansion of the 6D PES, $V(X, Y, s, \theta, \phi, v)$, used in the present calculation along the reaction path s . From [53].

We calculate the scattering probabilities $R_{mnjm_j}^{m'n'}(E_{\text{tot}})$, as functions of the final states of the rotational motion (j, m_j), and the initial (m', n') and final (m, n) states of the surface parallel translational motion of H_2 , for the scattering dynamics on $\text{Cu}(001)$. Note that in evaluating the $R_{mnjm_j}^{m'n'}(E_{\text{tot}})$, we summed the results over all the possible initial rotational states of impinging H_2 (j', m'_j), and we fixed the initial and final vibrational states of H_2 to the ground state. In Fig. 14, we show the surface parallel wave vector $G(m, n)$ distributions for CLR H_2 ($j = 1, m_j = 0$) and HLR H_2 ($j = 1, |m_j| = 1$) scattered from $\text{Cu}(001)$, in the case of $E_{\text{tot}} = 0.2$ eV. In Fig. 14(a) and (b), the surface parallel wave vector of the impinging H_2 is fixed to $\mathbf{K}_i = G(1, 0)$, along the $[100]$ direction of $\text{Cu}(001)$, which corresponds to an incident angle $\Theta_i \approx 10^\circ$ with respect to the surface normal, for $E_{\text{tot}} = 0.2$ eV. As we can see in Fig. 14, the angular distributions of the CLR H_2 (Fig. 14(a)) are quite different from those of the HLR H_2 (Fig. 14(b)). The CLR H_2 exhibits strong specular scattering, i.e., there is a sharp peak at $\mathbf{K}_f = \mathbf{K}_i$, while the HLR H_2 exhibits off-specular scattering, i.e., there is no peak at the $\mathbf{K}_f = \mathbf{K}_i$, instead, there are small peaks around $\mathbf{K}_f = \mathbf{K}_i$. \mathbf{K}_f corresponds to the surface parallel wave vector of scattered H_2 .

These results can be understood in terms of the coupling between the surface parallel translational motion and the rotational motion of H_2 . When the H_2 impinges on the surface, the corrugation (X and Y dependence) of the PES, as well as the rotational anisotropy (θ and ϕ dependence) of the PES influence its dynamics. On the corrugated surface, the surface normal translational motion of the impinging H_2 couples with its surface parallel translational motion, and the impinging H_2 exhibits off-specular scattering, while on the less corrugated surface (i.e., a nearly flat surface), the impinging H_2 exhibits specular scattering. However, these corrugation

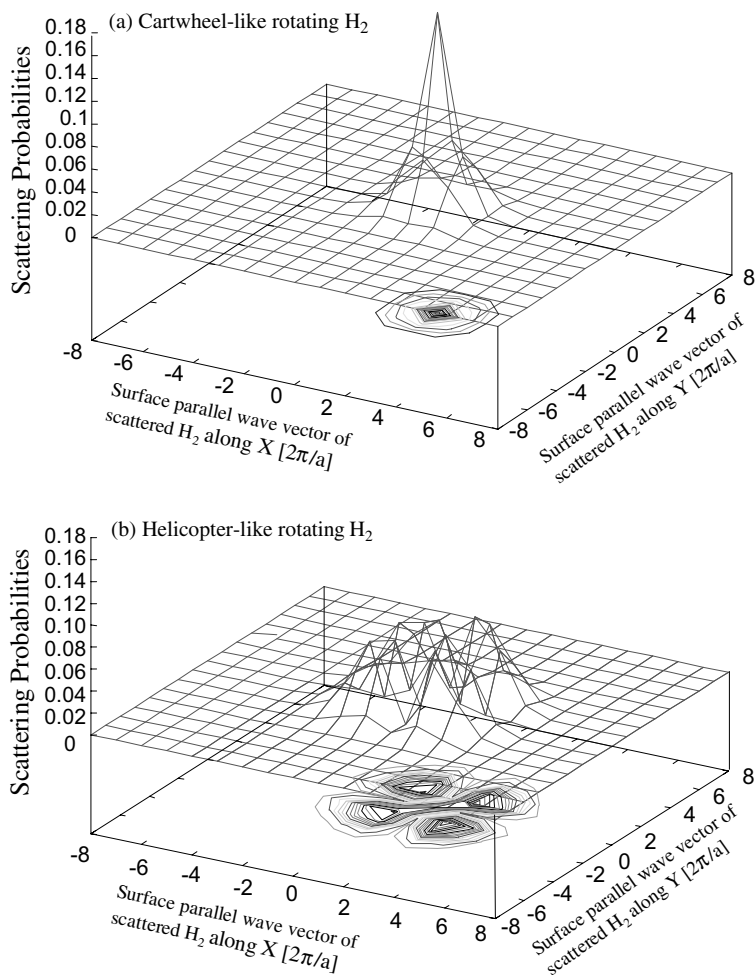


Fig. 14. Surface parallel wave vector $G(m, n)$ ($G = 2\pi/a, a = 2.55 \text{ \AA}$) distributions for a CLR H_2 ($j = 1, m_j = 0$) (a) and a HLR H_2 ($j = 1, |m_j| = 1$) (b) scattered from $\text{Cu}(001)$, in the vibrationally ground state ($v = 0$) for the case when $E_{\text{tot}} = 0.2 \text{ eV}$. From [53].

effects on the scattering process also strongly depend on the rotational motion of the impinging H_2 , i.e., whether the H_2 is doing CLR or HLR. Since the CLR H_2 rotates on an axis parallel to the surface, it is mainly affected by the polar orientational (θ) dependence (anisotropy), which is included as $\cos^2 \theta$ terms in (44). According to the ab initio PES calculation results for H_2 on $\text{Cu}(001)$ [80], as H_2 approaches the surfaces, the coefficient (of the $\cos^2 \theta$ terms) $V_{2000}(s)$ becomes large compared to $V_{2011}(s)$ and $V_{2010}(s)$ (see Fig. 13). This means that the CLR H_2 is less susceptible to corrugation effects during the scattering process, because the $V_{2000}(s)$ term includes no corrugation term (i.e., no X and Y dependence, see (44)). Therefore, the coupling

between the surface normal translational motion and surface parallel translational motion is very small, and the CLR H_2 is mainly scattered in the specular direction. On the other hand, the HLR H_2 rotates on an axis perpendicular to the surface, thus it is strongly affected by the azimuthal orientational (ϕ) dependence (anisotropy), which is included as $\sin^2 \theta \cos 2\phi$ term in (44). Since there is only one $\sin^2 \theta \cos 2\phi$ term in (44), and its coefficient $V_{2210}(s)$ (see Fig. 13) depends on the corrugation (i.e., X and Y dependence), there is a strong coupling between the surface normal translational motion and the surface parallel translational motion of the HLR H_2 occurs during the scattering process. Thus, HLR H_2 are mainly scattered in the off-specular direction.

To obtain the spatial distributions (orientational preference) of H_2 scattered from Cu(001), we calculate the quadrupole alignment factor $A_0^{(2)}(E_{\text{tot}})$, which is given by [81],

$$A_0^{(2)}(E_{\text{tot}}) = \frac{\sum_{m_j} [3m_j^2 - j(j+1)] R_{m_j m_j}^{m' n'}(E_{\text{tot}})}{\sum_{m_j} j(j+1) R_{m_j m_j}^{m' n'}(E_{\text{tot}})}. \quad (46)$$

The quadrupole alignment factor $A_0^{(2)}(E_{\text{tot}})$ can be experimentally determined by using REMPI [82,83] and LIF [84], and gives us information regarding the degree of alignment and orientational preference of H_2 . It assumes values in the range $[-1, 3j/(j+1) - 1]$, i.e., CLR H_2 ($m_j \approx 0$) has $A_0^{(2)}(E_{\text{tot}}) < 0$, while HLR H_2 ($|m_j| \approx j$) has $A_0^{(2)}(E_{\text{tot}}) > 0$. A spatially isotropic distribution of the angular momentum vector \mathbf{j} is described by $A_0^{(2)}(E_{\text{tot}}) = 0$. In Fig. 15, we show the $A_0^{(2)}(E_{\text{tot}})$ as a function of the scattering angle Θ_f of H_2 , which can be evaluated from the surface normal translational energy and the surface parallel translational energy of scattered H_2 . In Fig. 15(a) and (b), the surface parallel wave vector of the impinging H_2 is fixed to $\mathbf{K}_i = G(1, 0)$ along the $[100]$ direction of Cu(001) which corresponds to the incident angle $\Theta_i \approx 10^\circ$ with respect to the surface normal. In Fig. 15(a), we can observe a strong rotational alignment of H_2 scattered from Cu(001), where the H_2 scattered from Cu(001) in the region of the scattering angle $\Theta_i - 20^\circ < \Theta_f < \Theta_i + 20^\circ$ exhibits $A_0^{(2)}(E_{\text{tot}}) < 0$, while the H_2 scattered from Cu(001) in the region of the scattering angle $\Theta_f < \Theta_i - 20^\circ$ and $\Theta_f > \Theta_i + 20^\circ$ exhibits $A_0^{(2)}(E_{\text{tot}}) > 0$. A similar result can be seen for different $E_{\text{tot}} (= 0.4 \text{ eV})$ in Fig. 15(b).

These results indicate that the orientational preference varies with the scattering angle of H_2 from Cu(001), and we can obtain H_2 with aligned angular momentum vector \mathbf{j} through the scattering process. The microscopic mechanism of the rotational alignment of scattered H_2 can be attributed to the strong coupling between the surface parallel translational motion and the rotational motion of H_2 . A HLR H_2 is more susceptible to the surface corrugation than a CLR H_2 . The azimuthal (ϕ) dependence of the PES mainly influences a HLR H_2 , whereas the polar (θ) dependence of the PES mainly influences a CLR H_2 . Because of the generality of this behavior, we expect to observe DQF on the scattering dynamics of other gas–surface systems. In general, a molecule which rotates on an axis parallel to the surface will exhibit specular scattering, while a molecule which rotates on an axis perpendicular to the surface will exhibit off-specular scattering.

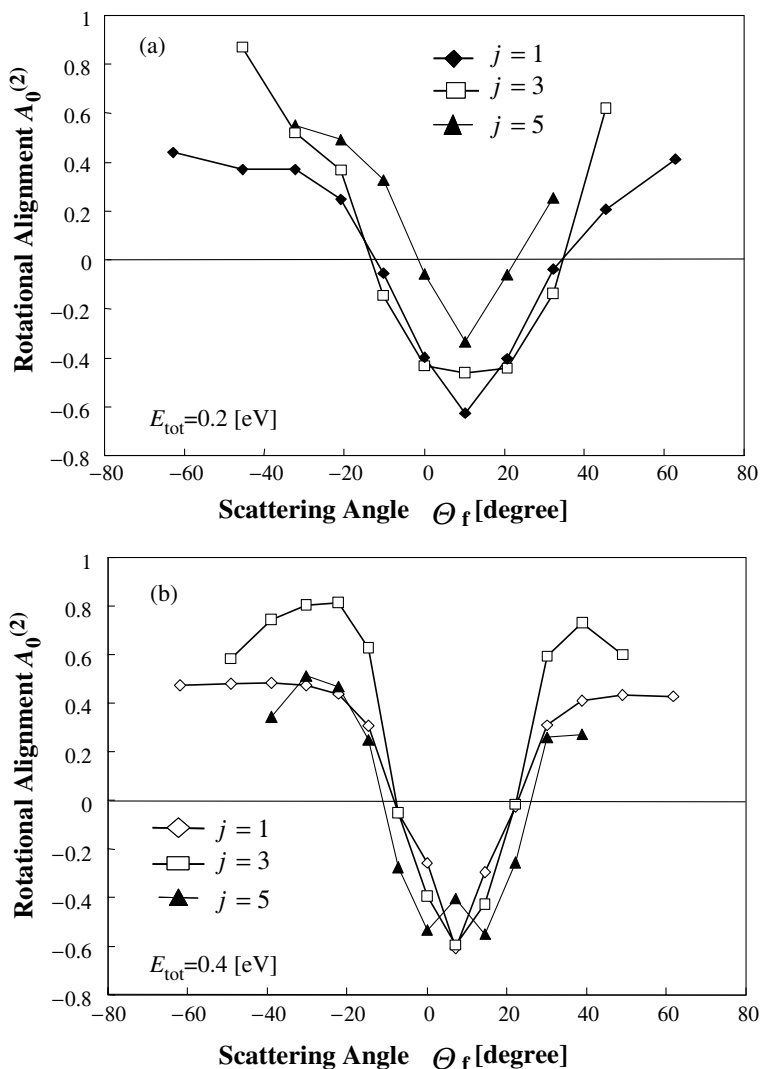


Fig. 15. Rotational alignment $A_0^{(2)}(E_{tot})$ of H_2 scattered from Cu(001), in the vibrationally ground state ($v = 0$), as a function of the final scattering angle along the [100] direction of Cu(001) for the case when (a) $E_{tot} = 0.2$ eV and (b) $E_{tot} = 0.4$ eV for the rotational states $j = 1, 3, 5$. From [53].

6. Increasing the $o-p$ H_2 conversion yield

Here, we describe a new method to enhance the $o-p$ H_2 conversion yield/rate of H_2 interacting with a solid surface based on reaction design of H_2 -surface/catalyst reactions. It consists of two stages. The first stage involves the DQF process [14,47–49,53], and the second stage relies on the SE on the $o-p$ H_2 conversion [58–62]. The

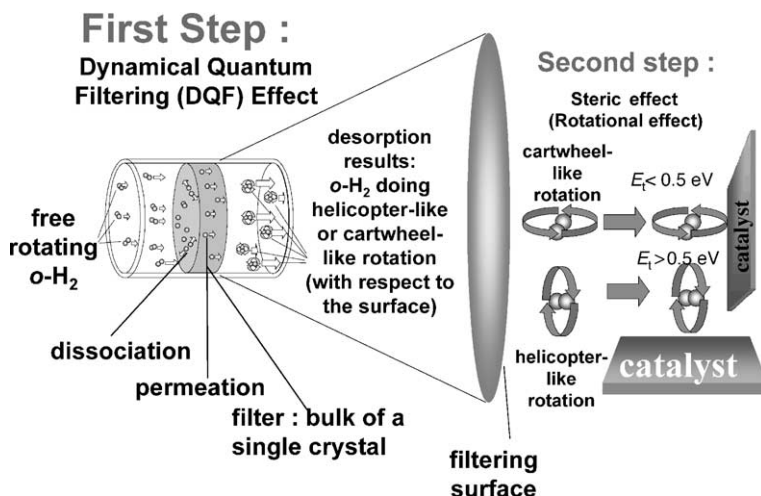


Fig. 16. The new method to enhance the $o\text{-}p$ H_2 conversion yield/rate we propose here consists of two steps [61]. The first step involves the dynamic quantum filtering process [14,47–49,53], and the second step relies on the SE on $o\text{-}p$ H_2 conversion [60]. The purpose of the DQF process is to align the free rotating $o\text{-H}_2$ such that we have only HLR H_2 or CLR H_2 [14,47–49,53].

purpose of the DQF process is to align free-rotating $o\text{-H}_2$ such that we have only H_2 doing HLR or H_2 doing CLR. This DQF process could be performed, e.g., by permeating H atoms through some metal crystal. After permeation, the desorbing H_2 will, depending on their final translational energy upon desorption, be exhibiting either CLR or HLR. As shown in Fig. 12, if we can devise a means to either select only slow desorbing molecules or fast desorbing molecules, we can obtain, respectively, either CLR H_2 or HLR H_2 , only. We can also do this by scattering H_2 on a solid surface.

In the second process, as shown in Fig. 16, we bring these aligned $o\text{-H}_2$ close to a catalyst surface (e.g., metal oxide surface). Based on the SE, cartwheel-like rotating $o\text{-H}_2$ will be converted to $p\text{-H}_2$ with higher rate than helicopter-like rotating $o\text{-H}_2$, as shown in Fig. 11. We estimate that if this method could be performed, we can enhance the $o\text{-}p$ H_2 conversion yield by around one order of magnitude.

7. Conclusions and discussion

In the following we list and give a brief description of the key factors considered in this study.

Fermi contact interaction. In the presence of a surface, the nuclear spin of a H_2 may couple with the electrons at the surface. The electron–nucleus coupling is magnetic in origin, and may be either a dipolar interaction between the electron and the nucleus spins or a Fermi contact interaction [39]. The latter depends on the very close approach of an electron to the nucleus. The coupling of the nuclear spin to

electron spin by the Fermi contact interaction is most important for proton spins. A 1s electron in a H atom experiences a field of about 50 mT as a result of its Fermi contact interaction with the central proton.

Steric effect. Symmetry considerations tell us that the *o-p* H₂ conversion would be more efficient when we have a H₂ with the H–H bond oriented parallel to the surface normal, than one with the H–H bond oriented perpendicular to the surface normal. In the former, only one of the nuclei comes into contact with surface electrons. Starting with pure *o*-H₂, via the Fermi contact interaction, flipping of the nuclear spin occurs. In the latter case, both of nuclei come into contact with the surface electrons, and both nuclei would have almost the same probability of having their spins flipped. Actual calculations show approximately one order of magnitude increase in the *o-p* H₂ conversion yield/rate with the H–H bond oriented parallel to the surface normal, compared to one with the H–H bond oriented perpendicular to the surface normal [58–62]).

Dynamical quantum filtering. This pertains to the process in which we can utilize the inherent orientation dependence of H₂-solid surface interaction to, in this case, use the surface as an effective filter to separate HLR H₂ from CLR H₂. We could do this in either of two ways, we could permeate H atoms through a solid sample [14,47–49] or scatter a stream of H₂ on one side of a solid sample [53], and then collect the corresponding associative desorbing H₂, or the scattered H₂, respectively. (Note that for efficient conversion, it would be necessary to use a surface having a particularly high activation barrier for H₂ dissociation. Otherwise, we would lose the H₂ supply to surface adsorption/absorption.) By employing either resonance-enhanced multi-photon ionization (REMPI) [82,83,85,86] or laser-induced fluorescence (LIF) [84,87–92], we could then distinguish between HLR H₂ from CLR H₂ by measuring the quadrupole alignment factor $A_0^{(2)}(j)$. $A_0^{(2)}(j) > 0$: predominantly HLR H₂ and $A_0^{(2)}(j) < 0$: predominantly CLR H₂. We can then separate these two types of rotating H₂ by coupling the above-mentioned experiments with (angle-resolved) time-of-flight (TOF) detection techniques. HLR H₂ will desorb with a much higher translational energy compared to CLR H₂. On the other hand, most of the specularly scattered H₂ will be doing CLR. Either procedure enables us to separate HLR H₂ from CLR H₂.

We hope that we have convincingly demonstrated that through systematic theoretical and experimental studies, we were able to present a simple, cost-effective method for solving a timely and urgent problem such as that of increasing the *o-p* H₂ conversion yield, using insights from surface science. We hope that this would serve a catalyst for further efforts to apply surface science-based insights into solving some of our more pressing needs, particularly in the design and fabrication of novel, energy efficient, user, and environmental-friendly materials, and devices.

Acknowledgements

We are grateful to Dr. Hiroshi Nakanishi and Dr. Yoshio Miura for helpful discussions and comments on this work. This work is partly supported by the

Ministry of Education, Culture, Sports and Science and Technology of Japan (MEXT) through their grant-in-aid for COE Research (10CE2004), Scientific Research (11640375, 13650026) programs, MEXT Special Coordination Funds for Promoting Science and Technology (NDR—Nanospintronics Design and Realization), and by the New Energy and Industrial Technology Development Organization (NEDO) through the Materials and Nanotechnology program, the Japan Science and Technology Corporation (JST) through their Research and Development Applying Advanced Computational Science and Technology program, and the Toyota Motor Corporation through their Cooperative Research in Advanced Science and Technology program. Some of the calculations presented here were done using the computer facilities of the Japan Science and Technology Corporation (JST), the Yukawa Institute Computer Facility (Kyoto University) and the Institute for Solid State Physics (ISSP) Supercomputer Center (University of Tokyo). W.A.D. gratefully acknowledges Fellowship grant from the Japan Science and Technology Corporation (JST) through their Research and Development Applying Advanced Computational Science and Technology program, and support from the Marubun Research Promotion Foundation. R.M. acknowledges support from the Marubun Research Promotion Foundation. This work is part of an officially recognized program/activity in commemoration of the “ASEAN-Japan Exchange year 2003”.

References

- [1] P.J. Feibelman, J. Harris, *Nature* 372 (1994) 135.
- [2] A. Farkas, *Orthohydrogen, Parahydrogen, and Heavy Hydrogen*, Cambridge University Press, Cambridge, 1935.
- [3] I.F. Silvera, *Rev. Mod. Phys.* 52 (1980) 393.
- [4] H. Kasai, A. Okiji, *Prog. Theor. Phys. Suppl.* 106 (1991) 341.
- [5] E. Ilisca, *Prog. Surf. Sci.* 41 (1992) 217.
- [6] H. Kasai, A. Okiji, *Prog. Surf. Sci.* 44 (1993) 101.
- [7] H.A. Michelsen, C.T. Rettner, D.J. Auerbach, in: R.J. Madix (Ed.), *Springer Series in Surface Science*, vol. 34, Springer-Verlag, Berlin, 1994, p. 185.
- [8] G.R. Darling, S. Holloway, *Rep. Prog. Phys.* 58 (1995) 1595.
- [9] H. Kasai, W.A. Diño, A. Okiji, *Butsuri* 52 (1997) 824 (in Japanese).
- [10] D. Fariás, K.-H. Rieder, *Rep. Prog. Phys.* 61 (1998) 1575.
- [11] A. Gross, *Surf. Sci. Rep.* 32 (1998) 291.
- [12] G.P. Brivio, M.I. Trinio, *Rev. Mod. Phys.* 71 (1999) 231.
- [13] G.J. Kroes, *Prog. Surf. Sci.* 60 (1999) 1.
- [14] W.A. Diño, H. Kasai, A. Okiji, *Prog. Surf. Sci.* 63 (2000) 63.
- [15] A. Hodgson, *Prog. Surf. Sci.* 63 (2000) 1.
- [16] G.O. Sitz, *Rep. Prog. Phys.* 65 (2002) 1165.
- [17] W.A. Diño, H. Kasai, A. Okiji, *J. Phys. Soc. Jpn.* 69 (2000) 993.
- [18] W.A. Diño, H. Kasai, A. Okiji, *Appl. Surf. Sci.* 169–170 (2001) 36.
- [19] W.A. Diño, H. Kasai, A. Okiji, *Surf. Sci.* 482–485 (2001) 318.
- [20] W.A. Diño, H. Kasai, A. Okiji, *Surf. Sci.* 493 (2001) 278.
- [21] P.M. Holmblad, J.H. Larsen, I. Chorkendorff, L.P. Nielsen, F. Besenbacher, I. Stensgaard, E. Lægsgaard, P. Kratzer, B. Hammer, J.K. Nørskov, *Catal. Lett.* 40 (1996) 131.
- [22] F. Besenbacher, I. Chorkendorff, B.S. Clausen, B. Hammer, A.M. Molenbroek, J.K. Nørskov, I. Stensgaard, *Science* 279 (1998) 1913.

- [23] B. Cagnac, M.D. Plimmer, L. Julien, F. Biraben, *Rep. Prog. Phys.* 57 (1994) 853.
- [24] Y. Fukai, *The Metal–Hydrogen System*, Springer-Verlag, Berlin, 1993.
- [25] B.M. Andreev, E.P. Magomedbekov, G.H. Sicking, *Interaction of Hydrogen Isotopes with Transition Metals and Intermetallic Compounds*, Springer-Verlag, Berlin, 1996.
- [26] H. Wipf, *Hydrogen in Metals III*, Springer-Verlag, Berlin, 1997.
- [27] M.S. Daw, M.I. Baskes, *Phys. Rev. Lett.* 50 (1983) 1285.
- [28] H. Vehoff, in: H. Wipf (Ed.), *Topics in Applied Physics*, vol. 73, Springer-Verlag, Berlin, 1997, p. 215.
- [29] D.P. Gregory, *Sci. Am.* 228 (1973) 13.
- [30] P. Dantzer, in: H. Wipf (Ed.), *Topics in Applied Physics*, vol. 73, Springer-Verlag, Berlin, 1997, p. 279.
- [31] G.E. Smauch, A.H. Singleton, *Ind. Eng. Chem.* 56 (1964) 20.
- [32] E.P. Wigner, *Z. Phys. Chem. B* 23 (1933) 28.
- [33] K.G. Petzinger, D.J. Scapalino, *Phys. Rev. B* 8 (1973) 266.
- [34] E. Ilisca, A.P. Legrand, *Phys. Rev. B* 5 (1972) 4994.
- [35] E. Ilisca, S. Sugano, *Phys. Rev. Lett.* 57 (1986) 2590.
- [36] E. Ilisca, *Chem. Phys. Lett.* 168 (1990) 289.
- [37] E. Ilisca, S. Paris, *Surf. Sci.* 363 (1996) 347.
- [38] K. Makoshi, M. Rami, E. Ilisca, *J. Phys.: Condens. Matter* 5 (1993) 7325.
- [39] E. Fermi, *Z. Phys.* 60 (1930) 320.
- [40] W.A. Diño, H. Kasai, A. Okiji, *J. Phys. Soc. Jpn.* 64 (1995) 2478.
- [41] H.A. Michelsen, C.T. Rettner, D.J. Auerbach, *Phys. Rev. Lett.* 69 (1992) 2678.
- [42] H.A. Michelsen, C.T. Rettner, D.J. Auerbach, R.N. Zare, *J. Chem. Phys.* 98 (1993) 8294.
- [43] W.A. Diño, H. Kasai, A. Okiji, *J. Phys. Soc. Jpn.* 66 (1997) 3344.
- [44] W.A. Diño, H. Kasai, A. Okiji, *Phys. Rev. Lett.* 78 (1997) 286.
- [45] M. Gostein, G.O. Sitz, *J. Chem. Phys.* 106 (1997) 7378.
- [46] A. Gross, S. Wilke, M. Scheffler, *Phys. Rev. Lett.* 75 (1995) 2718.
- [47] W.A. Diño, H. Kasai, A. Okiji, *J. Phys. Soc. Jpn.* 67 (1998) 1517.
- [48] W.A. Diño, H. Kasai, A. Okiji, *Surf. Sci.* 418 (1998) L39.
- [49] W.A. Diño, H. Kasai, A. Okiji, *Surf. Sci.* 427–428 (1999) 358.
- [50] W.A. Diño, K. Fukutani, T. Okano, H. Kasai, A. Okiji, D. Fariás, K.-H. Rieder, *J. Phys. Soc. Jpn.* 70 (2001) 3491.
- [51] W.A. Diño, *J. Phys.: Condens. Matter* 14 (2002) 4379.
- [52] D. Fariás, R. Miranda, K.-H. Rieder, W.A. Diño, K. Fukutani, T. Okano, H. Kasai, A. Okiji, *Chem. Phys. Lett.* 359 (2002) 127.
- [53] Y. Miura, H. Kasai, W.A. Diño, *J. Phys.: Condens. Matter* 14 (2002) L479.
- [54] W.A. Diño, H. Kasai, A. Okiji, *Surf. Sci.* 363 (1996) 52.
- [55] H. Kasai, W.A. Diño, A. Okiji, in: A. Okiji, H. Kasai, K. Makoshi (Eds.), *Springer Series in Solid-State Science*, vol. 121, Springer-Verlag, Berlin, 1996, p. 99.
- [56] H. Kasai, W.A. Diño, A. Okiji, in: K. Tanaka (Ed.), *Chemical Processes at Surfaces based on Atomic Scale Structures and Dynamics*, WORDS Publishing House, Tokyo, 1996, p. 223.
- [57] A. Okiji, H. Kasai, W.A. Diño, in: J.L. Moran-Lopez (Ed.), *Current Problems in Condensed Matter: Theory and Experiments*, Plenum Press, New York, 1998, pp. 275–282.
- [58] R. Muhida, W.A. Diño, A. Fukui, H. Kasai, H. Nakanishi, A. Okiji, K. Fukutani, T. Okano, *Surf. Sci.* 493 (2001) 285.
- [59] R. Muhida, W.A. Diño, A. Fukui, Y. Miura, H. Kasai, H. Nakanishi, A. Okiji, K. Fukutani, T. Okano, *J. Phys. Soc. Jpn.* 70 (2001) 3654.
- [60] R. Muhida, W.A. Diño, Y. Miura, H. Kasai, H. Nakanishi, A. Okiji, K. Fukutani, T. Okano, *Surf. Sci.* 514 (2002) 273.
- [61] R. Muhida, W.A. Diño, Y. Miura, H. Kasai, H. Nakanishi, K. Fukutani, T. Okano, A. Okiji, *J. Vac. Soc. Jpn.* 45 (2002) 448.
- [62] R. Muhida, Y. Miura, W.A. Diño, H. Kasai, H. Nakanishi, A. Okiji, K. Fukutani, T. Okano, *J. Appl. Phys.* 93 (2003) 644.
- [63] P.A. Cox, *Transition Metal Oxide*, Clarendon, Oxford, 1992.

- [64] T. Wolfram, E.A. Kraut, F.J. Morin, *Phys. Rev. B* 7 (1973) 1677.
- [65] P.E. Cade, A.C. Wahl, *Atomic Data Nucl. Data Tables* 13 (1974) 339.
- [66] M. Tsukada, C. Satoko, H. Adachi, *J. Phys. Soc. Jpn.* 48 (1980) 200.
- [67] M.O. Selme, P. Pecheur, *J. Phys. C Solid State Phys.* 21 (1988) 1779.
- [68] A. Szabo, N.S. Ostlund, *Modern Quantum Chemistry*, Macmillan, New York, 1988.
- [69] Y. Tokura, N. Nagaosa, *Science* 288 (2000) 462.
- [70] A. Okiji, H. Kasai, A. Kato, *J. Phys. Soc. Jpn.* 51 (1982) 3291.
- [71] A. Fukui, H. Kasai, A. Okiji, *J. Phys. Soc. Jpn.* 12 (1998) 4201.
- [72] J.C. Slater, *Quantum Theory of Molecules and Solids*, McGraw-Hill, New York, 1954.
- [73] W. Brenig, H. Kasai, *Surf. Sci.* 213 (1989) 170.
- [74] W. Brenig, T. Brunner, A. Groß, R. Russ, *Z. Phys. B* 93 (1993) 91.
- [75] C.C. Rankin, J.C. Light, *J. Chem. Phys.* 51 (1969) 1701.
- [76] Y. Miura, H. Kasai, W.A. Diño, A. Okiji, *J. Phys. Soc. Jpn.* 68 (1999) 887.
- [77] B. Hammer, M. Scheffler, K.W. Jacobsen, J.K. Nørskov, *Phys. Rev. Lett.* 73 (1994) 1400.
- [78] J.A. White, D.M. Bird, M.C. Payne, I. Stich, *Phys. Rev. Lett.* 73 (1994) 1404.
- [79] P. Kratzer, B. Hammer, J.K. Nørskov, *Surf. Sci.* 359 (1996) 45.
- [80] G. Wiesenekker, G.J. Kroes, E.J. Baerends, *J. Chem. Phys.* 104 (1996) 7344.
- [81] R.N. Zare, *Angular Momentum*, Wiley, New York, 1988.
- [82] S.J. Gulding, A.M. Wodtke, H. Hou, C.T. Rettner, H.A. Michelsen, D.J. Auerbach, *J. Chem. Phys.* 105 (1996) 9702.
- [83] H. Hou, S.J. Gulding, C.T. Rettner, A.M. Wodtke, D.J. Auerbach, *Science* 277 (1997) 80.
- [84] D. Wetzig, R. Dopheide, M. Rutkowski, R. David, H. Zacharias, *Phys. Rev. Lett.* 76 (1996) 463.
- [85] E.E. Marinero, C.T. Rettner, R.N. Zare, *Phys. Rev. Lett.* 19 (1982) 1323.
- [86] S.L. Anderson, G.D. Kubiak, R.N. Zare, *Chem. Phys. Lett.* 105 (1984) 22.
- [87] U. Fano, J.H. Macek, *Rev. Mod. Phys.* 54 (1973) 553.
- [88] C.H. Greene, R.N. Zare, *Ann. Rev. Phys. Chem.* 33 (1982) 119.
- [89] C.H. Greene, R.N. Zare, *J. Chem. Phys.* 78 (1983) 6741.
- [90] D. Wetzig, R. Dopheide, M. Rutkowski, R. David, H. Zacharias, *Phys. Rev. Lett.* 76 (1995) 463.
- [91] D. Wetzig, M. Rutkowski, R. David, H. Zacharias, *Europhys. Lett.* 36 (1996) 31.
- [92] D. Wetzig, M. Rutkowski, W. Etterich, R. David, H. Zacharias, *Surf. Sci.* 402–404 (1998) 232.